UNIVERSITÀ DEGLI STUDI DI CATANIA

Dottorato di Ricerca in SCIENZE CHIMICHE

Ciclo XXIX

Surface engineering of oxide systems for energy and molecular electronics applications

Stefania Vitale

Tesi di dottorato di ricerca
Gennaio 2017

Tutor: Prof. A. Licciardello

Coordinatore: Prof. S. Sortino

*A chi ha **sempre** creduto in me,*

*a volte facendolo **anche per me**.*

"It is our responsibility as scientists, knowing the great progress and great value of a satisfactory philosophy of ignorance, the great progress that is the fruit of freedom of thought, to proclaim the value of this freedom, to teach how doubt is not to be feared but welcomed and discussed, and to demand this freedom as our duty to all coming generations."

Richard Feynman, "*The Pleasure of Finding Things Out"*

"Science is not everything, but science is very beautiful."

J. Robert Oppenheimer

Riassunto

La modifica di superfici mediante deposizione di film sottili di molecole funzionali costituisce un interessante approccio tecnologico per il miglioramento di varie proprietà superficiali di un materiale. Sono virtualmente infinite le possibilità di progettazione di superfici funzionali con proprietà speciali impartite dai sistemi molecolari utilizzati, poiché virtualmente infinite sono le molecole che possono essere sintetizzate e le proprietà che in esse possono essere introdotte (ottiche, elettriche, strutturali, ecc…). Quando tali molecole vengono integrate sulla superficie di un materiale avente anch'esso *per se* proprietà speciali, il risultato è un nuovo sistema allo stato solido avente dimensioni nanometriche e caratteristiche derivate dalle "fusione" di quelle delle molecole ancorate e quelle della superficie. Per ottenere un'efficace "combinazione" molecola-superficie, tuttavia, l'approccio sperimentale utilizzato per la preparazione del substrato e per l'integrazione del sistema molecolare sono di importanza cruciale per l'ottenimento di un buon risultato. In questo contesto le metodologie impiegate devono essere messe a punto in maniera mirata, per garantire l'ancoraggio stabile di specifiche molecole su specifiche superfici.

Il presente lavoro di tesi è stato dedicato alla modifica di superfici mediante ancoraggio di sistemi molecolari funzionali per future applicazioni nell'ambito dell'elettronica molecolare e dell'energia. L'obiettivo principale è stato la messa a punto di una metodologia sperimentale che consentisse un ancoraggio stabile delle specie molecolari desiderate su superfici di ossidi di interesse tecnologico, quali gli ossidi trasparenti e (semi)conduttori (TCOs). Per fare ciò è stato sfruttato un approccio basato sulla chimica dello zirconio fosfato-fosfonato, che consiste in un *priming* superficiale preliminare (ZP-*priming*) attraverso la deposizione di uno strato sottilissimo (*monolayer)* di fosfato di zirconio direttamente alla superficie di ossido. Tale strato, come dimostrato dalle evidenze sperimentali riportate, funge da robusta "piattaforma" per il successivo ancoraggio di sistemi molecolari recanti un gruppo fosfonico, su ossidi di diversa morfologia e natura chimica.

La strategia di *priming* ZP è stata applicata con successo al trattamento di substrati nanostrutturati, di spessore micrometrico (5-10 μm) di TiO_2 ed SnO_2.

L'ottenimento di un *priming* uniforme è stato confermato attraverso l'acquisizione di profili di profondità (*depth profiling)* mediante spettrometria di massa di ioni secondari ToF-SIMS. ZP-TiO_2 e ZP-SnO_2 sono stati in seguito utilizzati come substrati per la preparazione di elettrodi fotoattivi, che possono trovare utilizzo in celle solari colorante-sensibilizzate (*dye-sensitized cells*). È stato dimostrato che il trattamento ZP produce un'ottima piattaforma di ancoraggio per le molecole di colorante fotoattivo RuP (un terpiridil-triazin complesso di rutenio (II) funzionalizzato con un gruppo fosfonico), mentre misure di *depth profiling* ToF-SIMS hanno permesso di monitorare la diffusione del colorante nel *layer* di ossido nanostrutturato, mostrando che tutto lo strato micrometrico viene sensibilizzato con il colorante. Inoltre, da misure di spettroscopia UV-Vis è emerso che il trattamento preliminare ZP introduce alcuni vantaggi, ovvero un incremento della stabilità del legame molecola fotoattiva-ossido, nonché un maggiore *uptake* di molecole di colorante. Da misure fotoelettrochimiche (caratteristiche JV sotto irraggiamento) si è visto inoltre che la presenza dello strato di fosfato di zirconio all'interfaccia fra ossido e molecole di colorante non influisce negativamente sul processo di iniezione di carica dal colorante all'ossido (alla base del funzionamento delle celle solari a colorante), e di conseguenza la funzionalità dell'elettrodo è del tutto paragonabile a quella di un classico elettrodo colorante-sensibilizzato "non ZP".

L'utilizzo di ZP-TCOs è stato inoltre esteso alla preparazione di fili molecolari conduttivi, questi ultimi "assemblati" depositando complessi metallo-polipiridinici direttamente alla superficie di ossido, attraverso successive reazioni di coordinazione. In una prima fase, è stata preparata una superficie funzionalizzata con unità terpiridiniche, mediante ancoraggio del sistema molecolare ditopico PPTP (acido (4-(2,2': 6'-2''-terpiridin-4-ile) benzen-fosfonico) su ZP-FTO; le unità terpiridiniche libere alla superficie sono state in seguito utilizzate come sito di ancoraggio per le molecole bifunzionali di $RuDT_2$ (Ru(II)-bis[4′,4‴-(1,4-fenilene)bis(2,2′:6′,2″-terpiridina)]), attraverso reazione di coordinazione metallica da parte di ferro (II) delle una terpiridine in superficie con una delle due unità terpiridiniche della molecola $RuDT_2$. Attraverso cicli iterativi di reazioni di coordinazione, sono stati preparati fili molecolari contenenti diverse unità Fe-$RuDT_2$, e l'avvenuta crescita è stata confermata mediante misure ToF-SIMS e spettroscopia UV-Vis. La conduzione elettrica lungo i fili molecolari è stata studiata mediante *liquid-metal EGaIn junction*, e i dati raccolti mostrano una buona conduzione della carica elettrica, comparabile a quella di sistemi simili preparati su superfici di

oro. La possibilità di integrare sistemi elettricamente conduttivi di complessi metallo-polipiridina su superfici di ossidi conduttori e trasparenti, attraverso la piattaforma ZP-PPTP, permette di prendere in considerazione applicazioni nell'ambito dell'elettronica molecolare, con possibile estensione all'elettronica "fotoresponsiva", considerato che le unità metallo-terpiridina sono notoriamente dei centri fotoattivi.

Table of contents

Preface

Surface engineering has become an indispensable tool for the improvement of a number of properties of solid surfaces. Nowadays modification techniques such as thin film deposition, (photo- and electron-)lithography, laser and plasma treatments are largely employed to tailor various surface properties and lead to new functional materials being used in different fields, such as advanced electronics, optoelectronics, optics, energy harvesting and medical devices.[1]

A particular interesting and relatively simple modification technique consists in the chemical deposition of thin molecular layers at the materials' surface. This approach has been extensively studied in the last decades, both for fundamental studies on intermolecular interaction at solid interfaces (but also generic intermolecular interactions) and functional surfaces development.[2, 3] The main advantages of molecular surface engineering are: i) specific functional molecular systems can be purposely synthesised to tailor specific properties to the desired surface ii) the flexibility and the relatively ease and low-cost manufacturing of organic synthesis could provide virtually infinite variety of molecular systems having diverse properties (optical, electrical, tribological, etc..), iii) the extremely small size of molecules (< 1 nm) allows for the preparation of nanometre-scale systems through a "bottom-up" approach. The latter point fulfils, among others, the requirements of the miniaturisation trend in the development of modern devices and allows to tackle all the physical and technical limits faced by established surface technologies such as photolithography.[4]

In molecular engineering of solid surfaces the choice of the molecular systems if crucial for the achievement of the desired properties. This choice, of course, is strongly affected also by the nature of the surface to be modified so that, globally, the achievement of the particular desired goal, in terms of system properties, must take into account both the counterparts (molecular system and solid substrate) as well as their interaction. In other words, parallel to the choice of specific molecular systems to be anchored, the selection of the substrate to be functionalised is not of least importance. Specific materials have specific chemical composition, structures and surface properties, which must be taken into account when thinking about a successful "molecule-surface" match for a well-defined application.

In the last two decades, significant scientific and technological interest has been addressed to oxide materials, especially metal oxides. A good summary of the reasons which justify this widespread interest can be found in a review by Diebold *et al.:*[5] "*Among metal oxides are superconductors and the best insulators; some oxides are inert enough to act as corrosion protection layers, whereas others are chemically active as catalysts. Some of the most interesting magnetic, optical and electronic properties are found within this class of materials.*"
Particular interest is focused on transparent conductive oxides (TCOs). The importance of those materials arises from their good electrical properties coupled with the transparency in the visible region.[6]

As a consequence of the above mentioned appealing properties, the scientific interest in molecular engineering of technologically-relevant oxide surfaces expanded rapidly in the last years, and the research on this topic led to functionalised-surface ("engineered") oxides that can actually find application in various fields such as electronics,[7-11] optoelectronics,[12, 13] catalysis[14] and sensors.[15, 16]

One of the most interesting field of application of oxide molecular surface engineering deals with the development and realisation of molecular devices which are able to perform light-induced functions, the so called Photochemical Molecular Devices (PMD).[17] In such devices the molecular system is chosen to fulfil specific light-induced functions (like photo-induced electron transfer), and it is subsequently integrated on a convenient solid substrate, which would be both a "support" for the immobilisation of the molecular system and, most important, an active component of the final device. Such a system can find application in a number of technological areas, such as those involving light harvesting, elaboration of optical signal information, energy production and biological applications.
In this framework, a remarkable example of photoactive devices which are able to photochemically convert the energy of the solar radiation in electric energy (or energy fuels) are the so-called Dye Sensitized Cells, such as Dye Sensitized Solar Cells (DSSCs) and Dye-Sensitized Photoelectrochemical Cells (DSPECs). The working principle of these devices is based on sunlight absorption by a photoactive dye molecule anchored onto the surface of a nanostructured, transparent, micrometres-thick semiconductor oxide, followed by injection of an electron from the excited state of the dye to the conduction band of the semiconductor.

Another interesting example of application of surface-integrated photoactive molecules consists in the preparation of nanometric solid state photoresponsive molecular junctions,[18] consisting in a thin film of light-sensitive molecules densely packed between two electrodes. Light-induced excitation of this molecular layer leads to charge dissociation and subsequent collection at the electrodes, making this system suitable for working as an optoelectronic switch or an optically responsive memory.

Apart from the choice of a molecular system bearing specific chemical and electronic structures capaple to be practically exploited for "actual" devices realisation, the development of all the above mentioned photoactive devices relies critically on a proper integration of the functional molecules onto the solid substrate. The molecular film has to be firmly bound to the surface through a stable interface, which has to allow for a robust anchoring of the molecules and, at the same time, for the "communication" between substrate and molecular system. Usually this goal is achieved by exploiting the chemical affinity of some specific functional group (which the molecular system would be equipped with) to the surface of a substrate. A general and easy approach involves the anchoring by chemisorption of the molecules onto the surface from liquid solutions, by simply immersion of the solid substrate in a low-concentration (usually millimolar) solution of the molecular system. As example of application of this approach, Self-assembled monolayers (SAMs) and Langmuir-Bodgett films are certainly amongst the most famous.[19] These solution-based methods, however, require a careful planning of each reaction step, with special concern on the reaction conditions (solvents, temperature, reaction time,…) and all the experimental parameters involved.

Parallel to the development of reliable and reproducible methods for the preparation and modification of functional molecular surfaces, specialised analytical techniques are necessary for the precise characterisation of the surface properties (such as chemical composition, structure, optical and electric properties, etc..), in order to elucidate the variety of physico-chemical phenomena down to the single molecule level and their effect on the macroscopic properties of the modified surface.
Among the available surface analysis techniques, time-of-flight secondary ions mass spectrometry (ToF-SIMS) can be considered one of the most powerful, because it allows for the chemical characterisation of the surfaces with very high sensitivity and good spatial resolution, allowing not only the detection and bi- or three- dimensional mapping of all elements (including hydrogen) but

also providing a large amount of molecular information on the species present at the surface and, with some limitations, along the depth of molecular films.

This thesis work is focused on the modification of oxide surfaces *via* anchoring of functional molecular systems, for applications in solar energy conversion and in molecular electronics. In particular, a functionalisation strategy based on the zirconium phosphate/phosphonate chemistry has been investigated, with the aim of developing an effective experimental strategy for achieving a robust and reproducible anchoring of functional molecules on oxide surfaces of different chemical nature (TiO_2, SnO_2, fluorine-doped tin oxide) and morphology (flat and nanostructured). Some specific preparation methodologies have been developed and optimised for the assembly of different special photoactive molecules on technologically-interesting oxide substrates. The obtained systems were extensively characterised by ToF-SIMS technique, jointly to UV-Vis spectroscopy. "Functional" characterisation was also carried out by means of photoelectrochemical measurements and liquid-metal junction technique.
The thesis is divided in different sections. The first, **"Introduction and state of the art"**, is an overview of the state of art and acts as an "introduction" to the experimental work performed. It gives some background information about the context of application of some molecular-functionalised oxides in the field of dye-sensitised cells for solar energy conversion and nanoscale molecular electronics. The second section **"Results and discussion"** deals with the description and discussion of the experimental results, and it is divided in two subsections. In the first one, results are presented on the functionalisation of nanostructured, transparent, semiconducting oxide surfaces by means of photoactive dye molecules, whilst in the second section the assembly of conductive molecular wires on a transparent conductive oxide is reported, along with some results on their electrical properties. Finally, some general C**onclusions and perspectives** are outlined. In order to render more fluid the presentation and discussion of the experimental results, many experimental details are reported in a separate appendix **"Material and Methods"**.

1.Introduction and state of the art

1.1. Progress in photovoltaics: the molecular approach for solar energy conversion

Progressive depletion of fossil fuels imposes to look for new energy sources for the (always increasing) needs of industrial, commercial and everyday-life activities. The supply of renewable and environmentally sustainable energy has become one of the major task of modern society, in order to limit fossil fuels depletion and also the environmental effects of their employment (pollution, global warming, etc..).

Among all the renewable energy technologies proposed over the years, photovoltaic technology based on solar energy exploitation is considered as the most promising one.

Solar radiation amounts to 3.8 million EJ/year ($3{,}8 \cdot 10^{24}$), which is approximately 10,000 times more than current world energy needs[20]. The idea of converting part of this huge amount of energy in an exploitable form has led to the development of solar photovoltaic cells, devices that convert solar energy directly to electric energy. The "conventional" first and second generation solar cells are based on semiconducting materials, mainly silicon, but also other semiconductors such as CdTe and CIGS. These cells are inorganic solid-state junction devices, which can convert sunlight radiation in electricity with 15-20% of efficiency. Despite their good performances, their production requires high manufacturing and maintenance costs, which prevents limits their actual widespread diffusion. Meanwhile, other alternatives are being explored such as molecular-based solar cells, namely heterojunction organic photovoltaic cells, polymeric thin films-based solar cells and nanocrystalline semiconductor-based ones. Similarly to the processes involved in the natural photosynthesis, all the above mentioned systems operate in virtue of a charge-separation achieved by electron injection from a molecular photoinduced excited state to the conduction band of a semiconductor material. Due to this molecular-based charge separation, those kind of cells generally show worse efficiency in sunlight conversion if compared to silicon-based cells (in which light absorption leads directly to the generation of free conduction band electrons and valence band holes; see Figure 1 for a schematic representation), but this is – at least in principle - compensated by considerably cheaper manufacturing costs. The technological interest on such molecular-

based cells is also given by the possibility of specific market applications, like low temperature processing on plastic substrate and subsequent ease of integration into established printing lines.[21]

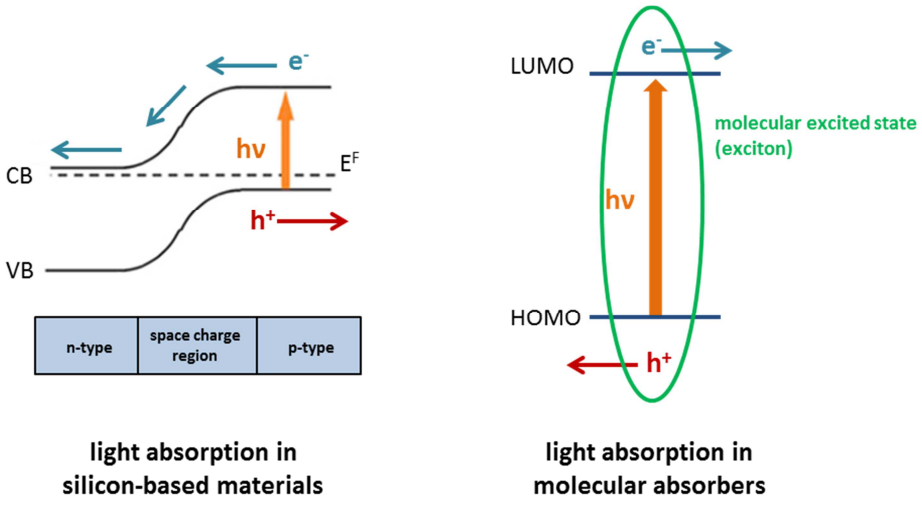

Figure 1: Schematic comparison between light absorption by molecular materials (left) and silicon-based materials (right). (Adapted from ref. [21]).

In this framework, one of the currently most attractive systems, for both scientists and engineers, is represented by the so-called Dye-Sensitized Solar Cells, which are going to be presented in the next paragraph.

1.1.1. Dye-sensitized solar cells (DSSCs)

A dye-sensitized-cell exploits a nanostructured, large-bandgap and transparent semiconductor oxide, in combination with a photosensitizer, usually a chromophore molecule.
The general configuration of a dye-sensitized solar cell and its operating principle are sketched in Figure 2.
The cell is normally built using the following components:

1. A photoanode, consisting on a mesoporous semiconducting oxide layer (usually TiO_2 in anatase phase), deposited onto a glass slide covered with a thin film of transparent conducting oxide (usually FTO, fluorine-doped tin oxide), and then sensitized with a monolayer of photoactive

dye molecules covalently attached to the surface of the mesoporous oxide;

2. a cathode, prepared with a glass slide covered with a catalyst (usually platinum);
3. an electrolytic medium, which is in direct contact with both electrodes, and contains a redox agent (usually the redox couple I^-/I_3^-, dissolved in an organic solvent, like acetonitrile).

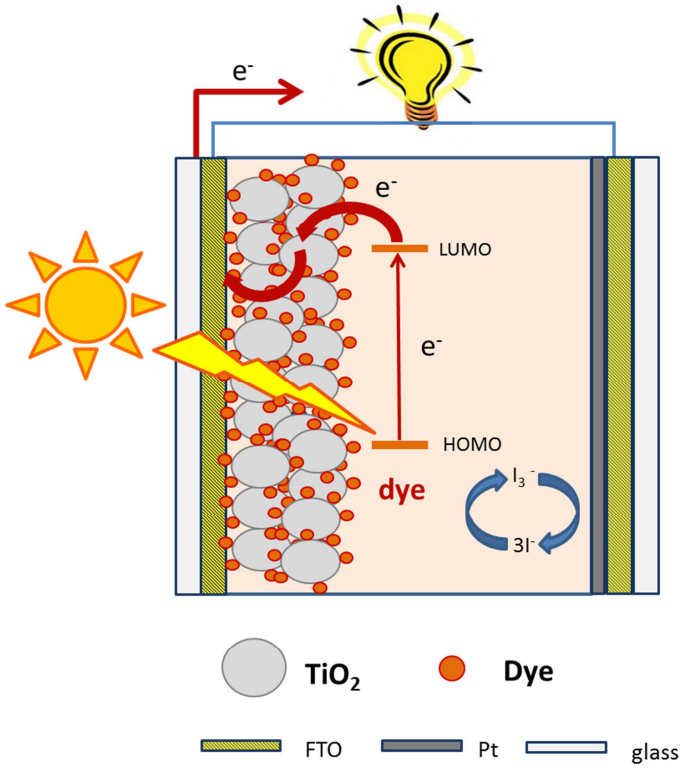

Figure 2: Scheme of a DSSC.

The process of solar energy conversion occurs through four main steps (listed below).[22] It starts with the absorption of a photon from the chromophore, which induces an electron transition from the fundamental state to an excited state (1). This process is followed by the injection of an electron from the excited state to the conduction band of the nanostructured oxide (2). Then, the oxidized dye molecule is reduced (and so regenerated) by the reducing agent present in the electrolytic solution (provided that the HOMO of the dye molecule is low enough to accept electron donation from the electrolyte) (3). The circuit is closed when the reducing agent that has been oxidized is again restored at the cathode, by receiving an electron through an external circuit (4).

1) $Dye + h\nu \rightarrow Dye^*$
2) $Dye^* + TiO_2 \rightarrow Dye^+ + (e^-, TiO_2)$
3) $2Dye^+ + 3I^- \rightarrow 2Dye + I_3^-$
4) $I_3^- + 2e^- \rightarrow 3I^-$

The performance of this kind of cell is evaluated on the basis of two parameters, efficiency (η) and fill factor (FF):

$$\eta = \frac{Voc\ Jsc\ FF}{P_{in}} \times 100\% \qquad FF = \frac{Vmax\ Jmax}{Voc\ Jsc} = \frac{Pmax}{Voc\ Jsc}$$

where J_{SC} is the short circuit current density (mA cm^{-2}), V_{OC} is the open-circuit voltage (V), P_{in} is the incident light power, J_{max} and V_{max} correspond to the values of current density and voltage, respectively, at the maximum power output given in the cell J-V curve (see Figure 3 for a graphic representation of the efficiency-related parameters).

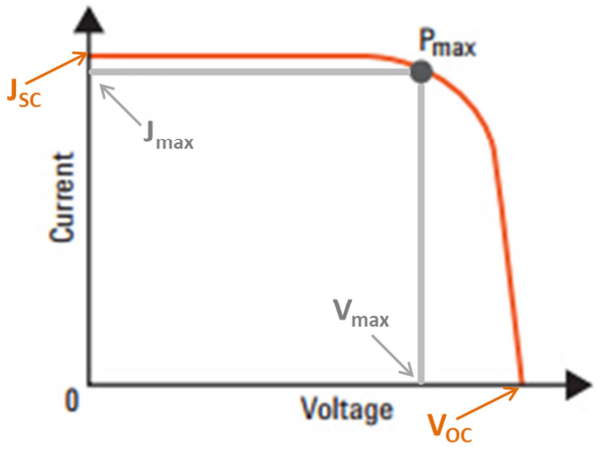

Figure 3: typical J-V curve for a DSSCs, where all the efficiency-related parameters are labeled.

The prototype of the first dye-sensitized solar cell was realised by O'Regan and Grätzel and the outcome results published in 1991.[23] In this paper, a photovoltaic device was described, which was based on a 10um-thick layer of optically transparent TiO2 film of small nanoparticles, coated with a monolayer of a charge-transfer dye to sensitize the titania film for light

harvesting. This cell showed an overall light-to-electric energy conversion higher that 7% in simulated solar light and 12% in daylight. The great performances of this "pioneering" photovoltaic device, combined with the low-cost and easy manufacturing largely justify the huge interest of both researchers and industries on the improvement of such a technology for solar energy conversion.
Following the leading work of O'Regan and Grätzel, a large number of dye-sensitized cells have been reported afterwards, with modified specific components (dyes, oxide electrodes, electrolyte, …) but with the same "backbone", remained mostly unaltered until present days.

1.1.1.1. The photoanode: molecular approach for dye-sensitization of TiO_2 electrodes

Among all the components of a dye-sensitised cell, the most crucial role on the cell functionality is played by the photoanode. Here are located the chromophore agents able to absorb the sunlight and here charge separation takes place after solar light absorption, with electron injection from the dye to the oxide conduction band.
In order to be used in a dye-sensitised cell photoanode, a nanostructured semiconductor oxide must meet different requirements, in particular:

1. a large band gap, allowing for transparency in the visible region of the solar emission spectrum;
2. large surface area;
3. long chemical and thermal stability under irradiation;
4. highly efficient electron collection and injection.

For DSSCs, the oxide material which fulfils all the above mentioned requirements, and has been chosen as substrate of election for photoanode preparation, is titanium dioxide. It occurs naturally in three phases: anatase, rutile and brookite. Anatase TiO_2 is the best suited phase for application in DSSCs, having a 3.2 eV bandgap, higher than the 3.0 eV of rutile (the latter being, however, the most thermodynamically stable phase), lower electron recombination rate [24] and it allows for the adsorption of a greater amount of dye molecules, due to the higher specific surface area. [25]

In addition, titanium dioxide is abundantly available, non-toxic and has cheap manufacturing costs. Despite many other oxide materials have been (and are still being) tested, such as ZnO [26-28], SnO_2[29, 30] and Nb_2O_5[31, 32], titanium dioxide still remains the one which gives the best cell performances in terms of efficiency.

For the preparation of the photoanode a mesoporous layer of oxide is needed, having a thickness of several micrometers (~ 10). The reason for the utilisation of electrodes with such a morphology lies on the large surface area available for the accommodation of the photosensitiser molecules. Given that the dye molecules actually make the DSSCs working, the more molecules we have at the photoanode surface, the more light can be absorbed and converted to electric energy. Furthermore, an oxide thickness in the order of 10 μm gives the right balance between TiO_2 electrode transparency in the visible region of the spectrum, efficient light harvesting and a pore size compatible with electron- as well as electrolyte solution diffusion.[23, 33-35]

The most common approach for the preparation of the mesoporous TiO_2 layer consists in spreading a mixed polymeric-TiO_2 nanoparticles paste over the FTO substrate, through either "doctor blade" technique or screen printing (Figure 4), following a 30 minutes sinterisation treatment at 450° C. Typical titania nanoparticles diameter ranges between 10 and 30 nm, and they are usually prepared by sol-gel synthesis or hydrolysis of $TiCl_4$.[36] Apart from nanoparticle-based electrodes, also other kind of nanostructure are under investigation for the constant improvement of photoanodes performances, such as nanotubes, nanorods, nanosheets, etc…[37]

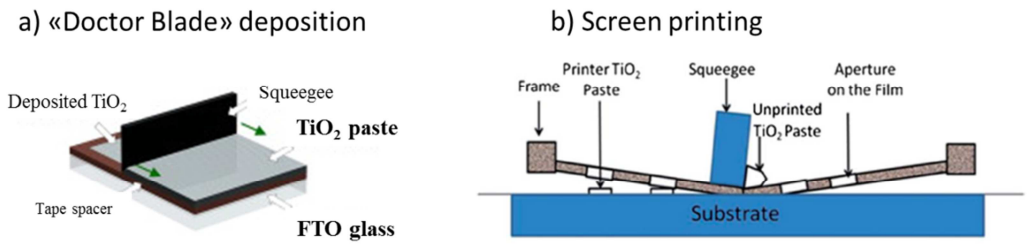

Figure 4: schematic representation of a) "doctor blade" deposition technique and b) screen printing. (Adapted from ref. [38]).

In parallel to the choice of the best suitable substrate to prepare the electrode with, serious attention must be paid on the selection of the dye to be used for sensitisation. The light-absorber molecule has to meet itself several requirements in order to give the desired functionality to the cell: [39]

1. it should absorb as much as possible the visible light up to a threshold of 920 nm (this limit has been extracted from thermodynamic calculations on the light conversion efficiency at different light wavelength)[40, 41];
2. it should be able to inject electron (upon photoexcitation) into the electrode conduction band with ideally unitary quantum yield, provided that the energy level of the excited state of the dye (i.e. LUMO of the molecule) matches with the edge of the conduction band;
3. It should have functional groups allowing for chemical anchoring onto the oxide surface (e.g. –COOH, $–PO_3H_2$,…);
4. its redox potential should be high enough to allow for the regeneration of the dye *via* reduction from the redox electrolyte;
5. it must be photostable, and electrochemical as well as thermal stability are also required.

Given the above mentioned requirements, during years of research several different photosensitizer dye have been synthesised on purpose, including a number of chemical compounds such as transition metal complexes, phtalocyanines, porphyrins and metal-free organic dyes.[42]
Among all those systems, Ru(II)-polypiridyl metal complexes emerged as excellent candidates for being exploited as photosensitiser in dye-sensitised cells.
Polypyridine-based ruthenium complexes are amongst the most interesting photoactive molecular systems, in virtue of a number of outstanding (photo)physico-chemical properties. They show strong absorption in the visible region (which could be also extended to near IR region through a suitable choice of lateral substituents of the polypyridyl units), strong electronic coupling between the MLCT excited state and the semiconductor conduction band (which allows for fast exctited state deactivation *via* dye-to-semiconductor electron injection, happening in a timescale of femtoseconds), and great chemical stability.[43, 44]
The first time when a solar-to-electric energy conversion efficiency of 10% was reached dates back to 1993, when Nazeeruddin and coworkers[45] published data on a dye-sensitized cell built with a cis-(SCN)2bis(2,2'-

bypyridyl-4,4'-dicarboxylate) ruthenium(II) photosensitizer, coded as N3 (Figure 5 a)). Subsequently, in a study of the effect of the proton content in N3 dye, it turned out that the double protonated form, indicated as N719 (Figure 5b) exhibited enhanced power conversion efficiency and a redox potential shifted to more negative potential in solution (condition that favourably increase the Jsc achievable).[46] In an attempt to continuously improve the efficiency of dye-sensitized cells, an extension of the absorption spectrum of the sensitizer to the IR region would be highly desirable; in this framework Gratzel and co-workers synthesised the N749 dye, also known as "black dye" (Figure 5c). With this molecule as photosensitizer, their cell showed a broad red-shift in absorption and a spectrum of IPCE (incident photon-to-current efficiency) over the entire visible range up to 920 nm in the near-IR, as well as an overall conversion efficiency of 10.4 %.[47]

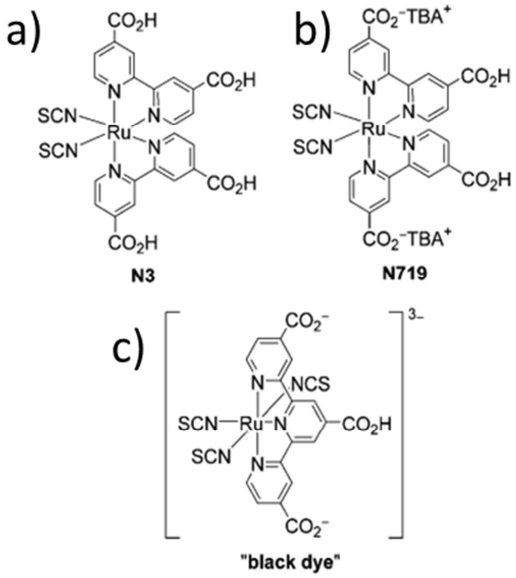

Figure 5: Chemical structures of ruthenium photosensitisers a) N3, b) N719, c) black dye.

From their first use as photosensitizer, N3, N719 and the black dye became reference points for the development of more efficient dyes, and they are today still used as a "starting" point for the design of new sensitizer bearing different ligands and substituents with respect to the "originals", in order to conveniently improve their optical and photophysical properties.

In order for the charge separation phenomena (whose proper functioning of the cell relies on) to properly occur, the availability of the "best" sensitizer, meeting all the previously mentioned conditions, is a necessary condition

although not sufficient *per se*. Among all the required conditions [25] one of the most crucial to be fulfilled is the good quality of the binding between the chromophore and the oxide surface. Given that the sensitizer ensures the solar light absorption, it has to be strongly bound to the surface in order to ensure the best functionality of the cell as well as long term durability. Moreover, the good "communication" must be guaranteed between chromophore molecules and semiconductor oxide, to allow for the dye-to-oxide charge injection. As a consequence of those issues, the obvious outcome is that the photoanode must be designed with utmost care, with a special focus on the dye-sensitization procedure of the nanostructured titania layer, in order to obtain the optimal performances and best device efficiencies achievable.

As previously mentioned, the sensitization procedure is usually carried out by attaching the photoactive system on the TiO_2 surface through a chemical bond between the oxide and a dye molecule carrying a functional group being able to bind to the surface.

The typical functionality currently in use is the carboxylic group, due to the large availability of natural and synthetic dyes, commercial accessibility and relatively good stability.[42] However, the carboxylic group-oxide bond is labile in certain conditions, for example in alkaline solutions,[48] and can be easily broken even with simple rinsing with organic solvents,[49] A number of other functional groups have been investigated, such as silane and sulphonate,[42] but currently one of the most valid alternative to carboxylic functionality appears to be given by the phosphonic groups. Since the first study reported by Péchy et al,[50] phosphonic units have been proven to bind to TiO_2 surfaces stronger than carboxylic groups, and they show greater stability after exposure to both organic solvents and aqueous media, as well as in a wide range of pH.[51-54] The different binding strength and stability can be ascribed to a different reactivity of the two functional groups, caused by the different number of coordination sites that they have, respectively two for the carboxylic unit and three for the phosphonic one. This leads to different anchoring structure in the two cases, that is mono- and bidentate for carboxylate linkages and mono-, bi- and tridentate for phosphonate linkages (Figure 6).[53]

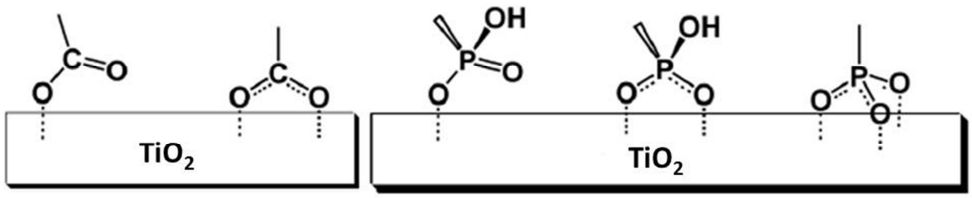

Figure 6: Surface bonding schemes for carboxylate (left) and phosphonate (right) linkages. (Adapted from ref. [53])

Although the stronger binding capability on TiO_2 surfaces and the more stable anchoring in comparison to the carboxylate one, it is known that phosphonate ester linkage on metal oxides (as well as the carboxylate) is susceptible to hydrolysis when exposed to aqueous media. Moreover, although in a smaller extent respect to carboxylated photoactive systems, desorption processes of the phosphonate dye in the common operating condition of the DSSC can occur and they negatively affect the performances of the cell and its lifetime. Later in the text (see paragraph 1.1.3), possible solutions will be discussed for the minimisation of desorption of photoactive molecules from the oxide surface.

1.1.2. Dye-sensitized Photoelectrosynthesis Cells (DSPECs) for photoinduced water splitting

As implicit in the very definition of photovoltaic solar cells, a DSSC can supply electric energy only in presence of the sunlight. Giving the fact that the sun is an "intermittent" source, in perspective of the ideal total replacement of energy production from fossil fuels, energy storage systems are required in order to provide power at night.[55]

A number of storage schemes have been proposed, or are in use,[56] but the only practical approach at the required scale is "Artificial Photosynthesis" with "solar fuels" as the product.

Solar fuels, according to Bolton definition, are reduced chemical substances produced by endergonic photochemical reaction, which are able to release the stored chemical energy upon reaction with oxygen.[57] Giving that their production would exploit only cheap and easily available "reagents" (i.e. water, CO_2 and sunlight), solar fuels hold great promise as a permanent,

environmentally friendly, long-term and globally-available renewable energy source.

An appealing approach to solar fuels generation by artificial photosynthesis is based on Dye-Sensitized Photoelectrosynthesis Cells (DSPECs) for photoinduced water splitting. These devices mimic the electrodes configuration used in DSSCs, but with a different goal: achieving a photoinduced reaction (rather than the generation of photocurrent), which leads to the production of oxygen and hydrogen, with the latter being a high energy solar fuel.

The configuration of a dye-sensitized photoelectrosynthesis cell is sketched in Figure 7.

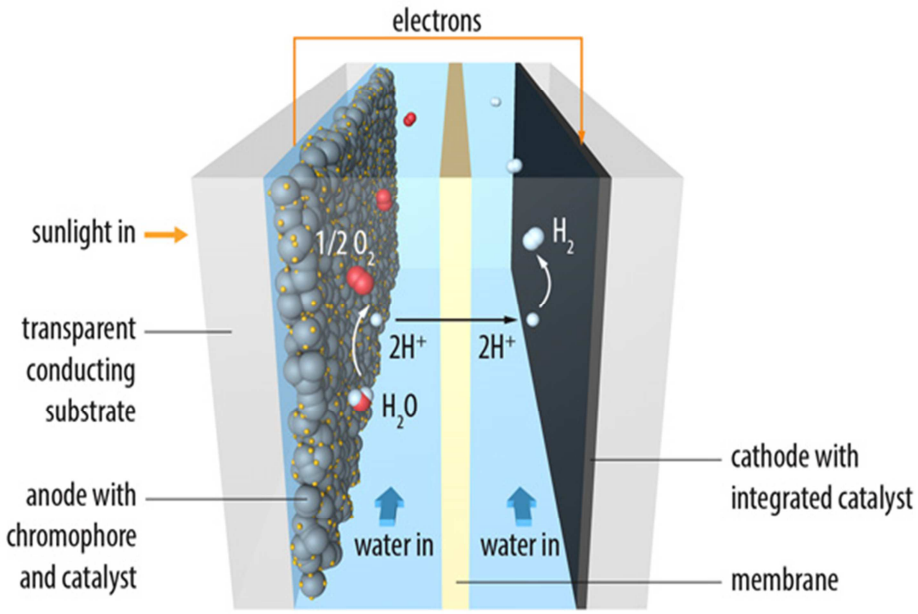

Figure 7: Scheme of a dye-sensitized photoelectrosynthesis cell for photoinduced water splitting (Graphic by Yan Liang, copyright L2Molecule.com).

The design of a DSPEC shares some component with a dye-sensitized solar cell, but also important different features are present. The configuration of these cells consists in the following crucial elements:

1. Photoanode: as in a DSSC, it is constituted by a nanostructured, transparent and semiconducting oxide sensitized with a photoactive molecular system, being able to capture the sunlight;
2. Water Oxidation Catalyst (WOC): it can be a molecular system or an inorganic compounds which uses oxidising equivalents to oxidise water to oxygen gas and H^+ ions; it must be assembled on the photoanode, together with the molecular dye;
3. Reduction Catalyst: it is the counterpart of the WOC, and it uses reducing equivalents to store energy in the form of reduced material (i.e. hydrogen); for photoinduced water splitting usually platinum is used (in the form of cathode), in virtue of its low overpotential (activation energy) and rapid turnover for proton reduction to hydrogen gas.

Water oxidation and H^+ reduction are achieved in two different compartments of the cell, kept separated by a proton exchange membrane (PEM), which allows for the diffusion of H^+ ions and charge balance.

The overall water splitting reaction (equation 3) takes place in virtue of two half reactions (equations 1 and 2):

$$2H_2O \rightarrow O_2 + 4H^+ + 4e^- \quad (1)$$

$$4H^+ + 4e^- \rightarrow 2H_2 \quad (2)$$

$$2H_2O \rightarrow 2H_2 + O_2 \quad (\Delta G^0 = +4{,}92 \text{ eV}) \quad (3)$$

This reaction is quite an energy demanding process: it request at least an input energy corresponding to 1,23 V (vs NHE at pH 0)[58] in order to take place. However, the application of a consistent overpotential is demanded in order to actually carry out the reaction due to the complexity of the process, which involves several intermediates for an overall four electron oxidation *per* molecule of water.
For a proper understanding of how each component of a DSPEC contributes to the overall water splitting process, a scheme of its working mechanism is presented in Figure 8.

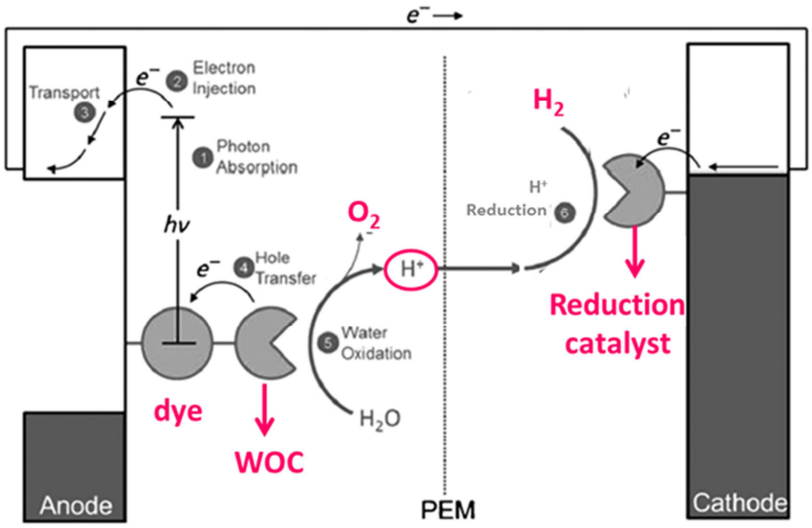

1) Dye + hν → Dye* (photoexcitation)
2) Dye* → $Dye^+ + e_{CB}^-$ (electron injection)
3) $Dye^+ + Cat \rightarrow Dye + Cat^+$ (electron transfer)
4) $4Cat^+ + 2H_2O \rightarrow 4Cat + 4H^+ + O_2$ (hole transfer)

Figure 8: Scheme of the water splitting process occurring in a DSPEC (top, adapted from [59]) and molecular reactions involved (bottom; Cat: water oxidation catalyst).

The process starts with the absorption of a photon from the molecular dye. This step is followed by an electron injection from the photoinduced excited state of the dye to the conduction band of the nanostructured oxide anode, and after the electron is transported to the counter electrode. Subsequently, the fundamental state of the dye is restored by electron transfer from the WOC and the latter uses the oxidising equivalent to oxidise H_2O to oxygen gas and H^+. Finally the generated protons diffuse through the PEM and migrate toward the reduction catalyst-equipped cathode, where they are reduced to hydrogen gas.

The first example of dye-sensitized photoelectrosynthesis cell dates back to 1999, when Meyer and co-workers published preliminary results on hydrogen production using a photoelectrosynthesis cell based on the absorption of a bis-ruthenium polypyridyl complex on nanocrystalline TiO_2 substrate.[60] The Ru-complex employed was actually the dpp-bridged molecular assembly $[(4,4'\text{-}(CO_2H)_2bpy)(4,4'\text{-}Me_2bpy)Ru_a(dpp)Ru_b(tpy)(OH_2)]^{4+}$ (Figure 9), which has $Ru(bpy)_3$-type part bearing two carboxylic units for the anchoring on TiO_2

and a ruthenium monoxo-terpyridyl part, whose structure is analogous to that of well-known redox Ru and Os complexes that show catalytic two-electron oxidation.[61]

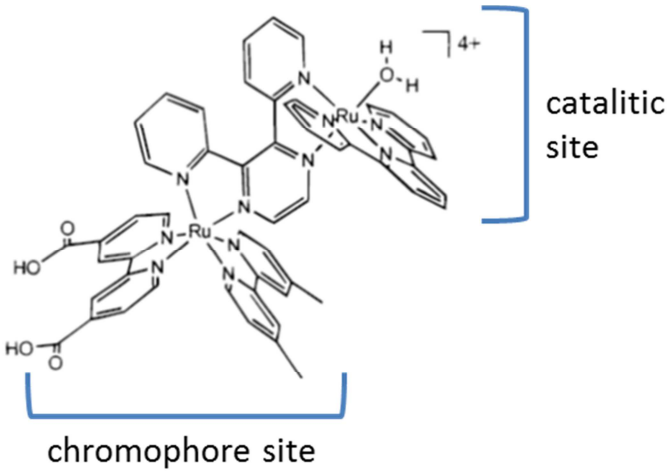

Figure 9: Structure of compound [(4,4'-(CO2H)2bpy)(4,4'-Me2bpy)Ru_a(dpp)Ru_b(tpy)(OH_2)]$^{4+}$. (Adapted from ref. [60])

The authors used a two-compartment cell, one compartment with the sensitized TiO_2 electrode immersed in 2-propanol solution and one containing a Pt counter electrode. Upon irradiation with visible light, production of H_2 was observed, with parallel oxidation of 2-propanol to acetone.

Similarly to the case of DSSCs, many studies on dye-sensitized photoelectrochemical cells have been carried out employing different chromophores, semiconductors oxide and oxidation catalyst, but the "skeleton" of the cell remains almost unchanged.

Ruthenium polypyridyl complexes are still the dyes of election for the photoanode preparation, in virtue of all the favorable photophysical and photochemical properties already mentioned previously (see paragraph 1.1.1.1).

Concerning the water oxidation catalyst, various possibilities have been explored. One of the most notorious example of material that has been used as WOC is given by nanoparticles of semiconductor oxides, most successful being IrO_2 nanoparticles. Due to its low electrochemical overpotential for water oxidation,[62, 63] IrO_2 (nanoparticulate or colloidal) has been widely studied as water oxidation catalyst by itself.[64, 65] In combination with a molecular light absorber such as $Ru(bpy)_3$,[66, 67] oxygen evolution takes place. However, various drawbacks take place as well, the more problematic

being the slow electron transfer from Ir(IV) to oxidised Ru(III), which result in poor catalytic efficiency and low turnover frequencies.[68]

Another class of molecular compounds that can be used for catalytic water splitting includes first-row transition metal complexes, whose chemical structure is tailored for mimicking that of the greatest water oxidation catalyst existing in nature, the oxygen evolving complex (OEC) of Photosystem II (PS II). This OEC is one of the main protein complex responsible for the light-induced oxygenic photosynthesis in plants, trees, algae, etc… Since the discovery of the existence of an Mn_4 cluster (Figure 10a) within the OEC of PSII,[69-71] several bioinspired tetramanganese complexes have been synthesised and tested for water splitting reaction, unfortunately showing poor catalytical activity.[72-74] Beside tetramanganese compounds, solid state cobalt cubane oxoclusters have also given promising results as WOCs, as Nocera and co-workers first reported.[75, 76] Subsequently several studies have been carried out on a particular cobalt cubane, namely $[Co_4(\mu\text{-}O)_4(\mu\text{-}CH_3COO)_4(C_5H_5N)_4]$ (Co_4O_4-H, Figure 10b), using $Ru(bpy)_3$ as photosensitiser.[77-79] The results of photoelectrochemical measurements conducted in buffer solution, using persulfate as sacrificial agent, showed promising photochemical quantum yield for water splitting. However, the overall efficiency of the reaction relies critically on the experimental conditions adopted (e.g. catalyst concentration, pH, influence of the sacrificial agent itself on the catalytic activity, photoinduced degradation of the sensitiser ,…), and furthermore self-oxidation of the organic ligand on the WOC contribute as well to the poor durability of the catalytic system over the time.[80]

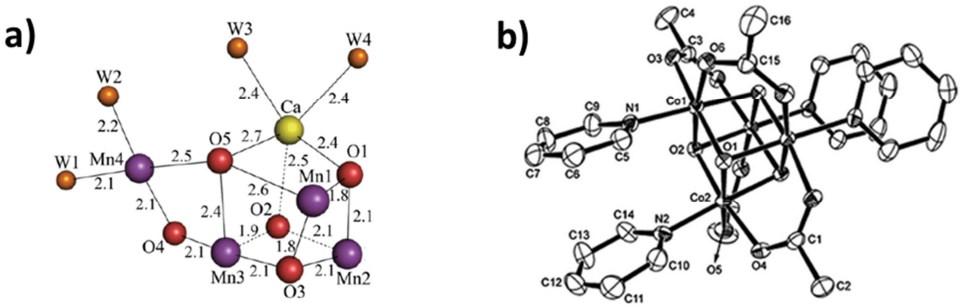

Figure 10: X-ray structures of a) $Mn4CaO_5$ cluster in PS II (reprinted with permission from ref. [81], copyright 2011 Nature Publishing Group) and b) cubane Co_4O_4-H (reprinted with permission from ref. [77], copyright 2007 American Chemical Society).

The issue of catalyst self-oxidation is overcome in the case of another class of molecular systems showing water splitting catalytic activity, namely polyoxometalates compounds (POMs). POMs are totally inorganic, polyanionic oxo-clusters of early transition metals (V, Mo, W, Nb, Ta) bound to a variety of other metals *via* oxo-bridges. The transition metals of POMs are normally in their highest oxidation state, and this is the reason of their great stability in strong oxidising conditions.[82] Among the various POMs tested for their perspective utilisation as WOCs, the $[Ru_4(\mu\text{-}O)_4(\mu\text{-}OH)_2(H_2O)_4(\gamma\text{-}SiW_{10}O_{36})_2]^{10-}$ (Ru_4POM) emerged as one of the most promising catalyst for water splitting.[83, 84] Its structure is reported in Figure 11. The photodriven water splitting activity tested in solution[83, 85] produced very promising overall performances, with high turnover numbers (up to 500) and turnover frequencies of ~ 0,60 s^{-1}, and a 100 times increment in reaction rate with respect to the experiment carried out without Ru_4POM. A reaction mechanism was proposed for the role of Ru_4POM in water splitting, in a system containing $Ru(bpy)_3$ as photosensitizer and persulfate as sacrificial agent (see Figure 12 for reaction scheme):[85] four photoexcited $Ru(II)(bpy)_3$* give electron-transfer reaction towards persulfate anions (which are reduced to sulfate), and the resulting four $Ru(III)(bpy)_3$ are then reduced by the Ru_4POM, the latter taking this four electrons from the oxidation of water. In later works by Orlandi and Toma [86, 87] Ru_4POM has also been studied as photocatalyst in heterogeneous phase, and it was demonstrated that its "oxygenic" activity is maintained in solid-state electrodes.

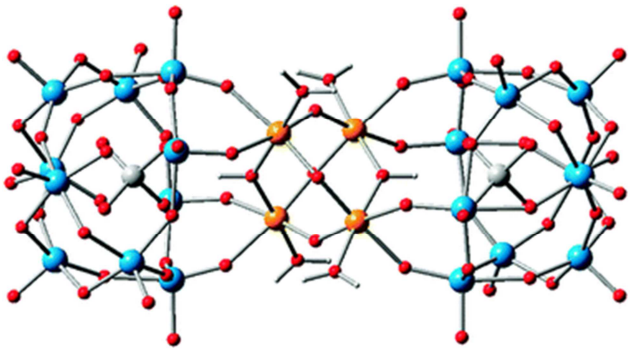

Figure 11: Structure of Ru_4POM (red: oxygen; grey: silicon; orange: ruthenium; light blue: tungsten). Reprinted with permission from ref.[80], copyright 2012 The Royal Society of Chemistry.

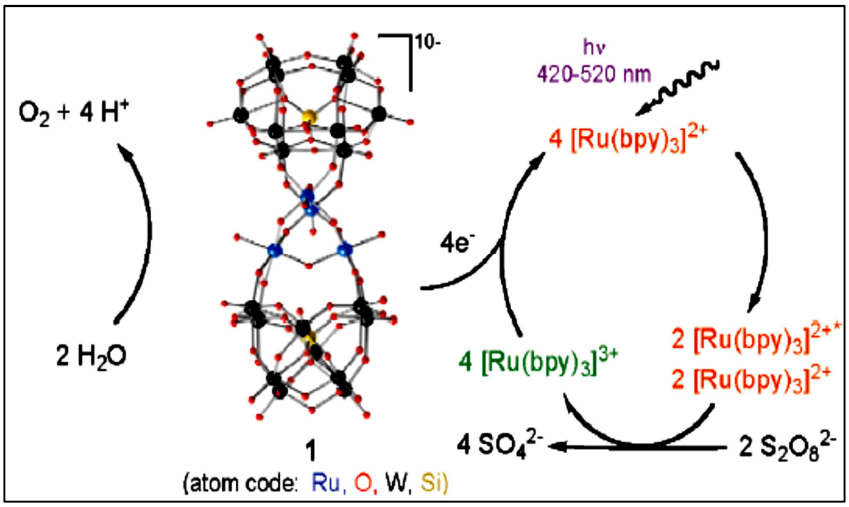

Figure 12: Reaction mechanism for photoinduced water splitting in solution, using Ru_4POM as catalyser, $Ru(bpy)_3$ as sensitiser and persulfate as sacrificial agent. Reprinted with permission from ref. [85], copyright 2009 American Chemical Society.

It must be underlined that the perfect match of photosensitiser and water oxidation catalyst that one can test in a "solution benchmark" has to be always studied as well in heterogeneous phase (i.e. on a solid electrode), given that the ultimate purpose is the development of a solid-state solar device. The transfer of all the above mentioned molecular components on a solid surface is not a trivial matter, because the molecular anchoring of dye and WOC at the surface must be carried in a way thatensures good "communication" between each component and functionality of the electrode and, at the same time, ensures long term durability of the cell.

As for DSSCs, nanostructured titanium dioxide in anatase phase has been the first-choice substrate for the realisation of electrodes for dye-sensitized photoelectrochemical cells. However, despite its unquestionable success as photoanode in DSSCs, other type of semiconductor electrodes are currently being explored for applications in DSPECs, mostly because the electronic structure of TiO_2 does not fit perfectly the ideal energetic requirements necessary for H_2 production from water splitting.

1.1.2.1. SnO_2 as alternative photoanode material for DSPECs

Nanostructured SnO_2 electrodes are recurring candidates for the replacement of TiO_2 electrodes. Tin dioxide is a n-type and wide band gap (~ 3.8 eV) semiconductor[29]. With respect to titanium dioxide, the conduction band of SnO_2 is more positive (about +0.5 V), and this makes tin oxide a better electron acceptor.[30] A comparative scheme for the electronic structure of TiO_2 and SnO_2 is presented in Figure 13, with respect to the redox potential of H_2O and CO_2 (the "fuels" for a DSPEC).

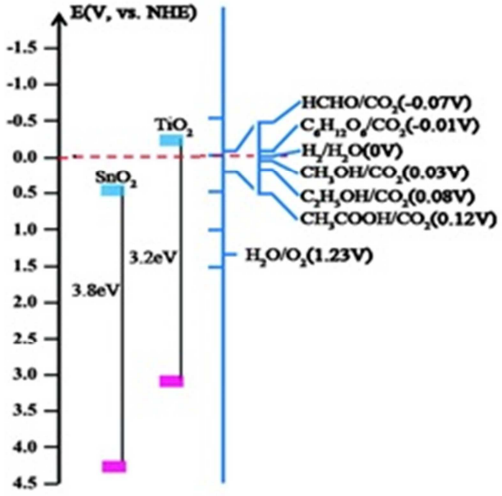

Figure 13: Electronic levels diagram comparing TiO_2 and SnO_2.(Adapted from ref. [88])

Tin dioxide substrates have been largely studied for applications in DSSCs[29-31, 89, 90], and the above mentioned energetic characteristic make it appealing also for application in realisation of DSPECs photoanodes. However, several drawbacks need to be overcome when using SnO_2 photoelectrodes. The most critical one is the significant slow regeneration of the dye by reaction with the electrolyte, caused by the competitive back-electron transfer reaction from the oxide to the redox electrolyte, whose rate is about three orders of magnitude faster than in the case of TiO_2[91]. This is probably caused by the presence of low-energy surface trap states on SnO_2 [92]. A widely exploited approach to limit this unwanted recombination phenomena is that of coating the nanostructured oxide electrode with a thin layer of high bandgap oxide, in

order to passivate it and lower (ideally block) the rate of undesired electron interception. Significant enhancement of the cell performances have been reported for dye-sensitized solar cells where the photoanode was covered with a layer of passivating-oxides such as Al_2O_3 (Figure 14)[93] or MgO[94]. Very satisfying results were obtained also for DSPECs with SnO_2 photoanodes[95] covered with Al_2O_3 and TiO_2 passivation oxides, deposited by ALD technique.

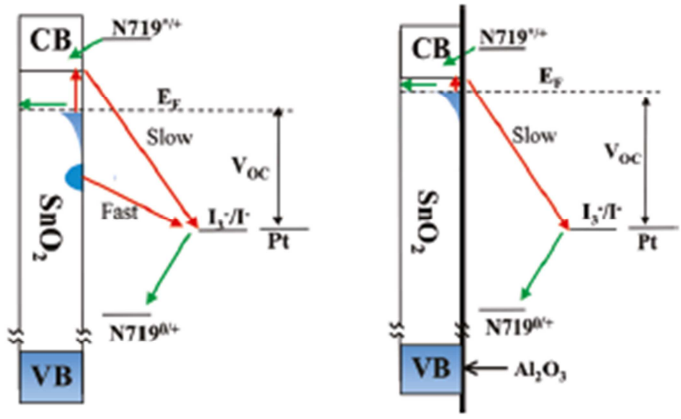

Figure 14: Proposed diagram for electron recombination phenomena in a DSSC with N719-sensitized SnO_2 photoanode without (left) and with (right) Al_2O_3 passivation layer. Reprinted with permission from ref. [93], copyright 2010 American Chemical Society.

1.1.3. Current challenges of Dye-sensitized Cells

In dye-sensitized devices for solar energy conversion (both DSPECs and DSSCs) molecular systems play the most important roles and account for most of the cell work, because they absorb light, transfer electrons and provide the sites for catalysis.[55]

The major role played by molecules in the light-to-electric energy conversion and in the water splitting process is a big point in favour of dye-sensitized devices, because the current chemists' abilities to synthesise molecular dyes and catalyst having specific optical properties and specific electronic structure allow for targeted modifications and improvements of the cell design and functionality. At the same time, however, the predominance of molecular reactions comes out with several drawbacks. Interfacial and intramolecular electron transfer dynamics are the most important factors to cite, because they

rely on the electronic structure of the employed molecules and determine the actual cell performances.

A scheme of the processes occurring at the interface of a dye-sensitized device (valid for both DSSC photoanode and DSPEC one) is presented in Figure 15.[96] In the normal operating conditions of a dye-sensitized cell, besides the molecular reactions that allows for the solar energy conversion (i.e. charge injection to the oxide conduction band from the excited state of the dye(1), electron collection at the electrode (2) and dye regeneration (3)), several competitive reactions take place, namely luminescence/non-radiative decay (4), electron recombination (5) and electron interception (6).

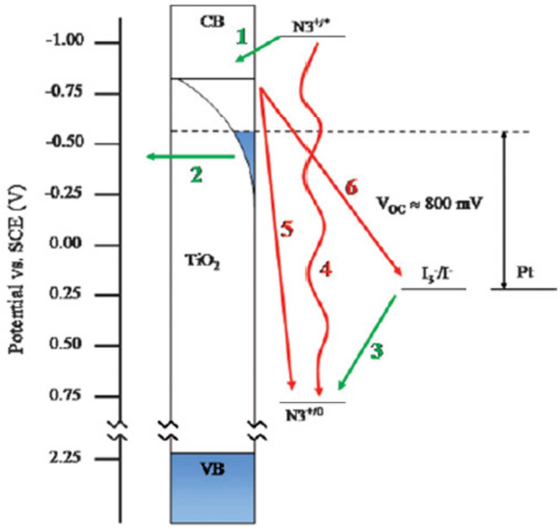

Figure 15: approximate energy diagram of a dye sensitized cell. Reprinted with permission from ref. [96], copyright 2008 The Royal Society of Chemistry.

The key for improving the solar cell performances is that of designing every single component as well as their "combination" in order to minimise reactions 4, 5 and 6 (i.e., ideally, they should be suppressed, or at least must happen in timescales much longer of those of the other desired reactions). Reaction 4 (luminescence/non-radiative decay) relies on the electronic structure, so in its respect the choice of the photoactive system must be done very carefully. On the other hand, reactions 5 and 6 (recombination and interception respectively) take place because of a "back-electron transfer" pathway between either the dye molecule or the redox electrolyte (or both of them). A possible strategy to minimise these reactions relies on the nanostructured electrode passivation,

which implies the realisation of an “interruption of communication” between the electrode and the “outside environment”. This approach, developed by covering the surface with a large bandgap insulating material has been broadly investigated, with good results and great improvement of the cell performances.[91, 97-99]

Another crucial point concerns the chemical linkage of the molecular dye/catalyst on the nanostructured oxide electrode, which should be strong enough to provide long term stability of the molecular binding and must be suitable for providing good “electronic communication” between chromophore/catalyst and the photoanode. Unfortunately, in the normal operating condition of DSSCs and DSPECs, dye-desorption phenomena occur, causing photoanode degradation and, as a consequence, severe cell efficiency losses.

Current research is exploring several approaches for minimising photoanodes degradation phenomena, the most promising being i) the use of co-adsorbed amphiphilic sensitizer and long alkyl-chain phosphonic acids,[100] and ii) chromophore binding stabilization *via* post-sensitizazion deposition of ALD coatings.[101, 102]

Another possible approach to enhance the stability of the dye-substrate linkage consists in creating an anchoring platform between the oxide surface and the photoactive molecular system. In our research group we developed a methodology that permits to create such platform on oxide surfaces, based on zirconium phosphate-phosphonate chemistry, and we refer to it as *ZP-priming*.[103, 104] This surface treatment method is based on the well-known chemical stability and robustness of ZP solids, and it consists in a stepwise procedure that leads to the deposition of a zirconium phosphate monolayer at the oxide surface, which can act as an actual anchoring platform for molecular systems bearing a phosphonic functional group. In the next paragraphs a more detailed description will be presented of zirconium phosphate-phosphonate systems and their use in surface modification.

1.2. Nanoscale molecular electronics

During the last decades the miniaturisation trend of silicon-based electronics predicted by the Moore's law[105] had to face the technological limits of its practical accomplishment. The main limitation consists in the "top-down" approach, which exploits preparation techniques, such as photolithography, for the realisation of patterned circuits. These approaches allow for a minimum lateral dimension in the order of hundreds of nanometres, due to the limits imposed by the wavelength of light (the magnitude needed to be in agreement with the prediction of Moore's law should be towards the nanometre scale). Among the most valuable approaches to obtain a system of a few nanometres size, the "bottom-up" approach has the merits that it is based on the use of functional molecules as "building blocks", which are assembled together in larger arrays. The creation of functional circuits starting from single molecular component is referred to as "molecular-scale electronics", and its relevance is not limited to the fulfilment of the technological needs for traditional electronic devices miniaturisation, but it also provides a precious platform for studying the properties of materials at the nanoscale level.

Presently, the realisation of practically useful molecular electronic devices relies critically on the preparation techniques used to bind and assemble the functional molecules on the solid supports. Already in 1959 the physicist Richard Feynman foresaw the possibility of preparing extremely small electronic devices, during the ever since famous lecture entitled "*There's plenty of room at the bottom"*;[106] however at that time the scientific knowledge was not yet ready to bring this visionary idea to life. But more than 10 years later the first proofs of the feasibility of Feyman's idea started to show up. In this framework, between the 70's and 80's the pioneering work of Kuhn, Mann, Sagiv and Polymeropoulos provided the earliest data about charge transport through molecular systems.[107, 108] The measurements were carried-out on thin films of saturated, long-chain fatty acids deposited on the substrate with the first effective self-assembly technique, where the molecular systems were chemically bound onto the substrate surface through molecular bond formation, and not simply by physisorption *via* dispersion forces. This achievement subsequently opened the way to the development of molecular surface modification via Self-assembled Monolayer (SAM) technique.

The possibility of chemically binding, and so integrating, functional molecules on solid surfaces, spontaneously and in ordered structures, significantly promoted the studies on molecular electronics, leading to a widespread interest in the use of single molecules as components for the construction of functional circuits.

It also provided a powerful driving force for the development of experimental platforms capable of characterising the surface properties and probing electric physical phenomena (such as charge transport) at the molecular level.
The concept of using single molecules as functional electronic components implies that an electrical signal must pass in and out of the molecule, via contact-coupled electrodes; so in order to actually measure the electrical characteristics of the system, a molecular junction needs to be build, i.e. a contact between the single molecule and a second electrode must be realised.

Several techniques are available for obtaining a molecular junction, but all of them have in common the same "basic" structure, given by the configuration metal-molecule-metal (sometimes indicated also as metal-insulator-metal). One of the milestones in this framework has come with the advent of Scanning Tunnelling Microscopy (STM) technique,[109] which gave the possibility to investigate both topography and electrical properties of the surfaces of molecular materials at the single-molecule level; other techniques include mechanically controllable break junctions (MCBJs),[110-112] electromigration breakdown[113, 114] and electrochemical deposition junctions.[115, 116]

It should be pointed out that, from an experimental point of view, the realisation of single-molecule junction is technologically challenging and not easy to implement in large-scale production systems, thus limiting the practical applicability in real devices.[8] On the other hand, more robust and easier to prepare systems are those made by ordered (self)assemblies of a large number of functional molecules packed between two electrodes to allow for large-area electric measurement, the so called ensemble molecular junctions.[117] Among the systems most widely exploited for the fabrication of these kind of junction, self-assembled monolayers (SAMs) play a major role, due to their thermodynamic stability and easy-processing method (Figure 16). The simple immersion of the substrate in a solution of a suitable molecule (bearing a head-group able to chemically anchor onto the substrate) can lead to the formation of highly ordered and densely packed molecular thin films at the material surface (for a review on this topic see reference [118]).

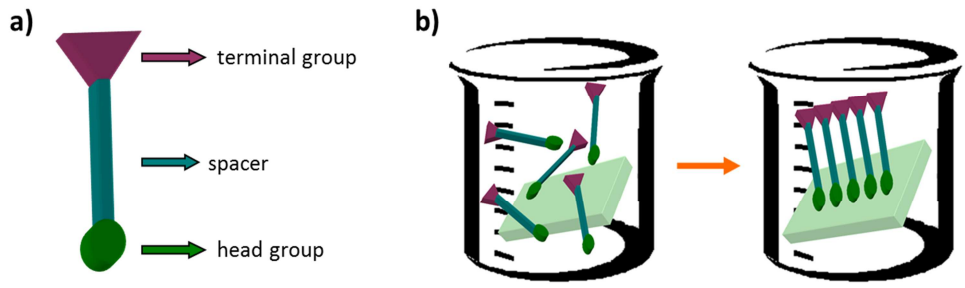

Figure 16: Schematic diagram of SAMs preparation; a) schematic representation of molecular structure needed for SAM formation; b) immersion of the substrate in SAM-forming molecules solution, leading to ordered SAM film at the surface.

By means of ensemble molecular junctions, the electrical behaviour of several molecules has been studied, such as simple alkyl hydrocarbons as well as conjugated molecules.[119-122] An interesting case of study, which has given promising results for future practical applications, is given by conductive molecular wires (the wording being similar to that of more "classic" conductive wires of domestic electric systems). This term designate a large variety of 1D molecular systems of nanometric size (5-100 nm), usually built by (self)assembly of organic conjugated molecules, chemically bound to the surface of a conductive substrate (e.g. metals, oxides, …), which acts as electrode. By similarity with macroscopic electrical conductive wires, the concept of molecular wires is based on intramolecular electron transfer, and the current flow through the junction, where molecular wires connect the electrodes, depends on the energy gap between the Fermi levels of the electrodes and the frontier energy levels of the molecules within the wire (usually HOMO or LUMO).[123] The first studies on conductive molecular wires in second half of the nineties identified polyphenylene-based chains and carbon nanotubes as potential backbones for current-carrying molecular electronics,[124] and molecular wires of the two classes were intensively studied from both theoretical and experimental point of view.[110, 112, 125-130] Particular focus has been given later to polyphenylene-based wires; because of their small size (with respect to carbon nanotubes), they have high current densities which, combined with the well-established knowledge of their chemistry and synthetic flexibility, create a perfect match between "electrical" functionality and ease of preparation.[124] Given the above mentioned

favourable conditions, a large number of studies were carried out and prototypical nanoscale electronic components such as molecular rectifiers and switches were realised, whose two examples, resulting from the word of Zhou[112] and Ellenbogen,[124] are presented in Figure 17.

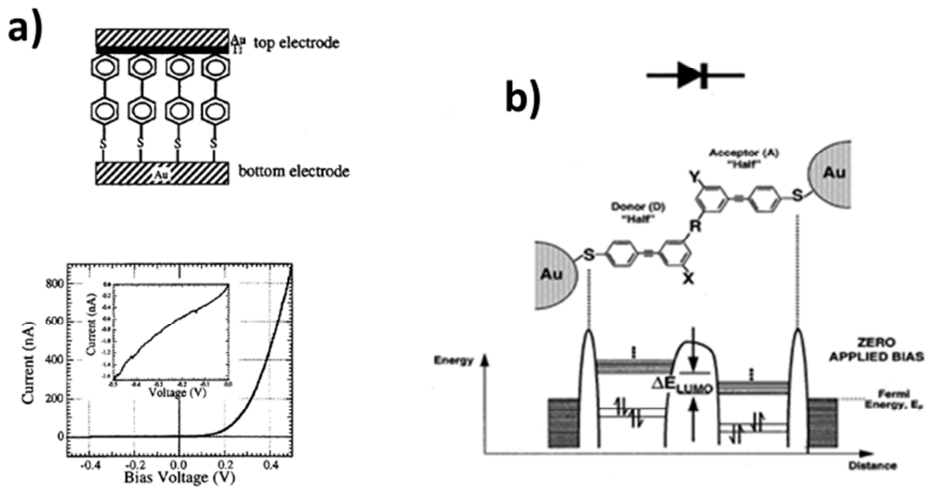

Figure 17: a) Molecular rectification demonstrated by Zhou et al.; b) Polyphenylene-based molecular rectifying diode switch, with scheme of predicted electron orbital energy levels. (Adapted from ref.[124]).

In order to improve the current flow through molecular wires, a well-known approach consists in the incorporation of redox-active sites within the organic backbone,[131, 132] especially metallic centres. As demonstrated by several studies,[133-136] in a (poly)metallic complex based wire the presence of metal redox sites provides low-lying, easy-to-reach, energy states, which promote the electron transfer rate through the wire.

The synthetic strategies used to assemble a polymetallic molecular wire can be roughly divided in two main approaches:

1- classic strategy: the redox-active complex is obtained by "classic" complexation reaction between the metal and a bridging ligand;

2- building-block strategy: metallic complexes are pre-synthesised and used as building-blocks for subsequently assembly of the wire.

An improvement of charge transport through the molecular wire can also be achieved by adding along the organic skeleton some photoactive centres, which upon irradiation undergo light-induced excitation; with the appropriate molecular systems, charge dissociation could follow photoexcitation, with subsequent photocurrent generation.[137-143] To this aim, many transition metal complexes are perfect candidates, because they can provide both a redox-centre, for charge transport improvement, and light-induced activity.[144-146] Among the most exploited coordinating ligands for those metal complexes, neutral sites of basic di- and trigonal nitrogen are often the preferred choice;[147] metal complexes with ligands such as bipyridine or terpyridine show exceptional rich electron-transfer chemistry, which makes them systems of election for application and studies on molecular-scale charge transport.[148]

The coupling between current flow and photo-responsivity eventually leads to photoactive conductive molecular wires, which - once integrated on suitable surfaces - can be used for the preparation of nanometric solid state photoresponsive molecular junctions,[18] consisting in a thin film of light-sensitive molecules densely packed between two electrodes. This molecular layer, “encrusted” with photoactive centres, is sensitive to light-induced excitation, which leads to charge dissociation and subsequent collection at the electrodes, making this system suitable for working as optoelectronic switch or optically responsive memory, or in electric current production from solar energy conversion. Very good candidates as convenient substrates for a winning match between molecular and surface properties are transparent conductive oxides (TCOs): the transparency in the visible range, coupled with their electrical conductivity (and also the relative cheaper manufacturing costs, with respect to noble metal substrates) make these oxides “active” substrates more than just a “solid support” for the assembly of functional molecules.

1.2.1. Charge transport mechanism in molecular systems

The charge transport mechanism of a molecular wire can be understood looking at the dependence between its electrical resistance and its length. It is well known that, if the wire is short enough, electrons can tunnel between the two electrodes; while in the case of longer wires electrons are transported thanks to a hopping mechanism.[149]
If a tunnelling mechanism occurs, electrons traverse a potential barrier and propagate on the other side without changing their phase. The tunnelling mechanism is often ‘‘non-resonant’’ in that the tunnelling electron energies are not precisely matched with the molecular orbital energies; however, the frontier molecular orbitals still assist the tunnelling process (i.e., they lower the junction resistance) by lowering the effective tunnelling barrier (Figure 18).[150]

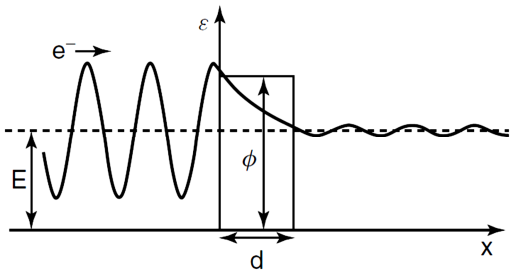

Figure 18. Transmission of electron wavefunction through a potential barrier. Reprinted with permission from ref. [151], copyright 2011 Wiley-VCH Verlag GmbH & Co. KGaA.

This kind of mechanism is usually described according to the Simmons model for tunnelling through a barrier of arbitrary shape;[152] normally, a simplified version of the Simmons equation is used, where the current density J (A/cm^2) that flows across the molecular system is described as:

$$J = J_0 e^{-\beta d}$$

where J_0 (A/cm^2) is a constant, d (Å) is the width of the tunnelling barrier (corresponding to the thickness of the organic layer) and β (Å^{-1}) is a a structure dependent attenuation factor, which value depends on the molecular system investigated. Efficient tunnelling is characterized by low values of β, in the range of 0.2-0.5 Å^{-1} in the case of delocalized π electrons[153, 154] and between 0.8 and 1.2 Å^{-1} in the case of saturated chains.[155, 156]

In conjugated molecular wires longer then few nanometres tunnelling mechanism cannot occur; the charge conduction occurs through a series of discrete steps, involving an initial charge injection in the molecular orbitals of wire, the field-induced drift of the charge carrier down the length of the molecule, and finally the extraction of the charge into the receiving contact (Figure 19).

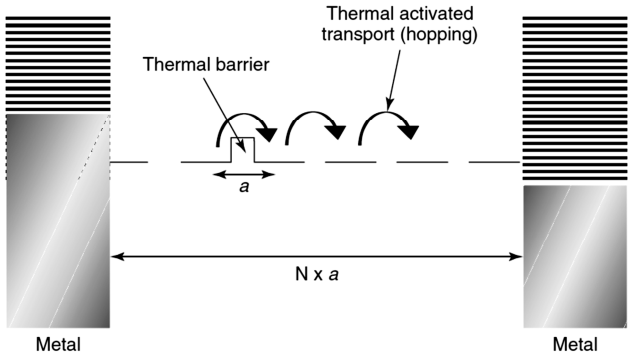

Figure 19. Schematic energy diagram for incoherent hopping through N sites. Reprinted with permission from ref. [151], copyright 2011 Wiley-VCH Verlag GmbH & Co. KGaA.

The hopping mechanism is thermally activated and can be described using an equation that follows a classical Arrhenius behaviour:

$$R=R_0 \exp(E_a/kT)$$

in which R is the system resistance, R_0 is the effective contact resistance, E_a is an activation energy and k is the Boltzmann constant. In tunnelling regime, as said before, there is an exponential dependence between R and molecular length; in case of hopping mechanism on the contrary there is a linear correlation in the low bias regime, and this different behaviour allows a charge transport over longer distances.

Through J/V measurements combined with temperature- and molecular length-variable measurements, in addition to tunnelling and hopping, various other classic conduction mechanism were identified which determinate the charge transport in molecular systems, such as field emission (or Fowler-Norheim tunnelling), space-charge limited conduction (SCLC), thermionic emission (or Schottky emission), and Poole-Frenkel effect.[117, 149] Often, the transition

from a certain conduction regimes to another occurs as a consequence of varying bias, electrical field or molecular length.
From the above considerations and discussion it is clear that electron conduction mechanism depends on several factors including electronic structure, molecular length, temperature, applied bias. For these reasons, a deep understanding of the electrical behaviour of a molecular junction involves both experimental and theoretical studies.

1.2.2. Polypyridine-based metal complexes

Polypyridines form a large class of multidentate N-heteroaromatic ligands which show various interesting properties. Some examples of most notorious and employed polypyridine ligands are presented in Figure 20. Notably, they form extremely chemically stable compounds, which can withstand thermal and electrical stresses and are also stable towards photodegradation. Metal complexes with polypyridinic systems are even more interesting, because they put together the stability of polypyridines with the chemical, optical, magnetic and electrical properties of the metal centre, creating a new molecular system which exhibits peculiar electro-, redox- and photochemistry. The properties of the new complex can be tailored by appropriate choice of metal centre and organic substituents of the polypiridinic ligand.

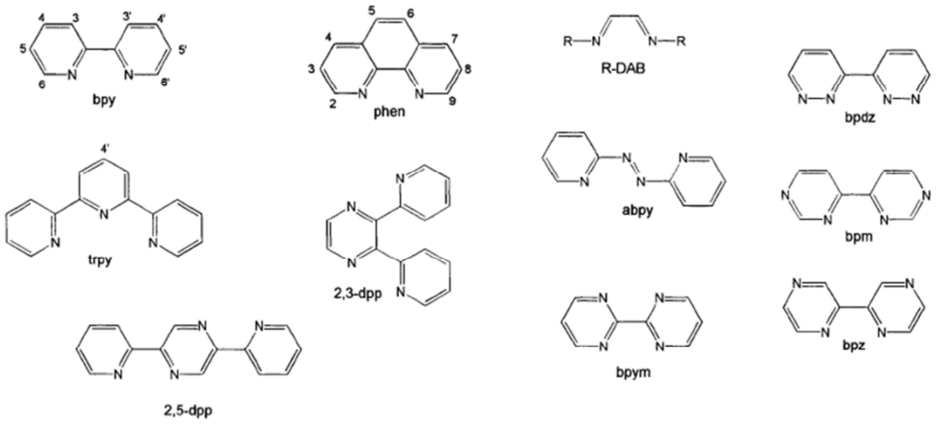

Figure 20: Chemical structure of ligands most employed for polypyridine metal-complexes synthesis.

The importance of these complexes has been demonstrated also within the field of supramolecular chemistry, where metal-polypyridine units are widely used as building blocks for the preparation of supramolecular macrocyclic architectures, [157, 158] oligonuclear metal complexes and metallo-dendrimers,[159, 160] as well as coordination polymers.[161-163] Because of their physico-chemical properties and structural characteristics, particular interesting complexes are those prepared by metal complexation of terpyridinic systems, in particular 2,2';6,6'-terpyridine (tpy) derivatives. These are tridentate ligands which complex a large number of transition metal ions with great binding constants, forming stereospecific assemblies with mostly octahedral symmetry (Figure 21). Terpyridine was isolated for the first time in 1932 by Morgan and Burstall, from a mixture resulted from dehydrogenation of pyridine by anhydrous ferric chloride.[164] Few years later the same authors presented proofs of terpyridine complexes formation with various metal ions, first of them being the purple-coloured $Fe(tpy)_2$.[165, 166]

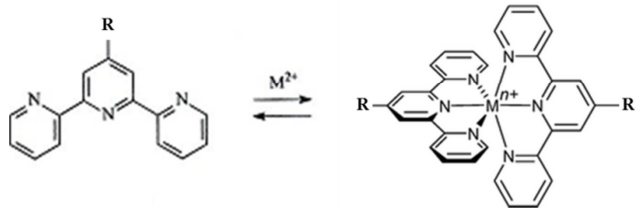

Figure 21: General scheme for metallo-terpyridine complexation, leading to $M(tpy)_2$ complex.

The combination of functional and structural properties of metal-tpy complexes has triggered a large number of research studies about their possible application in various areas.

Metal-terpyridine complexes of the class $Ru(tpy)_2$ were investigated with satisfactory results in the research groups of Krebs for applications in dye-sensitised solar cells and all-polymer photovoltaic cells. In particular, they used the $Ru(tpy)_2$ as both structural and functional component in the solar cell electrodes; in one case[167] they used the terpyridine complex as bridge between PPV-type donor polymer and PPV-type acceptor, (Figure 22) while in the other[168] the $Ru(tpy)_2$ unit carried a surface anchoring group on one side

and the light-harvesting polytiophene-type polymer on the other, acting finally as charge-injection centre towards the cell's electrode surface (Figure 23).

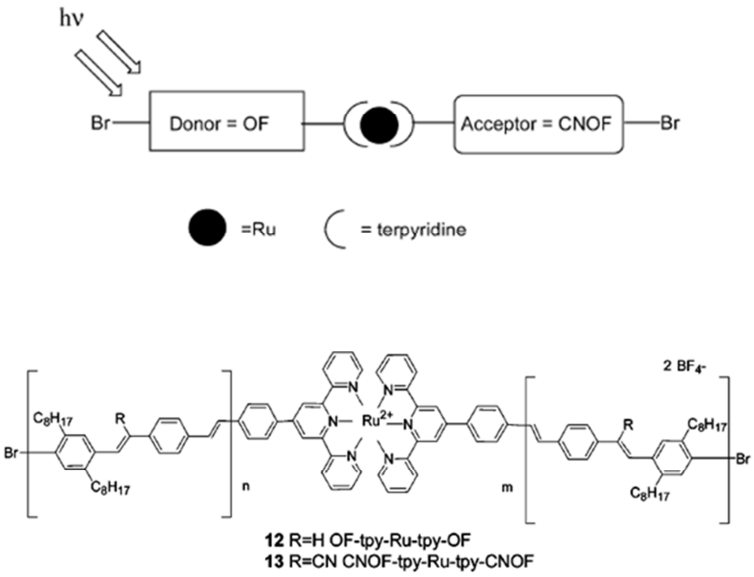

Figure 22: Donor-acceptor PPV chains bridged by Ru(tpy)$_2$ complex. Reprinted with permission from [167], copyright 2005 American Chemical Society.

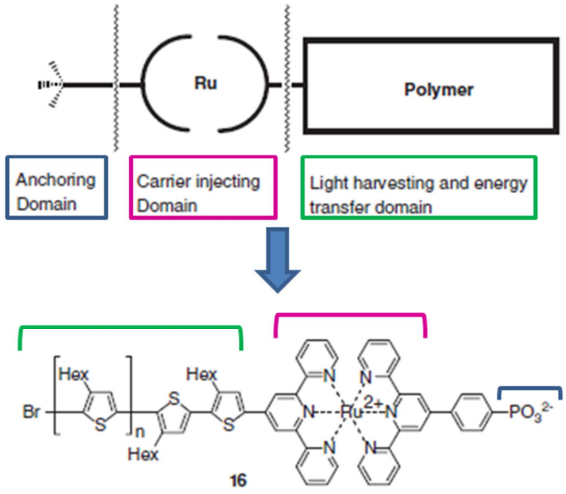

Figure 23: Light-harvesting polytiophene-type polymer functionalised with surface anchoring group *via* Ru(tpy)$_2$ complexation. (Adapted from ref. [168])

Higuchi et al. prepared a series of bimetallo-supramolecular terpyridinic polymers showing electrochromic behavior.[169] The polymers were synthesised by stepwise coordination of Fe(II) and Ru(II), in different molar ratios, with a bis-terpyridyl benzene ligand. The electrochemical properties were studied and the multi-colour electrochromic effect (Figure 24) analysed with respect to redox potential of the metal ion, stoichiometric ratio between Fe(II) and Ru(II) as well as applied voltage.

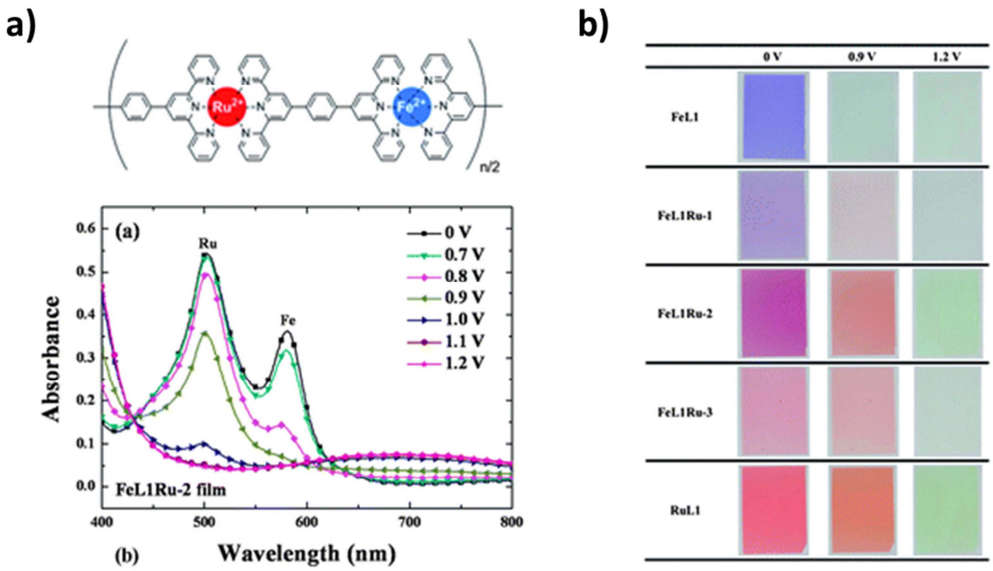

Figure 24: a) in-situ UV-Vis spectra at different applied voltage for compound FeL1Ru-2; b) colour switching at different applied voltages for FeL1Ru-x compounds (x: 0÷3, index of growing Ru-to-Fe ratio). Reprinted with permission from ref. [169], copyright 2013 The Royal Society of Chemistry.

Metal-terpyridine complexes have also been studied in the context of biomolecules immobilisation on solid substrates and sensing. In two different papers, Licciardello and coworkers presented the application of terpyridine-functionalised gold surfaces for DNA-strands recognition [170] and patterned adsorption of proteins (Figure 25).[171] In both cases, the surface functionalisation with terpyridine moieties was achieved by chemisorption of mercapto-phenyl terpyridine (MPTP) and mercapto-benzene (MB) on gold, leading to an ordered SAM of MB-MPTP in 1:1 ratio.[172, 173]

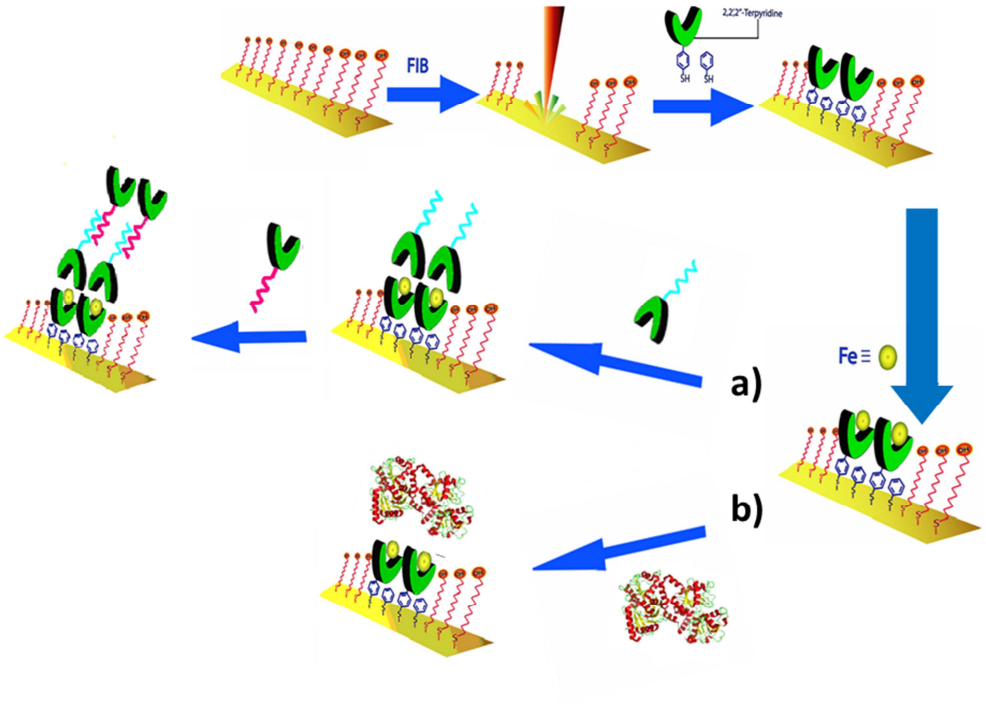

Figure 25: Preparation steps and application of patterned terpyridine-functionalised gold surfaces for a) DNA-strands recognition and b) spatially resolved lactoferrin absorption. (Adapted from refs. [170, 171]).

In the field of nanoscale molecular electronics, among the possible metallic redox-centre that form terpyridinic complexes, ruthenium(II) has become one of the most famous for several different reasons. Its complexes are kinetically stable and inert(characteristic required to avoid ligand scrambling), most of them of pseudo-octahedral geometry, achiral and highly symmetric with frontier orbitals involved in the redox processes essentially of non-bonding t_{2g} type.[147] In this respect, Ru-tpy units are excellent candidates for metallo-supramolecular architecture construction, especially linear arrays such as metallo-polymer chains or molecular wires. Furthermore, the assembly of oligonuclear Ru-tpy complex with organic conjugated units as spacers between Ru(tpy)2 cores has been demonstrated to improve the photophysical and photochemical properties with respect to mononuclear $Ru(tpy)_2$,[174] and the choice of a suitable spacer guarantees the electrical communication between the metal centres even for long linear wires.

The electrical behavior and the photoactivity of Ru-tpy complexes (with its consequent rich physico-chemistry) and their natural attitude for 1D-linear structures assembly,[175] make ruthenium-based terpyridine systems perfect candidates for the construction of solid-state conductive and photoresponsive molecular wires and molecular junctions, with a variety of possible application in light harvesting, solar energy conversion, artificial photosynthesis, as well as in catalysis and biomedical field.

1.2.3. Liquid metal junctions in molecular electronics

As previously mentioned, ensemble molecular junctions (i.e. junctions obtained by using an "ensemble" of molecules rather than single-molecule contacts) are in some extent more advisable with respect to single-molecule ones, mainly because of easier fabrication requirements and possibility of large-area systems preparation. One of the crucial point in making ensemble molecular junctions remains the realisation of the contact with a second electrode, which must be placed over the molecular film adsorbed on a metal or semiconductor substrate. Currently the experimental approaches for the realisation of the electrical contact with the second electrode are essentially three:[117]

1) direct deposition of a metal electrode by electron beam evaporation, thermal evaporation or electrochemical routes;
2) incorporation of conductive materials (polymers, nanomaterials, …), acting as an electrode;
3) use of liquid metals as electrodes.

Approaches 1) and 2) might bring some drawbacks, like mechanical or chemical degradation of the organic film, because of unwanted side reactions occurring in the experimental conditions required for the electrode deposition (metal atom penetration within the organic film, mechanical damage, thermal degradation, …). The use of liquid metals as electrodes overcomes those problems, giving the easy experimental set-up which requires no special facilities or harsh chemical reactions.

The very first use of liquid metal electrodes to prepare a molecular junction was introduced by Reynolds et al.[176] They measured the electrical behaviour of multilayer molecular films of barium stearate deposited on chromium

surfaces, by realising a molecular junction were the second electrode was a drop of mercury (Hg-drop) which was suspended above the sample and lowered with a micrometric screw to achieve the contact with the organic multilayers. Actually several liquid metals were tested, but mercury was found to be the most satisfactory in terms of junction stability and low resistance. Since that first utilisation, this Hg-drop method has been improved and refined, notably by the research group of Whitesides [177-179] and Majda,[119, 180] but nevertheless the basic principles and experimental approach remains almost unaltered. In Figure 26 a picture of an actual contact between Hg-drop and substrate is presented (right), as well as a representative sketch of the molecular junction of the kind Hg-SAM/SAM-Ag surface (left), studied by Whitesides and coworkers.[177]

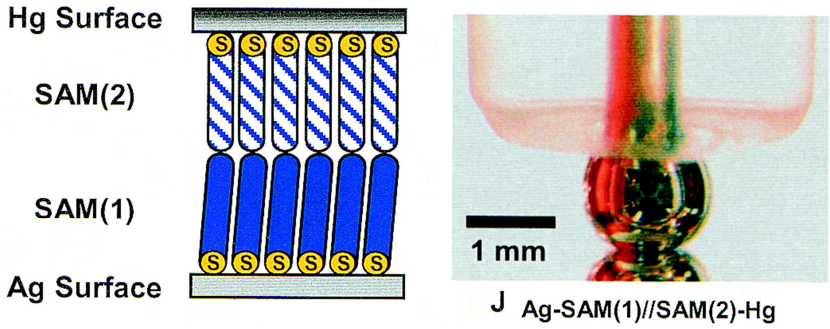

Figure 26: schematic illustration of Hg-molecule-Ag electrode junction (left), and picture of Hg-drop in contact with the substrate surface. Reprinted with permission from ref. [177], copyright 2002 American Chemical Society.

Other studies employing Hg-drop junctions include the investigation of charge-transport through molecular wires. Tuccitto et al. presented the investigation of the electrical properties of metal-centre molecular wires, assembled *in situ* on gold surfaces.[181] Molecular wires were grown *via* stepwise coordination of phenylene bis-terpyridine with either Fe(II) or Co(II), and electric characteristics were measured with Hg-drop electrodes (Figure 27).

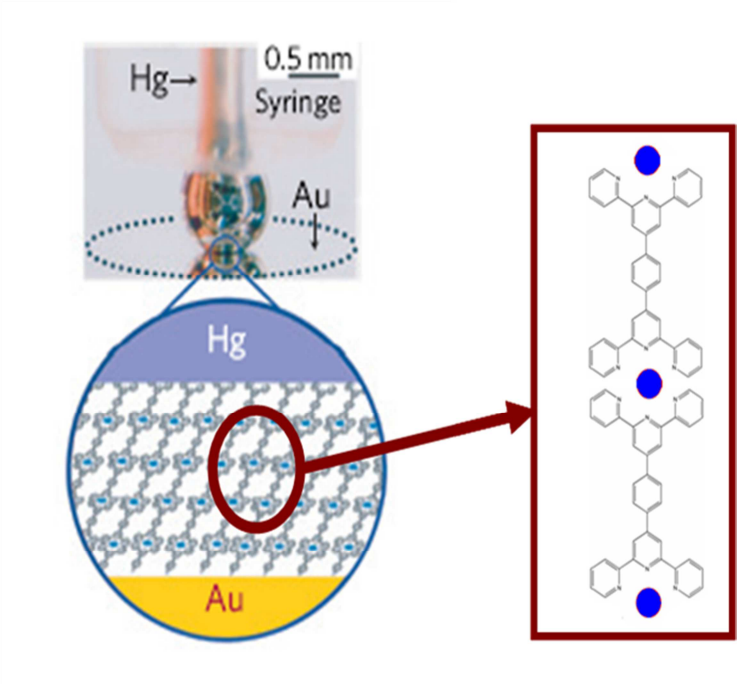

Figure 27: Metal-bisterpyridine molecular wires growth on gold and characterised by Hg-drop junction. (Adapted from ref. [181])

Although metals such as gold and silver are the substrate of election for SAMs deposition and immobilisation of organic molecules for Hg-drop measurements, the liquid metal junction has proven to be useful for the electrical characterisation of semiconductor oxide films such as indium tin oxide (ITO), both in dark condition and under illumination.[182] With this technique useful information could be extracted on the (opto)electronic behaviour of organic molecules film on ITO, as well as on other transparent conductive oxides (TCO).

The use of Hg as liquid metal has several advantages, such as junction mechanical stability, very good measurement reproducibility, good contact also on irregular surfaces and no intrinsic structural features (typical of solid electrodes) that can results in defects and poor electrical contact.[178] However, the infamous toxicity of mercury is a huge disadvantage for the operators health, thus the utilisation of "safer" substances is highly advised.

In this context, Whitesides and co-workers started to study the behaviour of liquid metal alloys as electrodes for molecular junctions. They introduced the use of gallium-indium eutectic (EGaIn) in replacement of mercury,[183-185]

given that its work function is comparable to that of Hg (respectively ~4.2eV and ~4.5eV) and it is non-toxic and far more safer to handle. The experimental set-up needed for EGaIn junctions fabrication is analogous to Hg-drop one, with a drop of liquid metal kept suspended on top of the other electrode and lowered to achieve the contact with the organic layer. Actually, the resulting contact, and so the charge transport, takes place through a very thin layer of Ga_2O_3 (1-2 nm), which forms spontaneously on the drop surface and acts as self-passivating oxide layer. A sketch representing the "bilayer" EGain-oxide interface is portrayed in Figure 28.[186] It has been demonstrated [185] that this thin oxide layer does not affect the current flow through the organic layer, being the electrical resistance of the latter far greater than the Ga_2O_3 layer one.

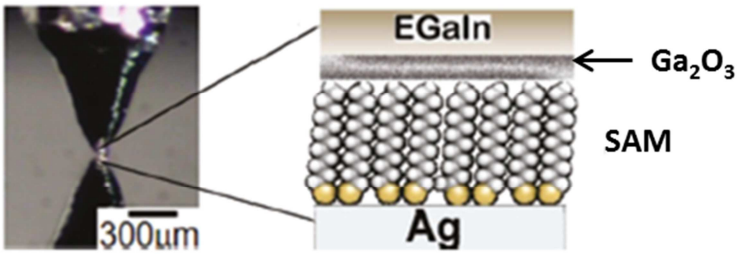

Figure 28: sketch representing the "anatomy" of a EGaIn junction, representing the contact between an organic layer (SAM onto Ag) and the Ga_2O_3/EGaIn drop electrode. Reprinted with permission from ref. [186], copyright 2011 American Chemical Society.

1.3. Surface modification using zirconium phosphate-phosphonate chemistry

In solid state chemistry, it is well known that the strong affinity between phosphate (or phosphonic) groups and numerous transition (tetravalent) metal ions leads to very stable and robust solid materials, with a highly ordered lamellar structure. The most famous example of this kind of compound is the α-zirconium phosphate (α-$Zr(O_3POH)$), whose structure (Figure 29) was first described and studied by Clearfield[187]. The same lamellar structure of α-$Zr(O_3POH)$, with a pseudo-hexagonal arrangement of phosphoric units above and below a plane of Zr^{4+} ions, has been found in compounds containing phosponic specimens bearing organic ligands.

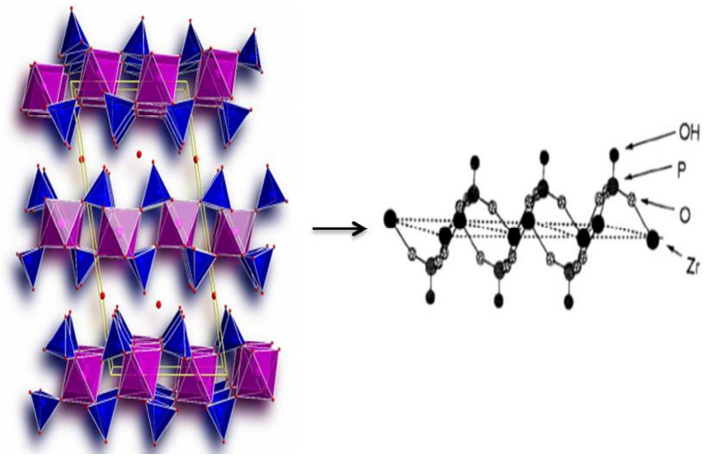

Figure 29: Structure of α-Zr(O_3POH).

The zirconium phosphate-phosphonate derivatives are particularly interesting for their practical applications, due to their strong chemical, mechanical and thermal stability, as well as for their ease of synthesis, which can be carried out at room temperature and in aqueous solution[188]. One of the most interesting characteristic of these materials is their tendency to form supramolecular assemblies, and this peculiar feature has been exploited for surface functionalisation.

The first examples of zirconium phosphonate thin film deposition was reported by Mallouk and coworkers[189, 190]. Their approach consisted in using ditopic molecules, containing a surface-active functional group and a phosphonic unit. They functionalized a silicon substrate by treatment with a bifunctional phosphonic acid bearing a silanol group, which can bind to the Si surface (see Figure 30 for the reaction scheme). In this way they obtained *de facto* a monolayer of phopshonic units on the surface. Then, after exposure to aqueous $ZrOCl_2$ solution and subsequently to an alkyl-bisphosphonate molecule solution, they obtained an ordered zirconium-phosphonate thin film at the substrate surface.

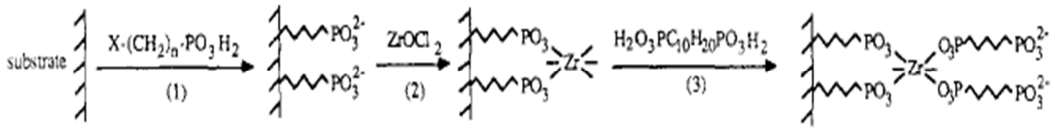

Figure 30: Reaction scheme for the deposition of zirconium-phosphonate thin film. Substrate = Si, X=(OH)Si(CH$_3$)$_2$. Reprinted with permission from ref. [189] copyright 1988 American Chemical Society.

To avoid all the practical issues related to the use of organosilane for the substrate surface priming (i.e. necessity of accurate monitoring of water content, high reaction temperatures, competitive crosslinking of polysiloxane, etc..), Kohli, Bakiamoh and Blanchard[191-193] proposed a protocol for direct priming of the oxide surface, using as phosphorylating agent $POCl_3$ and collidine in anhydrous acetonitrile (see Figure 31). This treatment provides a surface covered with a layer of phosphoric groups, which can react with a solution containing Zr^{4+} ions to form a monolayer of zirconium phosphate at the oxide surface.

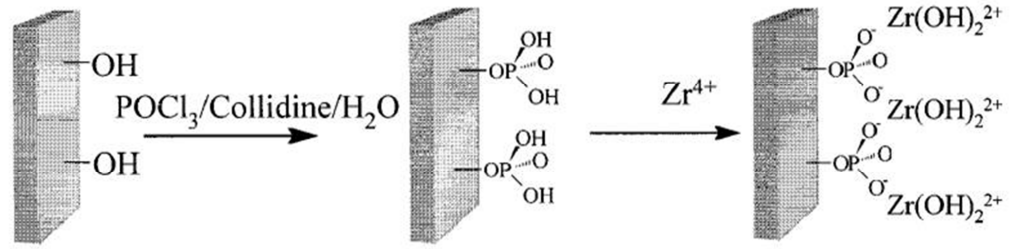

Figure 31: Scheme of Kohli and Blanchard surface priming protocol. Reprinted with permission from ref. [193], copyright 2000 American Chemical Society.

Kohli and Blanchard protocol for surface priming was further improved by Morotti[194] and Spampinato[103], who carried out the surface phosphorylation step by using pure $POCl_3$.
It has been shown for flat oxide substrates (quartz, thermally growth SiO_2 and ITO) [103, 195] that the application of this protocol for the functionalization of oxide surfaces with a zirconium phosphate layer actually provides an anchoring platform for ditopic molecules carrying a phosphonic group and a second functional unit exploitable for further molecular functionalization reactions (e.g. multilayer growth, (bio)molecules immobilisation, etc…).

Given the well-documented stability of zirconium phosphate-phosphonate compounds,[196] the existence of the zirconium phosphate monolayer at the oxide surface should ensure a good interfacial and structural stability of the anchored functional phosphonic (or phosphate) molecules, and this anchoring robustness should be (in principle) independent from the chemical nature of the underlying oxide.

The great molecular film stability would be a potential benefit for perspective practical applications for which long term durability are fundamental for guaranteeing the desired functionality.

2.Results and discussion

2.1. Introduction

In this section, results will be presented and discussed on oxide surfaces modification through the anchoring of functional molecular systems. The strategy, exploited for the modification, involved a preliminary surface priming based on the chemistry of zirconium phosphates/phosphonates (henceforth indicated as ZP-priming). The main focus was the development of an effective experimental strategy for robust anchoring of functional molecules on oxide surfaces. ZP priming is aimed to provide a stable anchoring platform for the anchoring of molecules bearing phosphate or phosphonic groups, virtually independently from the nature of the underlying oxide.

This priming method has been applied on oxides of different chemical nature (TiO_2, SnO_2, FTO), different morphologies (flat or nanostructured), and with different perspective applications. For each class of oxide the experimental approach has been optimised on-purpose and the surface physico-chemical properties have been studied. Moreover, specific evaluation of the "functional" behaviour of the prepared molecular surfaces was performed.

The discussion of the experimental work is divided in two parts. First, the chemical modification of nanostructured transparent oxides will be presented; special focus will be placed on the optimisation of ZP-priming for this kind of substrates, which will be the starting point for the subsequent anchoring of photoactive molecules at the oxide surface. Since nanostructured oxides whose surface is covered by photoactive molecules find application in the context of fabrication of dye-sensitized cells, in the perspective of possible application in this field, dye-sensitized electrodes of ZP-primed nanostructured TiO_2 and SnO_2 were prepared and their compositional and photoelectrochemical characterisation was carried out.

In the second part, deals with the growth and characterization of conductive molecular wires on a ZP-primed flat oxide (FTO). The wires were grown with a bottom-up approach, using a stepwise procedure involving metal-coordination reactions of bifunctional molecular conjugated systems, carried out directly at the oxide surface. In this context, again, the ZP-priming provides a "platform" to grow our wires on. Data on the molecular wires composition

and their spectroscopic characteristics are going to be presented, as well as preliminary data on their electrical behaviour, collected with EGaIn junction technique.

2.2. Anchoring of photoactive molecular systems on ZP-primed nanostructured oxide surfaces

As mentioned in the introductive part, the development of tailored experimental methodologies for the robust anchoring of functional molecules on oxides surfaces is a topic of interest in various applications. A notorious example in given by dye-sensitized cells: here the chromophore-oxide interaction dictates the proper functioning of the device itself, and any of desorption phenomenon arising from poor anchoring is detrimental and should be minimised.

In this work, ZP priming of nanostructured electrodes was tested as a possible strategy for achieving a stable anchoring of molecular dyes bearing a phosphonate group. At first, ZP priming of nanostructured TiO_2 surfaces of micrometric thickness will be described and experimental data on both surface and along-the-depth characterisation will be presented. The diffusion behaviour of Zr(IV) in different priming experimental conditions has been studied and will be discussed.

The relative stability of phosphonate dyes binding on ZP primed TiO_2 has been assessed, with respect to the anchoring of the same molecular system on bare titania surfaces. Moreover, the influence of the zirconium phosphate layer at the interface between photoactive system and TiO_2 electrode has been preliminarily investigated in a real DSSC, using a photoanode prepared with a ZP primed TiO_2 nanostructured electrode and a carboxylate dye, in order to evaluate the influence of the ZP-treatment on the charge separation and injection processes.

Subsequently, ZP-primed nanostructured TiO_2 substrates were sensitised with a photoactive molecule bearing a phosphonic moiety, and the photoelectrochemical properties of the obtained electrodes were studied in order to evaluate the effect of priming not only on the anchoring of the dye but also on the electrical interaction dye-oxide.

ZP-priming and dye-sensitization were finally extended to nanostructured SnO_2 substrates, as well as the same photoelectrochemical and compositional characterisation carried out for TiO_2 samples.

2.2.1. ZP priming of nanostructured TiO_2 surfaces

Many of the data presented in this paragraph of the thesis are also discussed in a recently published paper.[104]
The ZP priming procedure is a modification of that first described by Spampinato *et al* and for the modification of flat surfaces of silicon dioxide and ITO[195].
The experimental procedure, sketched in in Figure 32, consists in sequence of steps in which the substrate undergoes the following different surface reactions:

1. 15 minutes of treatment in UV-O_3 followed by rinsing in ultrapure water. This step is aimed to the enrichment of the oxide surface with –OH groups (as well as the elimination of organic contaminants);
2. Immersion in pure $POCl_3$, for one hour, in order to phosphorylate the –OH groups present at the oxide surface, leading to a layer of phosphate units;
3. 15 minutes immersion in aqueous $ZrOCl_2$ solution (10^{-4} M), in order to obtain the desired zirconium phosphate layer at the oxide surface.

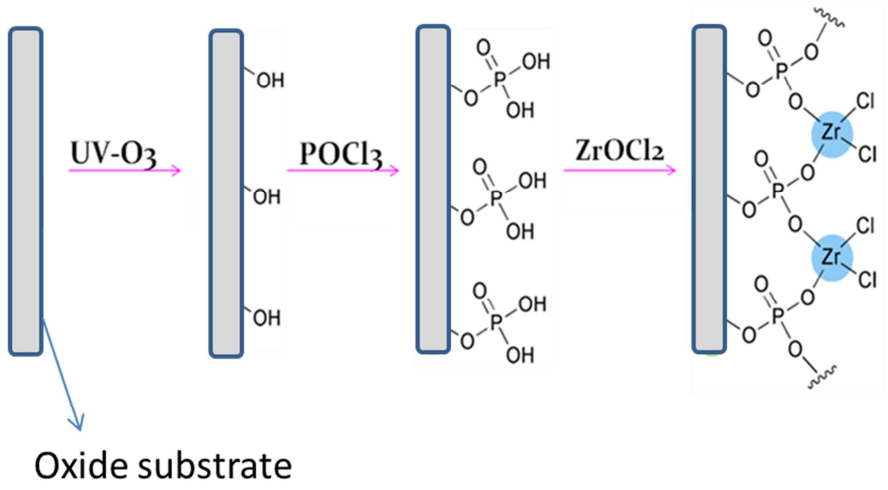

Figure 32: Scheme of ZP priming protocol on flat oxide substrates. Reprinted with permission from ref. [104], copyright 2016 American Vacuum Society.

The initial experiments were carried out on model, relatively flat, TiO_2 surfaces, obtained on purpose by deposition of a titania thin film onto a

FTO-covered glass substrate. Such titania film was obtained by hydrolysis of 0.4 M $TiCl_4$ solution (see "Materials and Methods" section for details).
The ZP-primed TiO_2 films were characterised by Time-of-Flight Secondary Ion Mass Spectrometry (ToF-SIMS), that is able to provide compositional information (both elemental and molecular) on from solid surfaces with great sensitivity (see "Materials and Methods" section).
Spectra were acquired with a reflector-type TOFSIMS IV spectrometer (ION-TOF GmbH, Münster, Germany) using 25 keV Bi+ primary ions. Static Sims conditions were used (Bi^+ primary ion fluence< 10^{12} ions·cm^{-2}) in order to preserve the molecular information from the surface.
Figure 33b reports some relevant regions of the positive ions ToF-SIMS spectrum (acquired in "static mode") of a typical ZP-primed TiO_2 film surface, in which peaks related to zirconium phosphate platform are identified, along with TiO_2-related peaks. For comparison, in Figure 33a the spectrum of the untreated titania substrate is reported.
Peak assignments were done on the basis of isotopic distribution and exact mass (the typical mass resolution being ΔM/M ≈8000, and mass accuracy of the order of 20 ppm).

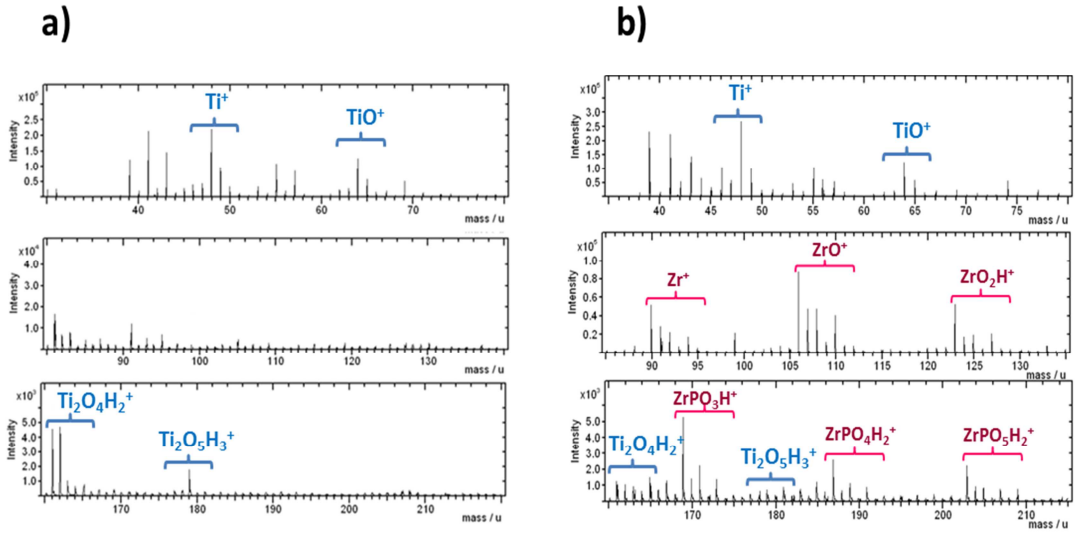

Figure 33: Relevant regions of positive ions ToF-SIMS spectra of a) untreated flat TiO_2 substrate, b) flat ZP-TiO_2.

The measured spectrum is consistent with the presence of a zirconium phosphate layer chemically bound to the oxide substrate, and it is stable towards prolonged immersion and rinsing in water. Also, the formation of the

"ZP" layer is demonstrated, *a posteriori*, by the fact that it undergoes successfully the reaction with phosphonate groups, as reported later on (see paragraph 2.2.4).The demonstration of the feasibility of ZP priming on a model TiO_2 flat substrate was propaedeutic to the functionalization of nanostructured titania films, that can be used as electrodes in dye sensitized devices. The substrates consisted in mesoporous, several micrometers-thick (5-10 μm) films of TiO_2 (anatase) deposited by doctor-blade technique onto FTO-covered glass slides (see "Materials and Methods" section for details). Static ToF-SIMS spectra of these mesoporous substrates after ZP priming, carried out following the above mentioned protocol, are virtually identical to the one shown in Figure 33b in the case of the flat substrare, and indicate, again, that the surface was successfully functionalised with the zirconium phosfate units.

In order to assess if the applied method is able to provide an uniform ZP priming along the whole thickness of the titania layer, the samples were analysed along the thickness by by ToF-SIMS depth profiling. Measurements were carried out in dual-beam mode, alternating analysis cycles (using a 25 keV Bi^+ primary ion beam) with sputtering cycles (by means of a 10 keV Cs^+ beam). Due to the stepwise approach of the priming, a strict monitoring of each preparation step is required in order to assess the effectiveness of the method for the obtainment of a uniform surface functionalisation over the entire thickness of nanostructured titania layer. With this aim, depth profiles of the sample were acquired after each step of the priming procedure,. In Figure 34 the negative ions ToF-SIMS profiles of nanostructured TiO_2 are reported for the untreated substrate (a), after its immersion in $POCl_3$ (b) and, finally, after the treatment with $ZrOCl_2$ solution (c).

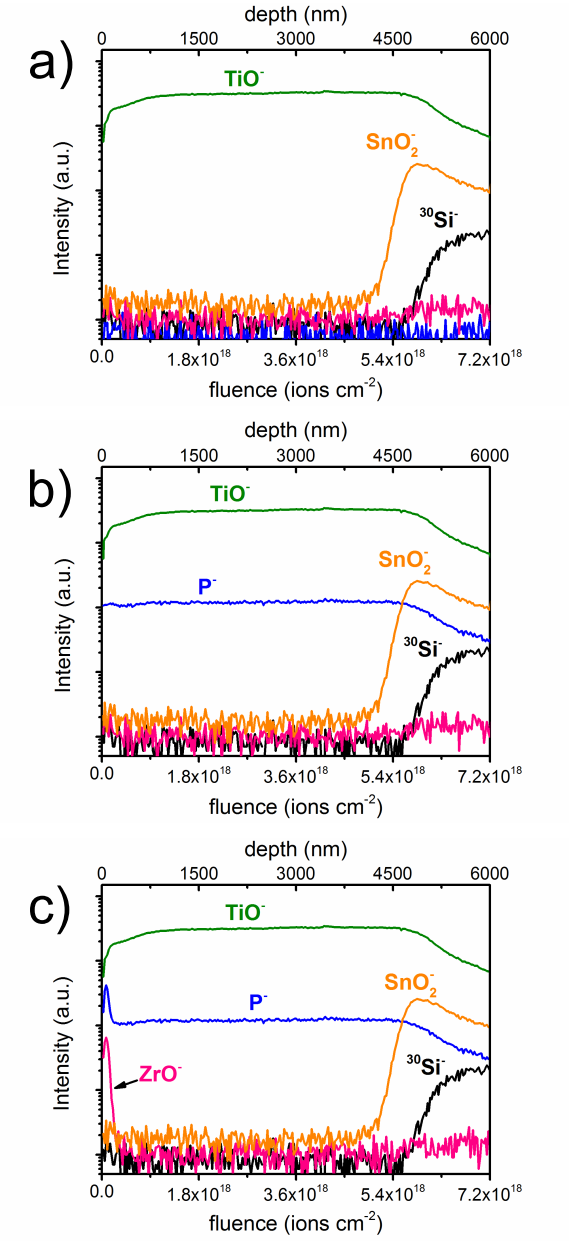

Figure 34: Depth profiles for nanostructured TiO_2 sample a) untreated, b) after 1 hour immersion in $POCl_3$, c) after 15 minutes immersion in aqueous $ZrOCl_2$. Reprinted with permission from ref. [104], copyright 2016 American Vacuum Society.

In each profile the signals representative of the substrate (TiO^- for the titania layer, SnO_2^- for the FTO layer and $^{30}Si^-$ for the glass surface) are reported together with those that are representative of ZP priming, namely P^- and ZrO^-.

These ions were chosen, among all the characteristic signals identified in the spectrum in virtue of their relatively high intensity (and high signal-to-noise ratio) as well as for the absence of significant non-resolvable mass interferences.

Comparing profiles from a) to c) we clearly note that, in the experimental conditions adopted, a uniform distribution of phosphorus is obtained throughout the entire nanoporous titania layer, while zirconium is detected only close the sample surface (Figure 34c). The uniform distribution of P in profiles b) and c) indicates that the phosphorylation of the nanoporous oxide was successfully achieved along the entire layer thickness. *Viceversa*, the ZrO^- profile shows that the penetration of zirconium is limited to the outer layers, meaning that the desired uniform functionalisation with zirconium along the depth was not achieved. In other words, SIMS results clearly show that treatment with $ZrOCl_2$ is the actual "limiting" step for the achievement of a uniform ZP priming. This observation prompted further investigations on this step, carried out by changing the experimental conditions for the zirconium impregnation step, namely treatment time and solvent, while leaving unchanged the preceding surface treatment steps (UV-O_3 and $POCl_3$ treatment). Several different conditions for $ZrOCl_2$ treatment were explored, which are summarized in Table 1. The corresponding ToF-SIMS depth profiles are reported presented in Figure 35.

Substrate	**$POCl_3$ treatment**	**$ZrOCl_2$ treatment**	**Profile**
Nanostructured TiO_2 on FTO	1 hour	30min in $ZrOCl_2/H_2O$ + 24h in C_2H_5OH	**1**
Nanostructured TiO_2 on FTO	1 hour	30min in $ZrOCl_2/H_2O$ + 24h in CH_3CN	**2**
Nanostructured TiO_2 on FTO	1 hour	24h in $ZrOCl_2/H_2O$	**3**
Nanostructured TiO_2 on FTO	1 hour	24h in $ZrOCl_2/C_2H_5OH$	**4**
Nanostructured TiO_2 on FTO	1 hour	24h in $ZrOCl_2/CH_3CN$	**5**

Table 1: List of investigated $ZrOCl_2$ treatments.

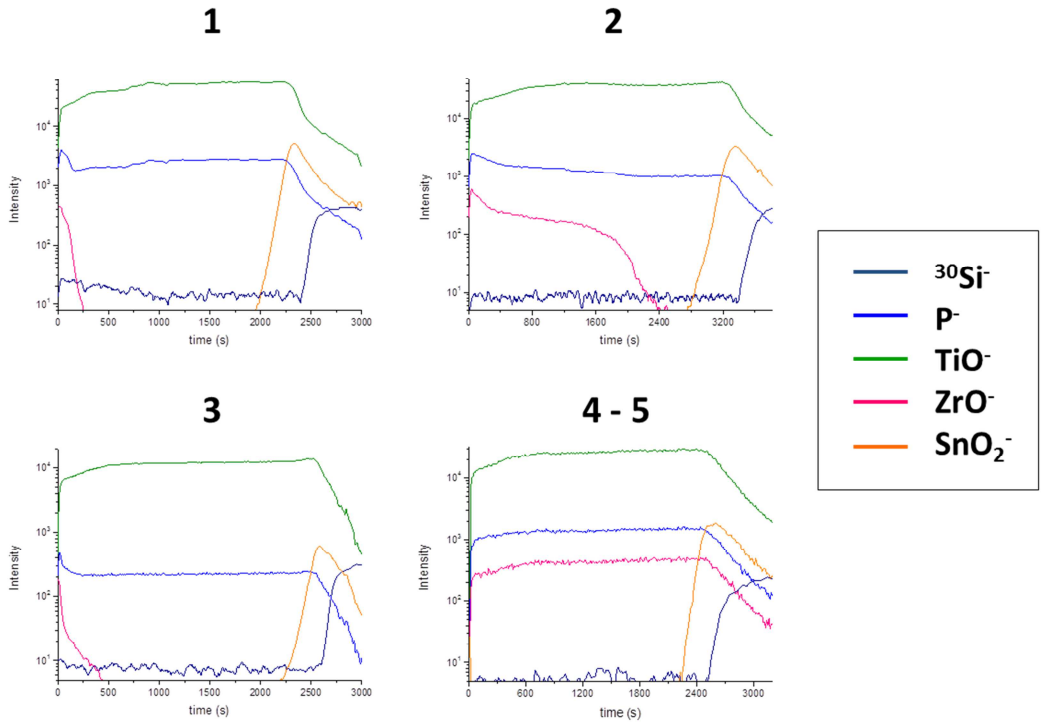

Figure 35: ToF-SIMS depth profiles for samples prepared using different ZP priming protocols on nanostructured TiO_2 substrates. Numbers refer to the conditions listed in Table 1. Only one profile is reported for treatments 4-5 because they are superimposable.

In profiles 1, 2 and 3 the ZrO^- signal decreases before the attainment of the TiO_2/FTO interface, indicating that no uniform zirconium distribution along the whole TiO_2 layer is achieved, even if the immersion in aqueous $ZrOCl_2$ is carried out for 24 hours (profile 3). However, a particular effect can be noticed where the samples, after 30 minutes immersion in aqueous $ZrOCl_2$, were post-treated by immersion in either acetonitrile or ethanol for 24 hour (samples 1 and 2). To all appearances, the post-treatment in organic solvent seems to promote the diffusion of zirconium within the nanostructured oxide layer. The influence of the solvent is evident in the profiles 4 and 5, referred to samples prepared by immersion for 24 hours in, respectively, ethanol and acetonitrile solutions of $ZrOCl_2$. Those profiles show that the Zr-related signal is present with constant intensity until the attainment of the interface TiO_2/FTO, meaning that the 24 hours treatment with $ZrOCl_2$ in ethanol or acetonitrile solution actually leads to the desired uniform distribution of zirconium along the entire layer of mesoporous titania. Given that the solubility of $ZrOCl_2$ salt was found

to be much higher in ethanol rather than acetonitrile, it was decided to use the ethanol as solvent for all the subsequent ZP-priming of nanostructured titania substrates. However, these interesting finding (that both time of immersion, solvent of the $ZrOCl_2$ solution and eventual post-treatment have a significant influence on the zirconium penetration) encouraged further investigations, focused on the elucidation of some aspects of the diffusion of Zr(IV) through TiO_2 mesoporous substrates.

2.2.2. Diffusion behaviour of Zr(IV) in nanostructured TiO_2 substrates

In order to gain information about the diffusion mechanism of zirconium (IV) within the nanostructured layer, the Zr migation was investigated by SIMS technique. Depth profiles were collected and Zr-related signals monitored with respect to both the time of immersion in the $ZrOCl_2$ solution and the solvent used to prepare the solution itself. For the sample preparation, the two initial priming steps conditions (i.e. UV-O_3 and $POCl_3$ treatment) were not changed.

- ***Treatment with aqueous $ZrOCl_2$ solutions***

The migration of zirconium supplied by aqueous $ZrOCl_2$ solution was the initial subject of investigation. The phosphate-functionalised TiO_2 substrates were immersed for, respectively 3, 7 and 24 hours in aqueous $ZrOCl_2$ (10^{-3} M), with the purpose of evaluating the diffusion depth of zirconium within the substrate as a function of the time of immersion.
ToF-SIMS profiles of ZrO^- signal for those samples are reported in Figure 36. As noted already in paragraph 2.2.1, even after 24 hours of immersion, the distribution of Zr within the nanostructured titania layer is not uniform, with the most part of zirconium remaining confined on the outer part of the oxide layer. Actually the depth distribution of zirconium after 24 hour treatment is only slightly changed with respect to the shorter treatment periods, just with a slightly deeper tail (note the logarithmic scale of the y-axis in Figure 36). These

data indicate that water is not the most suited solvent for triggering, in a reasonable timescale, the diffusion of Zr(IV) deeper in our substrate.

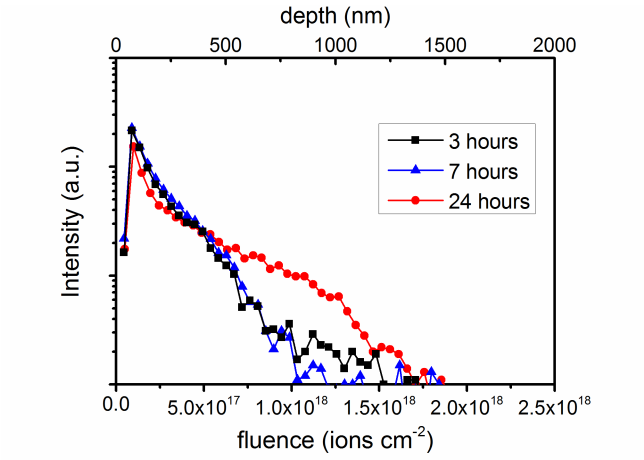

Figure 36: ToF-SIMS depth profiles relative to ZrO^- signal (in logarithmic scale), for three samples prepared at increasing time of immersion in aqueous $ZrOCl_2$. Reprinted with permission from ref. [104], copyright 2016 American Vacuum Society.

- ***Effect of post-treatment in C_2H_5OH***

In order to gain information on the mechanisms involved in the zirconium migration into the nanostructured titania layer, the initial stages of the process (shorter treatment times) were studied by SIMS depth profiling. Three different profiles, obtained after 15, 45, 120 minutes of immersion in $ZrOCl_2$(aq) are reported in Figure 37.

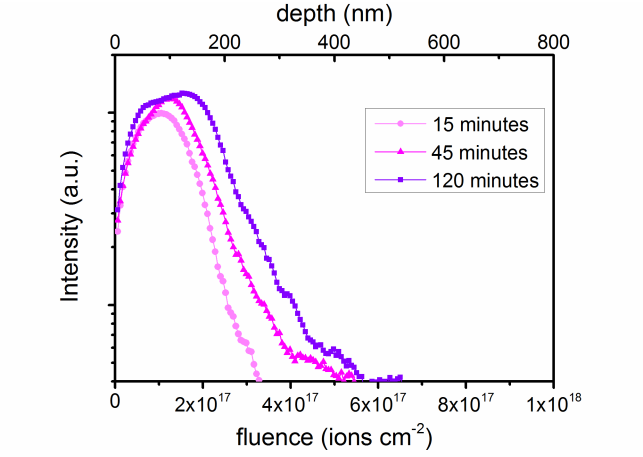

Figure 37: profiles relative to ZrO- signal (in logarithmic scale) for three samples prepared by 15, 45 and 120 minutes (respectively) of immersion in aqueous $ZrOCl_2$ solution. Reprinted with permission from ref. [104], copyright 2016 American Vacuum Society.

In the framework of a classical diffusion behaviour, in the presence of an infinite source [197] (in this case the zirconyl chloride solution) one expects that the total amount of zirconium in the sample should increase linearly with the square root of time. The total amount of zirconium can be calculated, in principle, from the area of the experimental profiles. However, the shape of profiles of Figure 37 cannot be simply transformed into a concentration profile, because the zirconium-related secondary ion intensities can be strongly affected by the fact that the most part of Zr signal comes from a region very close to the surface, i.e. in a transient signal region where a conversion of intensity into concentration is questionable.[198] In spite of this limitation, some information can be extracted thanks to an interesting post-treatment effect occurring in our samples. Indeed, we observed that the immersion of the samples (prepared as described above) in organic solvent (ethanol in particular) is very helpful in improving the in-depth distribution of zirconium through the nanostructured titania film (see discussion of Figure 35). The effect of a 24h C_2H_5OH post-treatment on the profile of zirconium is reported in Figure 38 in the case of a sample prepared by 2 hours immersion in aqueous $ZrOCl_2$. It is evident from the SIMS depth profiles reported in figure that, after the post-treatment, a migration of zirconium towards inner layers takes place. Thanks to this enhanced migration of zirconium, the most part of the profile is now far from the surface, where quantification is easier. By assuming that the loss of

zirconium caused by post-treatment is negligible, the area of the experimental profile can be considered proportional to the total amount of zirconium introduced in the sample by the treatment with $ZrOCl_2$ (aq).[199] Figure 39a reports the normalised ZrO^- profiles, acquired after 24 hours post-treatment in ethanol, of three samples prepared in the same way of those of Figure 37. It should be pointed out that the "normalisation" of ZrO^- profiles has been carried out point-by-point with respect to the matrix signal TiO^-, in order to eliminate possible effects (such as drifts or oscillations in the primary ion current) that could affect the intensity of ZrO^- signal. As already pointed out, being now the surface effects negligible, the normalised profile area is then indicative of the amount of zirconium actually present inside the sample. The plot in Figure 39b clearly shows that these areas are linearly correlated to the square root of the time of immersion in aqueous $ZrOCl_2$, thus indicating that a classic diffusion mechanism (Fick's law) governs the introduction of Zr(IV) in the titania film upon immersion in aqueous $ZrOCl_2$. The second diffusion step, that takes place during the post-treatment, is probably more complex, and would deserve further investigation.

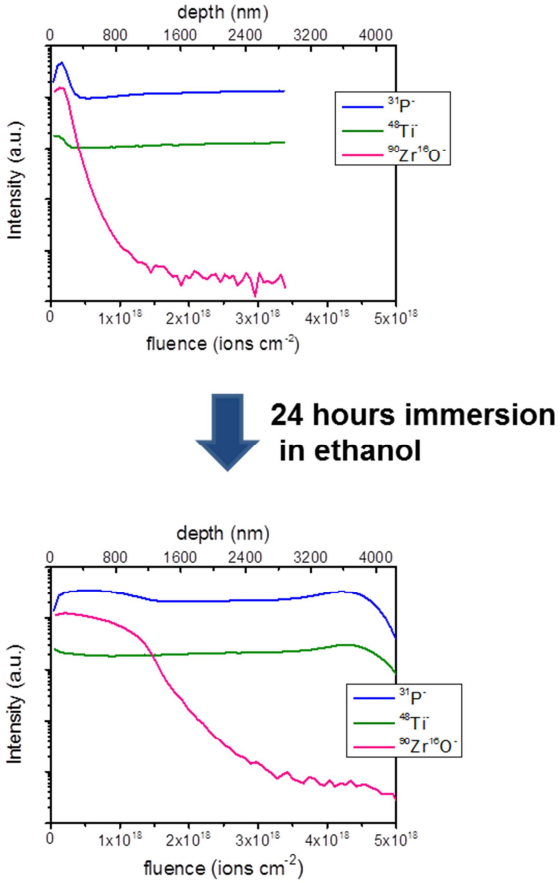

Figure 38: Effect of post-treatment (24 hours immersion in ethanol) on ToF-SIMS ZrO^- profiles (intensity reported in logarithmic scale). Reprinted with permission from ref. [104], copyright 2016 American Vacuum Society.

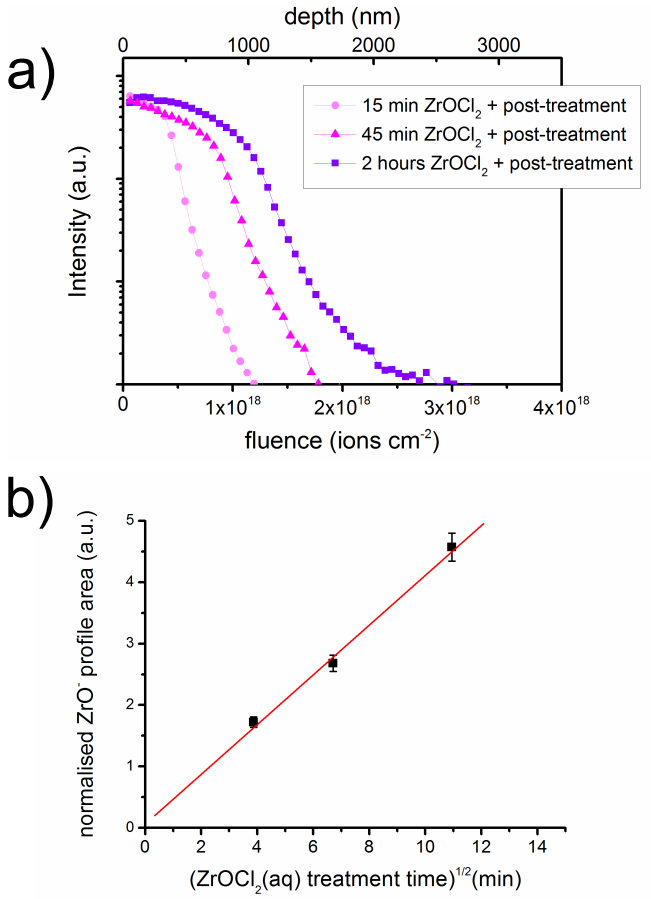

Figure 39: a) profiles relative to ZrO^- signal (in logarithmic scale) for three samples prepared at increasing time of immersion in aqueous $ZrOCl_2$ solution and post-treated by 24 hours immersion in ethanol; b) plot of integrated profile areas as a function of the square root of the immersion time in $ZrOCl_2$ solution. Reprinted with permission from ref. [104], copyright 2016 American Vacuum Society.

- ***Treatment with $ZrOCl_2$ in ethanol solutions***

The data presented above indicate that ethanol is rather effective promoting the diffusion of zirconium in TiO_2 nanostructured substrates. In view of this, we investigated the effect of impregnation with zirconium of the phosphate-terminated titania substrates starting from $ZrOCl_2$ ethanol solutions.

Figure 40 reports the ToF-SIMS depth profile of a nanostructured titania substrate after 45 minutes of immersion in a 10^{-3} M $ZrOCl_2$ solution in ethanol. The profile shows that after this relatively short period of immersion the zirconium has already penetrated the entire thickness of the TiO_2 film. By increasing the time of immersion, up to 24 hours, the only outcome is the

increase of the normalised intensity of ZrO^- signal, i.e. the increase of the amount of zirconium contained inside the titania layer. By plotting the normalised ZrO^- profiles area as a function of the time of immersion in $ZrOCl_2/C_2H_5OH$ solution (Figure 41), we obtain a growth trend that reaches a plateau after about 500 minutes; this can be explained as the achievement of an uniform and complete coverage of all the "sites" available for zirconium all over the entire thickness of TiO_2.

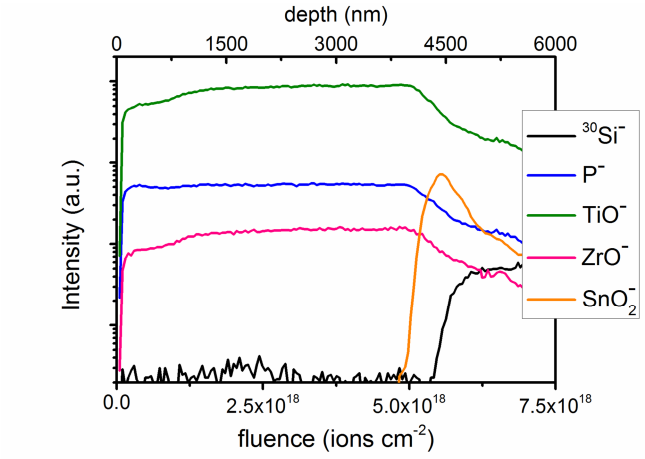

Figure 40: ToF-SIMS depth profile of ZP primed nanostructured TiO_2 after 45 minutes of immersion in $ZrOCl_2/C_2H_5OH$ (intensity reported in logarithmic scale). Reprinted with permission from ref. [104], copyright 2016 American Vacuum Society.

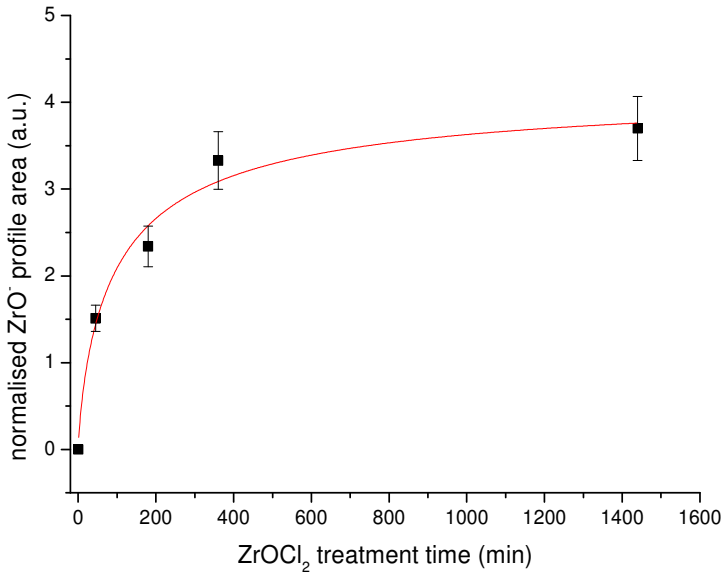

Figure 41: plot of integrated profile areas as a function of the immersion time in $ZrOCl_2/C_2H_5OH$ solution. Reprinted with permission from ref. [104], copyright 2016 American Vacuum Society.

From the above discussed data and considerations, 24 hours of immersion in ethanolic $ZrOCl_2$ solution (10^{-3} M) emerge as a suitable conditions for a uniform and complete priming of the nanostructured, micrometres-thick titania substrates. For this reasons, for all the subsequent surface treatment within this thesis work, the experimental ZP-priming protocol adopted is established as follows:

1. 1 hour of UV-O_3 treatment followed by abundant rinsing with water;
2. 1 hour of immersion in pure $POCl_3$, and subsequent rinsing with water;
3. 24 hours immersion in $ZrOCl_2$ 10^{-3} M solution in ethanol.

2.2.3. Effect of ZP layer on dye-to-oxide charge injection

Once the optimal procedure has been established for the functionalization of nanostructured TiO_2 substrates with the zirconium phosphate platform (that we indicate as ZP priming), the influence of the ZP layer on the functionality of a TiO_2 photoanode has been investigated. In particular, it is of crucial importance to understand whether the presence of the intermediate zirconium phosphate/phosphonate layer between the titania ssubstrate and the attached photoactive molecular systems affects somehow the good "communication" between dye and TiO_2, and so the efficiency of charge injection process.
Hanson et al[200] already showed that energy transfer occurs in chromophore bilayers on nanostructured TiO_2, in which two photoactive molecular systems are bound each other in multi-layered assemblies through a zirconium-phosponate linkage. We expect a similar non-detrimental effect of ZP layer in our samples, even if a substantial difference is given by the presence of zirconium phosphate directly bound to the titania surface.
To evaluate this issue, a ZP-primed TiO_2 electrode was used for the construction of a real dye-sensitized solar cell, and the functional parameters of the resulting device were tested and compared with those of a cell having a "classic" titania electrode. These experiments were carried out in collaboration with the research group of Dr. G. Di Marco, of the CNR-IPCF of Messina.
The photoanodes were obtained from screen printed nanostructured titania substrates (see materials and methods for details) by sensitization with the well-known carboxylic dye N719[46], either with or without the preliminary ZP priming. Although the carboxylic moiety is not expected to be the best suited for binding the dye at the ZP primed surface, in these preliminary experiments we chose the N719 molecule since it is a reference dye largely used as sensitizer in DSSCs and its photochemical behaviour is well-known. These photoanodes were inserted in identical standard Graetzel cell for a first evaluation of the influence of the ZP treatment. These devices (made either with a "normal" or ZP-primed photoanodes), were exposed to a solar sunlight simulator and the I-V curves registered (details in "Materials and Methods" section).
The results of such measurements are reported in Figure 42 and Table 2. In particular we observe that the overall efficiency η of the cell constructed with the ZP-primed photoanode is comparable to the one of the device made with the normal photoanode. The latter type of cell shows performances that are

slightly better, nevertheless the result must be considered very promising iconsidering that this slightly smaller efficiency found for ZP-primed DSSCs could be abundantly compensated by a gain in the long term stability of the dye anchoring, that will be demonstrated in the next paragraph

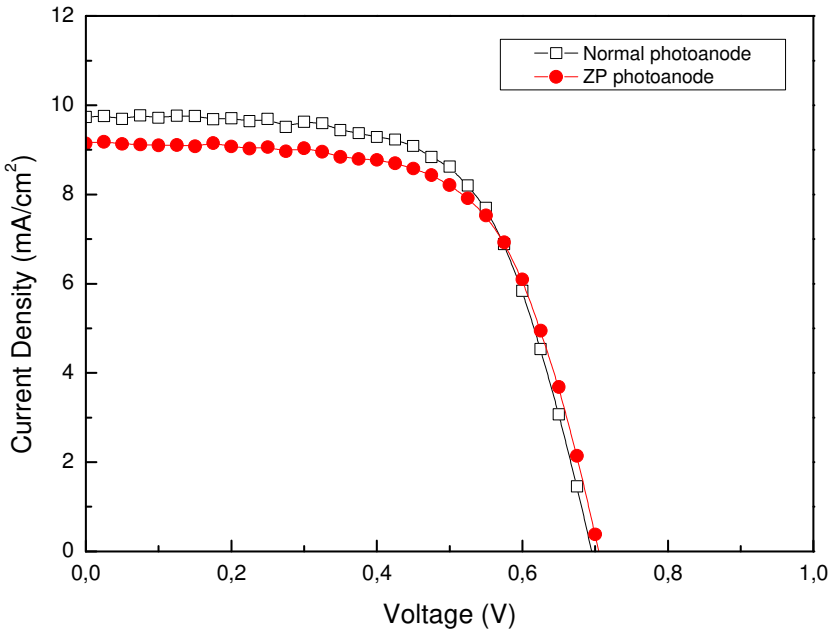

Figure 42: I-V characteristics for DSSC built with, respectively, a normal N719-TiO_2 photoanode and a ZP-primed N719-TiO_2 one.

.

Sample	Irradiated power (mW/cm^2)	η (%)	FF	Jsc (mA/cm^2)	Voc (mV)
Normal DSSC	100	4.31	0.63	9.73	695
ZP-DSSC	100	4.15	0.64	9.14	705

Table 2: Summary of measured functional parameters for normal N719-TiO_2 photoanode DSSC and ZP-primed-N719-TiO_2 photoanode one.

2.2.4. Anchoring stability of phosphonate-derivatised organic molecules on ZP-primed TiO_2 surfaces

Experimental results reported so far in this work, show that ZP-priming on micrometres-thick nanostructured TiO_2 substrates is feasible, obtaining a layer of zirconium phosphate at the oxide surface; in addition the concept of exploiting such a system as a molecular anchoring platform for dye-sensitized electrodes development is supported by experimental evidence of a non-detrimental effect of the ZP surface layer on the charge transfer processes that occurs between ZP-primed TiO_2 semiconductor and a chromophore adsorbed on it.

As mentioned before, given the well-known stability of zirconium phosphate solid compounds, we expect that a ZP-primed TiO_2 surface binds a phosphonate molecular system more firmly than a bare TiO_2 surface.

In order to evaluate the relative stability of phosphonate-based dyes anchoring on ZP-TiO_2, in comparison to that on bare TiO_2, stability tests towards hydrolysis and thermal stress in organic solvent were carried out, by setting up two different experiments. In such experiments "flat" TiO_2 films were chosen as model system, because of low surface roughness compared to that of thick nanostructured TiO_2 substrates, allowing better control and reproducibility of results, along with an easier characterization and comparison of results. Part of these substrates were ZP primed and subsequently all of them (either primed and non-primed) were allowed to interact with a solution of a properly chosen phosphonic-derivatised molecules in order to perform the anchoring. Finally, the stability of such anchoring was tested as detailed in the next paragraphs.

- ***Thermal stability in organic solvent***

This test consisted in prolonged immersion of the surface-engineered ("sensitized") ZP and non-ZP TiO_2 substrates in boiling ethanol (b.p. 78 °C) and monitoring the amount of "surviving" dye molecules on the surfaces of each type of substrate.

The chromophoric system anchored as "molecular probe" was a phosphonate-derivative of Rhodamine B (hereafter RhB-P), whose molecular structure is

shown in Figure 43. This molecule was synthetized on purpose by the group of prof. Amato (University of Catania). The choice of a rhodamine B derivative is due the high absorption coefficient ε ($10{,}6 \cdot 10^4$ $cm^{-1} \cdot M^{-1}$) which allows its monitoring by transmission UV-Vis spectroscopy even at very low concentration, and in virtue of the great thermal stability (rhodamine undergoes decomposition beyond 570 K)[201].

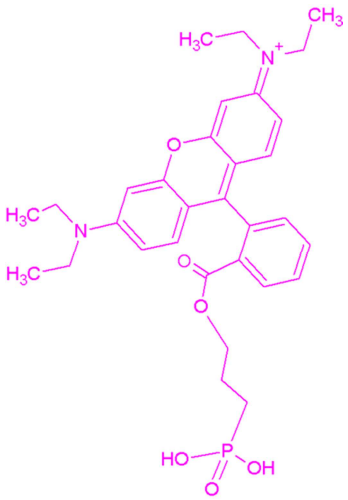

Figure 43: Molecular structure of phosphonate-derivative of Rhodamine B (RhB-P).

For the ZP-priming of flat TiO_2 the protocol already discussed and validated for flat oxide surfaces was applied (see Figure 32 for reaction scheme). Both bare TiO_2 substrate and ZP-primed one were immersed for 24h in a 10^{-4} M RhB-P solution in ethanol, in order to cover the oxide surfaces with a monolayer of dye molecules, and then rinsed abundantly with ethanol, in order to remove physisorbed molecules. Figure 44 shows the UV-Vis spectrum of a RhB-P layer onto a TiO_2 surface (solid line) compared with the one (dashed line) obtained from a ethanolic solution of the same molecule. The spectrum of the surface layer has the same shape of the one in solution, although it is red shifted; this is a quite usual behaviour, due to the different environment of the molecule in the two systems. When comparing the spectra of RhB-P bound to ZP-primed and non-primed surfaces we observe (Figure 45a) that the spectra are identical in shape and band position, but the one from ZP-primed sample is more intense, indicating that a larger amount of dye is chemisorbed at the zirconium-containing surface. In the rough assumption that the absorption

coefficient ε of RhB-P is not much affected when going from a diluted solution to a surface layer, one can estimate the amount of molecules present at the surface, that turns out to be $\approx 9.5 \cdot 10^{13}$ molecules$\cdot$cm^{-2} for the ZP-primed sample and $6.25 \cdot 10^{13}$ molecules$\cdot$cm^{-2} for the non-primed one. Considering that the that the estimated area of the dye molecule (estimated from molecular modelling) is about 10^{-14} cm^2, we can conclude that the coverage of the ZP-primed surface is approximately one monolayer and that the one of the non-primed sample is about 60% of a monolayer. After the anchoring of RhB-P, samples were immersed in boiling ethanol and the UV-Vis spectra recorded at increasing treatment times. The absorbance at λ_{max} was normalized to the initial value and plotted versus the time of treatment, thus permitting a direct comparison between the amount of dye desorbed from the ZP sample and the non-ZP one (Figure 45b); normalisation was necessary because of the different initial absorption of the two samples, which is larger for ZP-primed titania, as reported in Figure 45a.

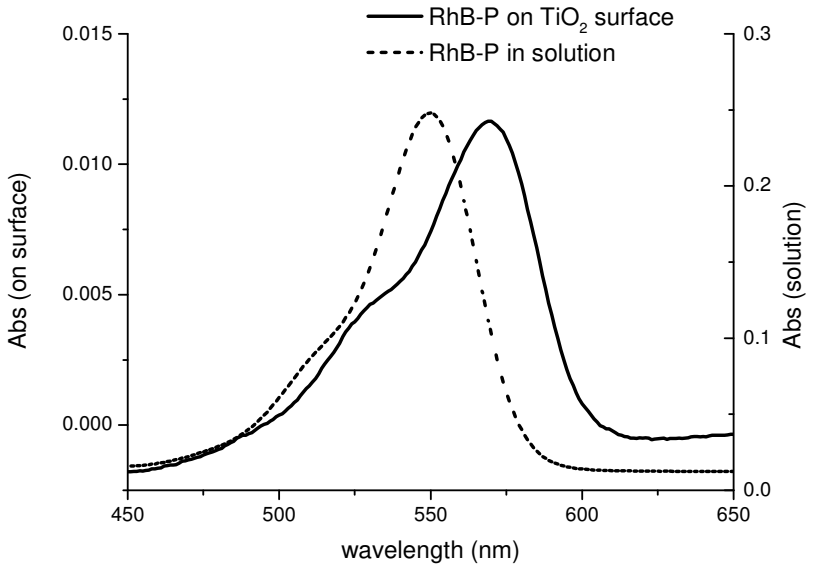

Figure 44: Comparison between RhB-P absorption spectrum on surface (continuous line) and in solution (dashed line).

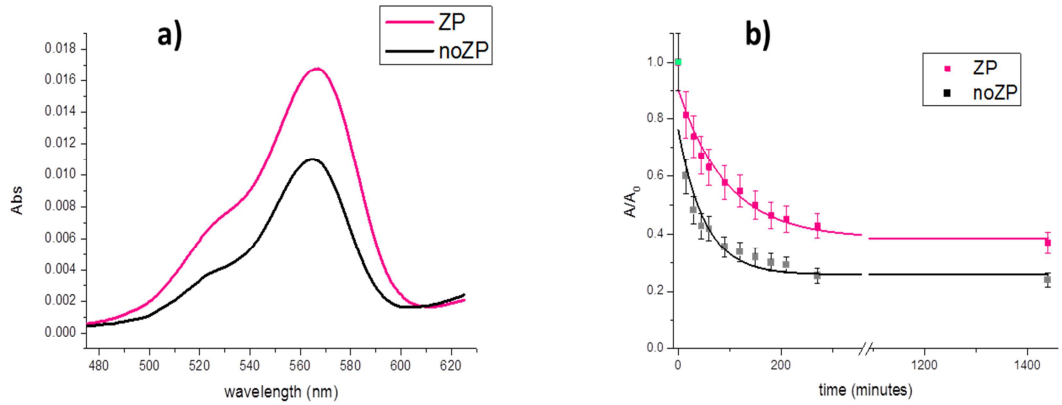

Figure 45: a) initial absorption spectra of ZP and noZP flat titania samples; b) normalized absorbance at λ_{max} for RhB-P functionalized TiO_2 on ZP and no-ZP substrates as a function of immersion time boiling ethanol.

The UV-Vis data show that, in the considered time range (≈24 hours) the non-primed sample undergoes a larger relative decrease in RhB-P absorbance in comparison to the ZP sample. Indeed the absorbance after 24 hours is reduced to approx. 40% of the initial value in the case of ZP-primed surfaces, to be compared with the 20% of the non-primed surface. Furthermore, considering that the ZP primed surface, upon immersion in the RhB-P solution, is able to bind an amount of dye molecules which is about 1.5 times larger than that adsorbed on the non-primed surface (see Figure 45a) the overall result is that, after a 24 hours of treatment in boiling ethanol, the "survived" surface concentration of dye on the ZP-primed surface is three times higher than that on the bare TiO_2 surface.
All above confirms that the binding of phosphonate-based molecules on ZP-primed oxide surfaces, as predicted, is stronger and more stable than the binding on non-primed substrates and, moreover, that ZP-priming has a positive effect on the amount of molecules that initially bind to the surface.

- ***Stability towards hydrolysis***

This test was carried out using an approach similar to that used for thermal stability tests; after the immersion of the substrate (ZP-primed and non-primed TiO_2 films) in the proper dye solution, the survival of the anchored molecular

layer was monitored by measuring the UV-Vis absorbtion spectra at increasing times of immersion in a slightly acid (pH 5.7) aqueous solution.
For this experiment it was not possible to use as a probe the RhB-P dye, because of the presence of the ester bond between RhB core and the alkyl chain bearing the phosphonic unit, that can undergo hydrolysis in these conditions. For this reason, a phosphonate-derivatised polypyridinic Ru(II) complex (hereafter RuP) was preferred for the experiment, whose structure is shown in Figure 46. This ruthenium chromophore was chosen because its absorption spectrum in CH_3CN did not show any modification in absorption band shapes or maxima after the addition of water, even after 24 hours (at variance of what observed when using, for example, $Ru(bpy)_3$-based dyes). Other details on RuP dye and its properties and applications are going to be discussed later in the text (paragraph 2.2.5.1).

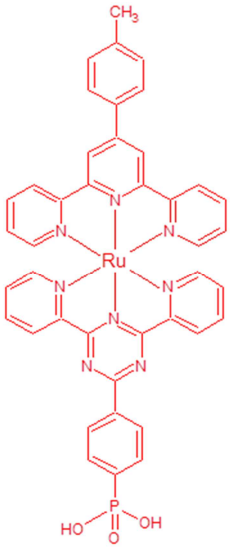

Figure 46: Molecular structure of RuP.

The sensitization process with RuP complex was carried out by immersion of both ZP-TiO_2 and noZP-TiO_2 flat substrates in a 10^{-4} M solution of the dye in acetonitrile, in order to bind thechromophore on the oxide surface. The absorption spectrum of the dye anchored on non-primed TiO_2 surface is reported in Figure 47 together with the spectrum of the molecule in CH_3CN solution.
Absorbance of the band at 480 nm (assigned to the MLCT transition typical of Ru(II) polypyridyl and Ru(II)-bis(pyridyl) complexes)[44, 202] was monitored for both ZP- and non-primed samples after different immersion times in water

(pH 5.7), and the normalised value as a function of time are reported in Figure 48, together with the absorption spectrum of the samples prior to the stability test.

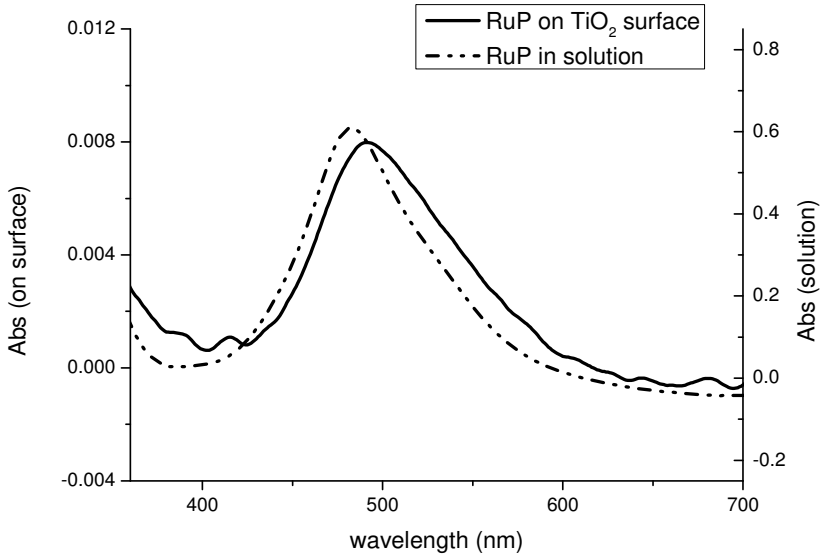

Figure 47: Comparison between RuP dye absorption spectrum on surface (continuous line) and in solution (dashed line).

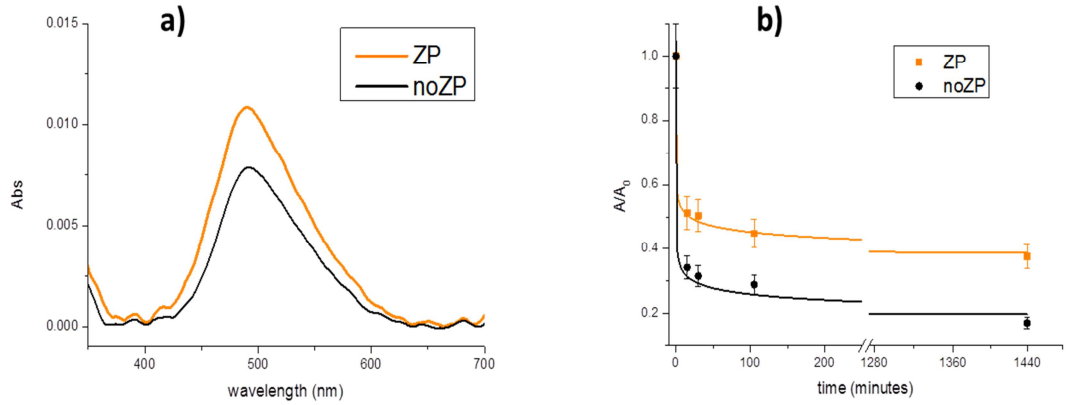

Figure 48: a) initial absorption spectra of ZP and noZP flat titania samples; b) normalized absorbance at λ_{MLCT} for RuP functionalized TiO_2 on ZP and no-ZP substrates as a function of immersion time in aqueous pH 5.7 solution.

The above results give a similar indication as those arising from the thermal stability test, i.e. that anchoring mediated by the ZP treatment provides a robust

anchoring of phosphonic derivatized molecules. In particular the ZP-primed surfaces, in comparison with the non-primed ones, undergo a smaller percentual loss of chemisorbed dye molecules upon prolonged exposure to acid solutions, combined with an higher initial surface coverage.
It interesting to note that higher dye uptake of the ZP-primed surface compared with the non-primed one is analogous to what observed in the case of RhB-P. In particular, comparing the spectra of the samples before the stability test (Figure 45a and Figure 48a), we observe that the intensity ratios between the spectra pertaining to the ZP-primed and non-primed system are almost identical for both kind of molecules. This supports the idea that the increased dye uptake upon ZP-priming is really due to an increased ability of such treatment to improve the interaction and binding of molecules bringing phosphonate anchoring groups.

2.2.5. Assembly of photoactive molecules on nanostructured ZP-primed TiO_2

Surface modification *via* anchoring of functional molecules is actually a double-sided process: both the surface and the molecular system must be chosen and, if required, conveniently modified in order to make possible not only their chemical interaction but (depending on the perspective application) also their electrical "communication". Often the two aspects (molecular and surface-related) cannot be treated separately but must be simultaneously dealt with. This aspect is particularly significant, among others, in the field of dye-sensitized cells. A clear example is given by the required match between the energy of the dye frontier orbitals and the edge of the oxide conduction band, mandatory for the charge-injection process at the basis of the cell operation. This energy match can be influenced, for example, by the application of an oxide overlayer at the dye-oxide interface or by placing a compact blocking layer at the nanostructured oxide-FTO interface, and this actions can either be positive (passivation of the electrode towards unwanted recombination reactions) or negative (the coating acts as a barrier, hindering the dye-to-oxide or oxide-to-FTO charge injection).[93, 203] Therefore, even if the most performant photoactive molecules and the ultimate nanostructured oxide substrate are available, once again the experimental strategy adopted for their

assembly and the modification perpetrated at the electrode surface are a crucial aspect for the correct functioning of the resulting photoanode.

According to the experimental results so far discussed, ZP-priming method on nanostructured TiO_2 substrates allows for a stronger binding of phosphonate-based chromophore on titania surfaces, thus limiting molecular-desorption processes. Moreover, it seems – from the preliminary experiments with N719 dye, described in paragraph 2.2.3 – that there is a negligible effect of the zirconium phosphate layer at the interface between chromophore and TiO_2 on charge injection processes. It must be pointed out, however, that more reliable data in this context would be given by measurements on electrodes sensitized with phosphonic-functionalised molecules, so where there is a strong chemical interaction and binding of the photoactive molecule onto the oxide surface.
The above mentioned observations could be exploited in the context of dye-sensitized photoanodes improvement, given that here dye-desorption form the oxide surface is a severe issue, which contributes to the functional deterioration of dye-sensitized devices. In the framework of the work carried out during this PhD thesis, a study was performed to explore the possibility of assembling photoactive dyes onto nanostructured TiO_2 substrate by means of the ZP-priming strategy, in order to provide an anchoring platform for the dye molecules. The modification of the surface and the characterisation of composition were performed, as well as a "functional" study, aimed to the investigation of the influence of the ZP-priming on the photoelectrochemical performances of the obtained electrode.

2.2.5.1. Synthetic approach for ZP-TiO_2 dye-sensitisation

The photoactive dye chosen for our investigations was the polypyridynic ruthenium complex Ru^{II}(4'-(tolyl)-2,2':6',2"-terpyridine)(dihydroxy-4-(4,6-di(pyridine-2-yl)-1,3,5-triazin-2-yl) phenylphosphonate) (Figure 49), henceforth indicated as RuP. This complex has been synthesised on-purpose by the research group of professor Campagna (University of Messina) with a molecular structure chosen and optimised for a possible use in devices for solar energy harvesting and conversion, especially DSPECs. The photoactive core constituted by the Ru(II)terpyridyl-bis(pyridyl)triazine, ensures reversible

electrochemistry, photochemical stability and an appropriate oxidation potential for driving water splitting in a DSPEC cell.[204, 205] The chromophore has a phosphonic group incorporated in the molecular backbone to allow for the anchoring on oxide substrates. The photoelectrochemical and photophysical behaviour of RuP complex in solution and anchored onto nanostructured TiO_2 and SnO_2 electrodes (without ZP treatment) has been recently published, showing the actual potential of this dye as efficient photosensitizer for DSPECs.[206] The sensitisation procedure of ZP-TiO_2 samples was monitored and assessed by means of ToF-SIMS and UV-Vis spectroscopy measurements.

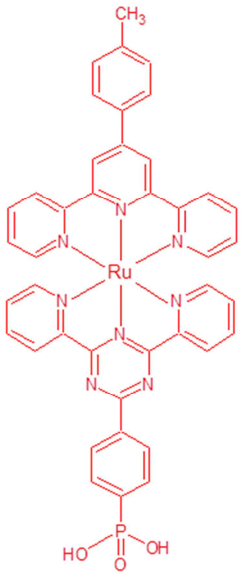

Figure 49: Molecular structure of the photoactive RuP dye.

For the preparation of the photoanode, nanostructured TiO_2 substrates have been first of all functionalised using the ZP-priming procedure, as optimized for thick nanostructured layers (see paragraph 2.2.1) and afterwards they have been sensitised with RuP dye. The sensitization was performed by overnight immersion in 10^{-4} M solution of the dye. This timespan was chosen to guarantee the saturation of the TiO_2 surface and a uniform dye distribution along the whole layer thickness (see next paragraph). For comparison of the spectroscopic and photoelectrochemical characteristics, other electrodes were prepared in parallel, according to the same experimental procedure but

excluding the ZP priming pre-treatment (from now on these samples will be indicated as “noZP” samples).

2.2.5.2. ToF-SIMS and spectroscopic characterisation

Both surface and along-the-depth ToF-SIMS characterisation of the RuP-sensitized ZP-TiO_2 were carried out. In Figure 50 the high mass region of the positive ions ToF-SIMS surface spectrum is presented, where a large number of peaks diagnostic of the presence of RuP are detected. In particular, the molecular ion signal M+ ($C_{41}H_{28}N_8PO_3Ru$) is visible at m/z 813, as well as the two fragment ions M-O^+ and M-PO_3^+ at m/z 798 and 735 respectively. Another intense peak is present at m/z 425, corresponding to the molecular fragment $C_{22}H_{16}N_3Ru$, i.e. the tolyl-terpyridine ligand plus ruthenium .
The same representative peaks are found on the surface spectra of the noZP analogous samples (not reported here).

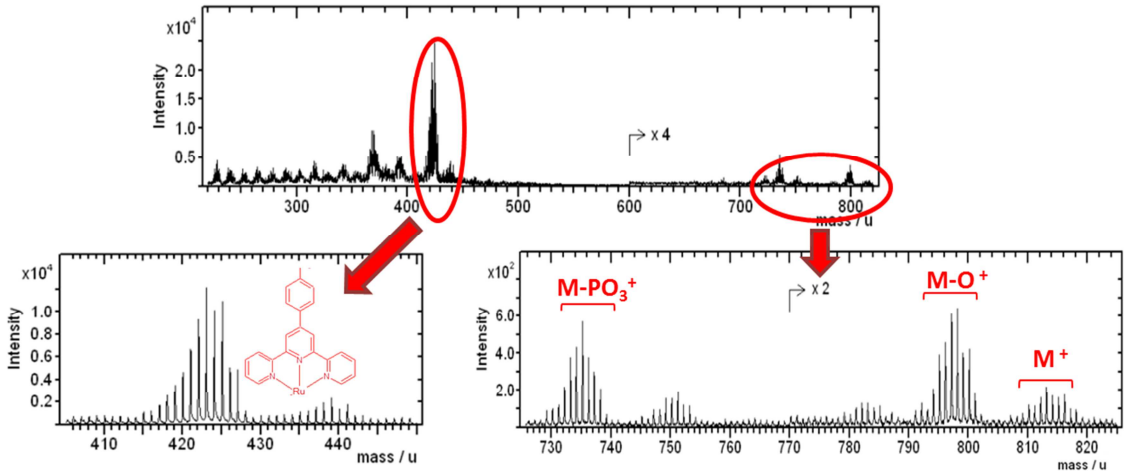

Figure 50: High mass region of positive ToF-SIMS spectrum, with details showing diagnostic RuP dye mass peaks.

It must be pointed out that the dye-related peaks in the mass spectra are due to the presence of these molecules chemically bound to the oxide substrate, given the fact that numerous washing cycles after each step of the preparation procedure ensure the elimination of physisorbed substances from the surface.
ToF-SIMS depth profiles of RuP-sensitised ZP-TiO_2 were acquired in order to monitor the distribution of the dye along the depth. In the dinamyc SIMS mode

used for depth profiling however, the molecular information is lost, only elemental and small cluster signals can be detected. The negative ions depth profile (Figure 51) reveals that the sensitization procedure (monitored by following Ru^- signal intensity), as well as ZP-priming, involved the entire thickness (several micrometres) of nanostructured TiO_2 substrate. In order to ensure the complete saturation of the whole mesoporous titania layer, the sensitization process was studied by measuring the depth profiles of samples prepared at different times of immersion in the RuP solution (respectively 45 minutes, 3, 5 and 16 hours). In all these samples, Ru^- signal shows a fairly constant intensity along the whole thickness (as exemplified in Figure 51 in the case of the five hours treatment) that is approximately parallel to that of phosphate and zirconium-related signals. By plotting the Ru^- profiles area (normalised to the matrix signal TiO^-) as a function of the time of immersion in RuP solution (Figure 52), we find that the plateau (indication of surface saturation) is reached after about 300 min of immersion in the dye solution.

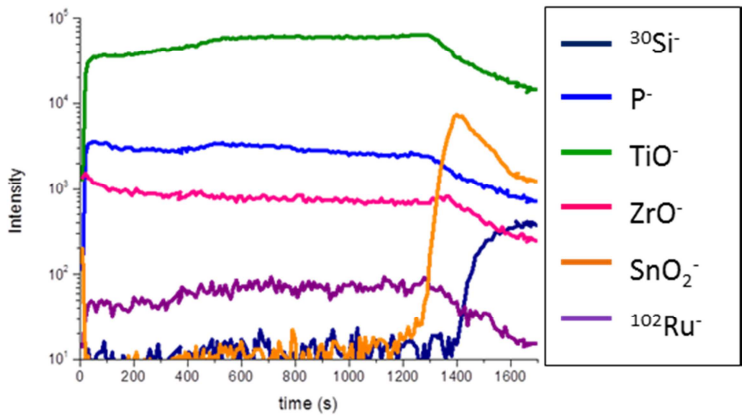

Figure 51: negative ions ToF-SIMS depth profile for nanostructured RuP-sensitized titania electrode, prepared by five hours immersion in the solution of the dye.

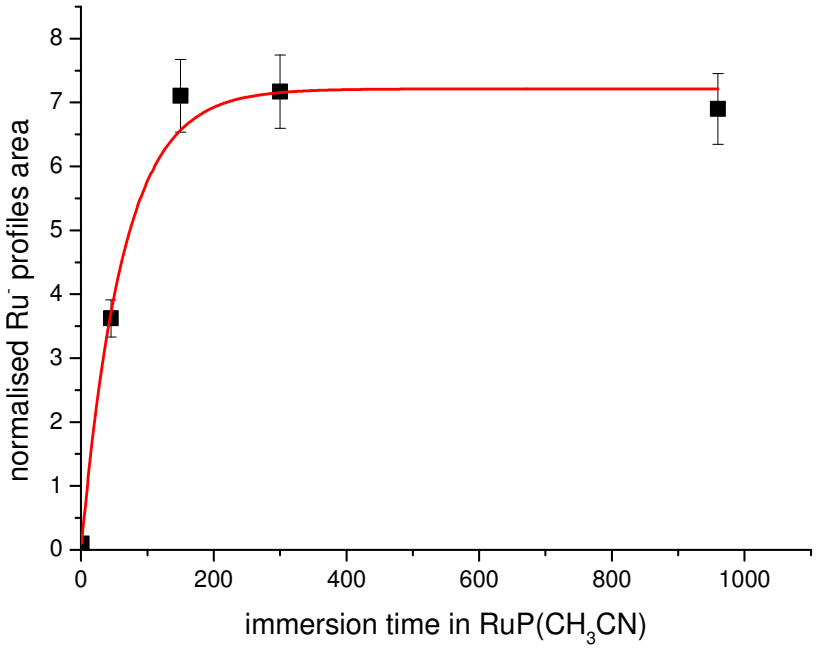

Figure 52: integrated ruthenium profile areas (Ru- signal normalized to matrix TiO- signal) as a function of the immersion time in RuP solution.

The absorption spectrum of the ZP-primed TiO_2 electrode after sensitization with RuP is shown in Figure 53 (continuous line), in comparison with the spectrum of the noZP sample. The spectrum is dominated by the MLCT band typical of Ru-polypyridyl compound located at 490 nm. It is clear that the ZP electrode shows higher absorbance, evidence of a greater amount of dye loaded on the primed substrate, with respect to the noZP one. This data is consistent with that arising from photoactive-dye anchoring onto flat TiO_2 (see paragraph 2.2.4). Given the perspective application of these samples, and in order to gather preliminary information about the anchoring stability of RuP onto the oxide substrate with respect to hydrolysis, the ZP and noZP sensitised samples were immersed for 24 hours in an aqueous solution at pH 5.7, and afterwards the amount of dye remained at the electrode surface was evaluated by UV-Vis spectroscopy. The comparative absorption spectra (as-prepared and after the aqueous treatment) are reported as well in Figure 53. A greater decrease of the absorbance is noticed for noZP sample with respect to the ZP one, respectively ca. 60% and 20%. This data is consistent with the previously discussed results

of relative stability tests (see paragraph 2.2.4), and it is a clear indication of improved binding stability of the phosphonic dye on ZP-TiO_2 with respect to bare TiO_2.

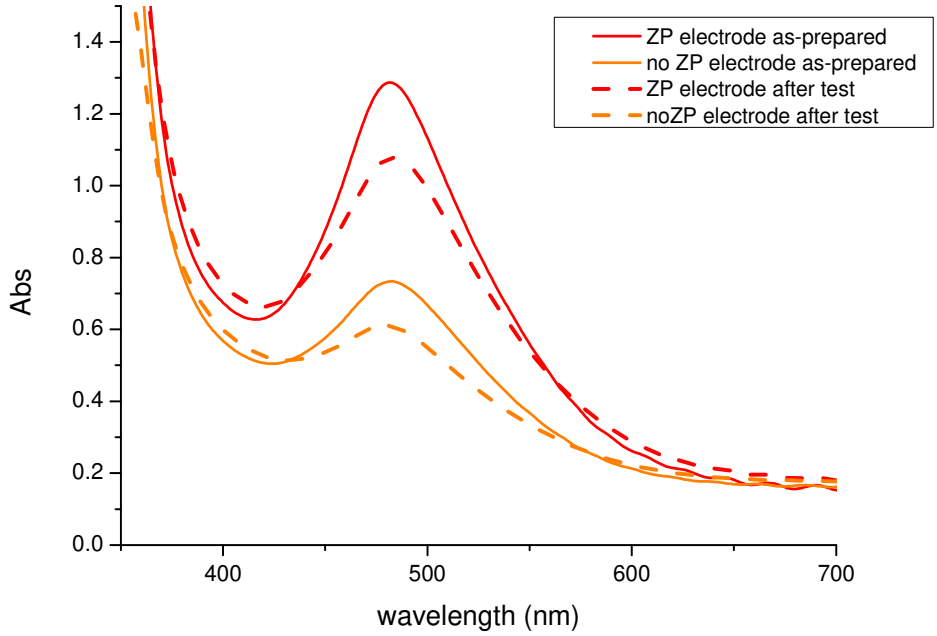

Figure 53: absorption spectrum for ZP and noZP photoanodes, as-prepared (continuous line) and after 24 hours of immersion in pH 5.7 aqueous solution (dashed line).

Summarising, ToF-SIMS data indicate a uniform distribution of the dye along the thickness of the nanostructured titania and from UV-Vis data it can be concluded that the new ZP-photoelectrode achieves a higher amount of dye loading with respect to a titania substrate with no ZP-priming. This is a positive aspect in view of the application in a real dye-sensitized cell, considering that the greater the absorption, the greater the light harvesting efficiency and the greater the performances). Moreover, the ZP-platform appears to be beneficial for the anchoring stability towards hydrolysis.

2.2.5.3. Photoelectrochemical measurements on dye-sensitized ZP-TiO_2

In order to evaluate the feasibility of using the RuP-sensitized ZP-titania electrode for application in "real" dye-sensitized cells, useful information can be extracted from the photoelectrodes electrical characteristics, namely the generated photocurrent, the open circuit voltage, the stability of the electrode under irradiation, etc… All the above mentioned parameters are fundamental for the functionality of the real device. For this reason, in collaboration with the research group of prof. Bignozzi (University of Ferrara), photoelectrochemical measurements were carried out on nanostructured ZP-TiO_2 electrodes, sensitized with the RuP dye. Measurements on the non-primed TiO_2 samples were carried out as well for comparison.
J-V characteristics were acquired in $NaClO_4$ 0.1 M at pH 3, under simulated solar irradiation (see "Materials and Methods" for details). The J-V curves are reported in Figure 54. The maximum generated photocurrent is lower than 0,5 μA in both kind of electrodes, being smaller in the case of ZP-electrode with respect to the noZP one. The low generated photocurrents obtained are consistent with the IPCE (Incident Photon-to-Current Efficiency) measurements reported in Figure 55. IPCE is and indicator of the quantum efficiency of a solar device and indicates the amount of current that the system produces when irradiated by photons of a particular wavelength. The low IPCE values reported in the plot of Figure 55 (less than 1% over the whole wavelength range considered) indicate a poor efficiency in the photocurrent generation (i.e. most probably due to poor electron injection from the excited state of RuP dye to the titania conduction band). However, we must note that the IPCE at a given voltage for the ZP-photoelectrode is appreciably greater with respect to the noZP one, and this would indicate a greater quantum efficiency at the given voltage. It should be pointed out that the apparent inconsistence between the JV outcome (i.e. poorer performances of ZP electrode) and the IPCE data (i.e. greater performances of ZP electrode) is only due to the experimental conditions adopted for the data acquisition: the JV characteristics are collected after several scan cycles, until a stable photocurrent value is reached; on the contrary the IPCE plot are acquired by measuring the J under shuttered light (while varying the wavelength) and taking the transient of photocurrent, which by definition have the maximum value.

Giving the fact that the obtained photocurrents (for both electrodes) are not high enough to allow for a correct comparison between the two kind of electrode in terms of performances, the J-V characteristic were acquired again with the assistance of a sacrificial agent (LiI). Actually, in the context of this thesis work, the main goal is that of understanding and evaluate the effect of the zirconium phosphate layer at the oxide on the photoelectrochemical properties of the final electrode, rather than the suitability of a particular dye. In this context the use of a sacrificial agent, which "helps" the charge injection processes, does not alter the information about the efficiency comparison between ZP- and noZP-electrodes. In other words, if the ZP-layer actually acts as a barrier to the dye-oxide electrical communication, no charge injection can take place, neither with nor without sacrificial agent support.

New J-V curves were collected in 0.1 M LiI in acetonitrile. LiI is a "hole scavenger", so it should promote charge injection and regeneration of the dye, thus enhancing the generated photocurrent. The J-V curves, acquired under shuttered illumination in presence of LiI are presented in Figure 56. In these conditions, the ZP electrode shows greater efficiency with respect to the untreated one, because it reaches higher photocurrent values and higher open circuit voltage, indicating a minimization of the recombination processes that usually compete with the charge injection and limit the performances of the electrode. The greater amount of dye adsorbed on the ZP electrode (see Figure 53) could play a role in the enhancement of the performances; in this case the increment in photocurrent should vary linearly with respect to the dye loading. Given that in the case under investigation there is not such a proportionality,[207] the hypothesis that the increase in J is due to the ZP treatment is strongly suggested, although other explanations cannot be completely excluded.

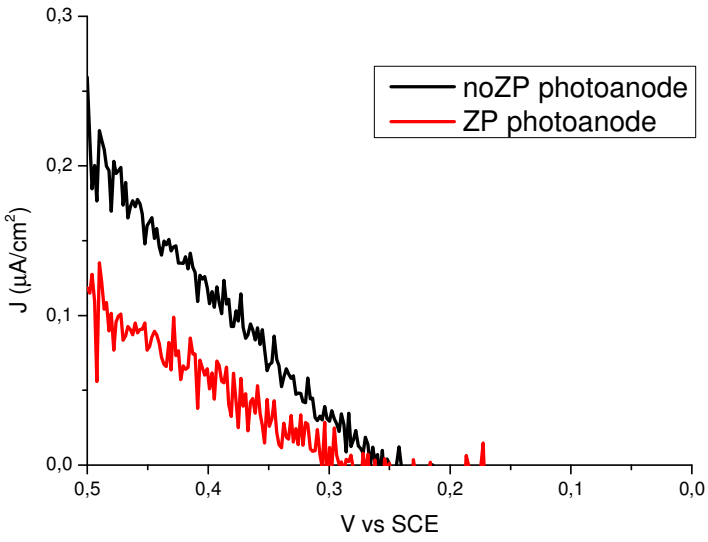

Figure 54: J-V curve for RuP-sensitized ZP and noZP electrodes.

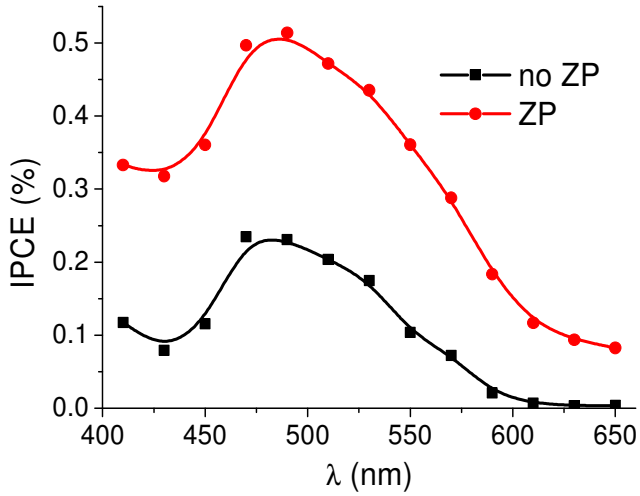

Figure 55: IPCE for RuP-sensitized ZP-titania electrodes and noZP ones at 0.5 V.

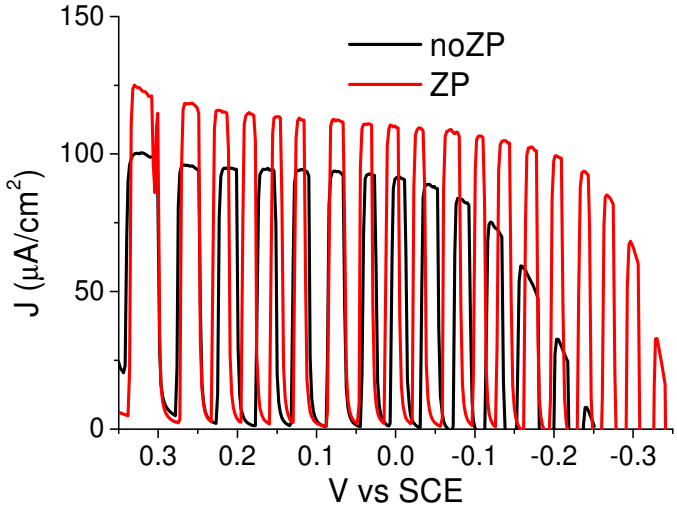

Figure 56: J-V curves in LiI 0.1 M, under shuttered illumination, for RuP-sensitized ZP-TiO_2 electrodes and noZP ones.

The poor photocurrent generation for RuP-sensitized TiO_2 electrodes deserves some further comment. Very recently, Ronconi et. al. [206] reported the results of photoelectrochemical and transient absorption spectroscopy measurements, which indicate that the low photocurrent observed on bare nanostructure titania electrodes is due to inefficient oxidative quenching of the excited state RuP* of the dye. In other words, charge injection from the excited state of the dye to the conduction band of TiO_2 (i.e. the oxidative quenching of RuP*) is not the preferred deactivation pathway, due to a modest oxidation potential of the excited state of the dye. Instead, reductive quenching of RuP* to RuP^- is the most thermodynamically favourable mechanism, following a so-called "antibiomimetic pathway", in contrast with the "biomimetic pathway" proceeding through the classic oxidative quenching (see Figure 57 for a scheme of the two mechanisms).

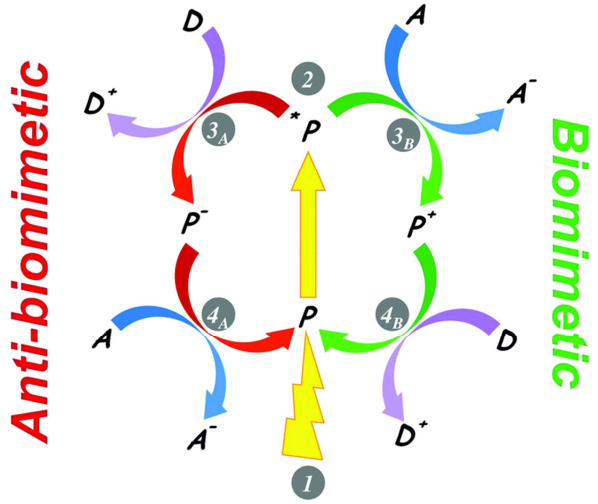

Figure 57: scheme for biomimetic and antibiomimetic pathways for charge transfer photosensitiser quenching; P: photosensitiser, D: donor, A: acceptor. Reprinted with permission from ref. [206], copyright 2016 The Royal Society of Chemistry.

However, the same authors observed a clear charge injection and good photocurrent generation for RuP-sensitized nanostructured SnO_2 electrodes in presence of LiI. In this case, the significant improvement of charge injection is ascribable to increased driving force for RuP* oxidative quenching to the low lying SnO_2 conduction band.

Given that measurements are necessary by using a dye-oxide systems whose components are more effectively able to "communicate", in order to assess without any doubt if the ZP priming has an actual positive effect on dye-sensitized electrodes, ZP-photoanodes sensitized with RuP were prepared and investigated.

In the next paragraph details about the preparation of ZP-SnO_2 photoanodes the results on RuP-sensitized ZP-SnO_2 photoanodes presented, concerning their composition and their photoelectrochemical properties.

2.2.6. Assembly of photoactive molecules on nanostructured ZP-primed SnO_2

The possibility of extending the ZP priming on SnO_2 nanostructured substrates was first tested. To this aim, 1 μm thick nanoporous SnO_2 were used (see materials and methods for details).
The priming procedure adopted was similar to the one already optimised for TiO_2 nanoporous electrodes, and consisting in the following steps:

1. One hour UV-O_3 treatment;
2. One hour immersion in $POCl_3$;
3. 24 hours immersion in $ZrOCl_2$ solution in ethanol.

After each step of the priming, several washing cycles are carried out, in order to eliminate the excess of physisorbed substances.

The ZP-primed systems were characterised by ToF-SIMS. The surface ("static") spectra (not reported here) show the signature of the ZP-platform presence, as already observed in the case of titania substrates. The depth profile (Figure 58) confirm that the priming involves the entire thickness of the nanostructured layer and demonstrate the feasibility of the ZP-priming also for SnO_2 nanoporous substrates.

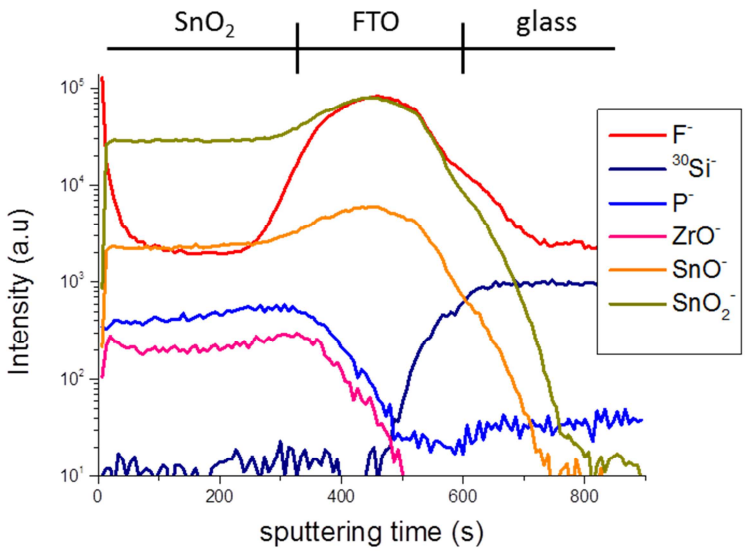

Figure 58: : negative ions ToF-SIMS depth profile of a nanostructured ZP-SnO_2 electrode.

Once the feasibility of ZP-priming was confirmed, RuP-sensitized ZP-SnO_2 electrodes were prepared, by immersion overnight in 10^{-4} M solution of the complex in acetonitrile. As for the case of titania photoelectrodes, for the comparison of the spectroscopic and photoelectrochemical characteristics, also "noZP" photoanodes was prepared, according to the same experimental protocol, but just excluding the ZP priming pre-treatment. The obtained samples were characterised by means of UV-Vis spectroscopy and ToF-SIMS.
The absorption spectrum of the ZP-primed SnO_2 electrode after sensitization with RuP is shown in Figure 59, in comparison with the spectrum of the noZP sample. It is clear that also in the case of SnO_2 surfaces, the ZP priming has a beneficial effect on the dye loading, as indicated by the greatest absorption of the ZP-electrode with respect to the noZP one.

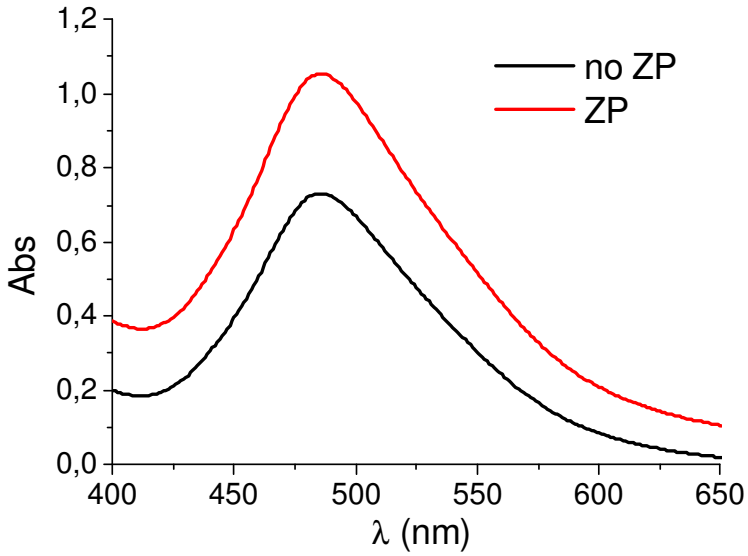

Figure 59: absorption spectrum for ZP and noZP SnO_2 photoanodes, sensitized with RuP dye.

The static ToF-SIMS spectra of the sample surface (Figure 60) show the clear signature of the presence of RuP complex, in a very similar way of what found in the case of RuP anchored on ZP-TiO_2 (see paragraph 2.2.5.2 and Figure 50).
The ToF-SIMS depth profiles (Figure 61) reveal that the sensitizer (probed by the Ru^- signal intensity), as well as ZP-priming, penetrated fairly homogeneously along the entire thickness of nanostructured SnO_2 substrate.

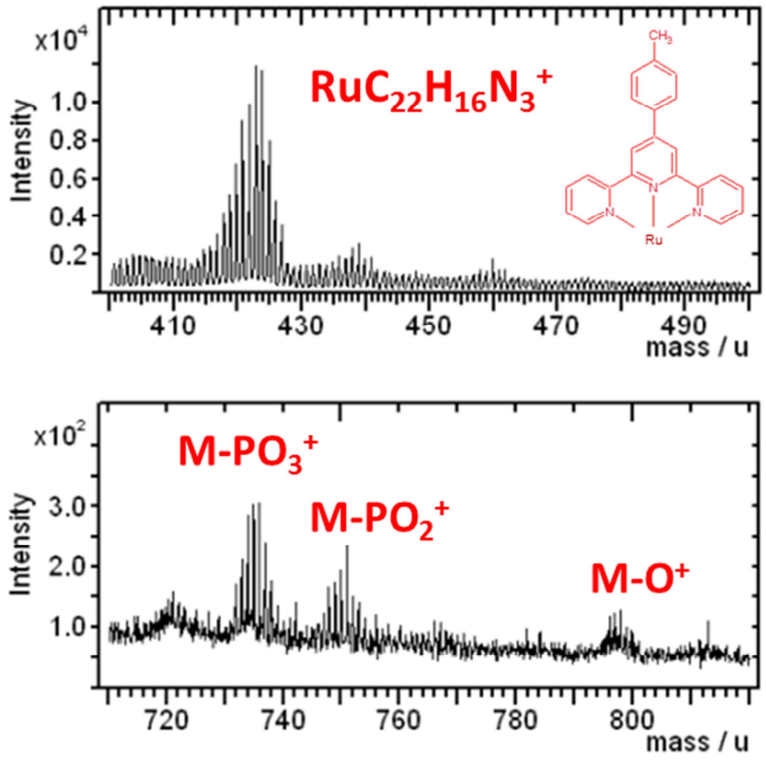

Figure 60: Details of the high mass region of positive ToF-SIMS spectrum for RuP-sensitized SnO_2 photoelectrodes showing diagnostic RuP dye mass peaks.

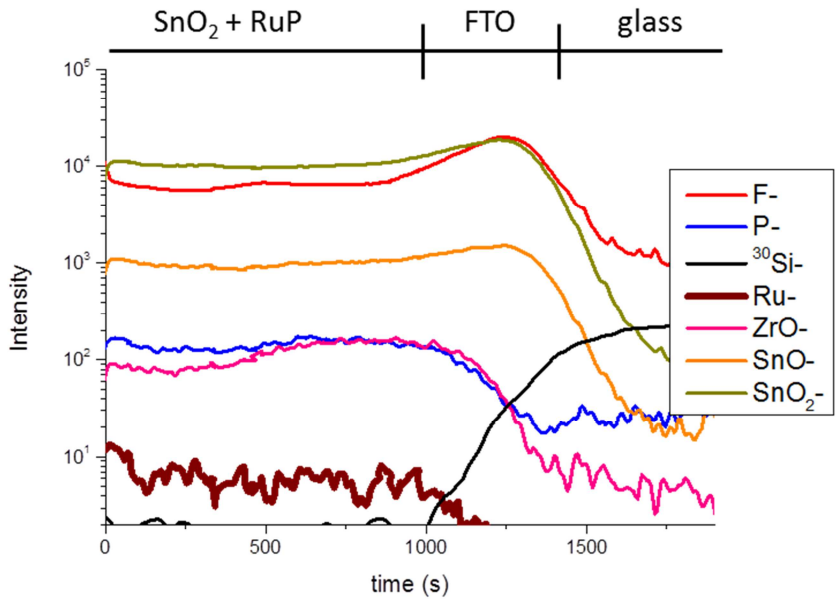

Figure 61: negative ions ToF-SIMS depth profile for nanostructured RuP-sensitized ZP-SnO_2 electrode.

J-V characteristics for ZP-SnO_2 photoanode and noZP one were acquired in 0.1 M LiI solution in acetonitrile, under simulated solar irradiation (details in "Material and Methods" section). The obtained J-V curves are reported in Figure 62. Higher photocurrent values are achieved, with respect to RuP-TiO_2 systems, for both ZP and noZP electrodes. In these conditions, a slightly higher open circuit voltage and a lower photocurrent at high potential are reached for the ZP photoelectrode. The higher V_{OC} value is a clear indication of a decrease in (unwanted) recombination reactions at the oxide surface, ascribable to the passivation of the electrode by the surface zirconium phosphate; at the same time, however, the slight decrease in photocurrent value would be index of less efficient dye-to-oxide charge injection.[96] These considerations were confirmed by J-V measurements carried out at increased LiI concentration (0.25 M). In these conditions we clearly see, from J-V plot (Figure 63) an increase of the Voc for the ZP-photoelectrode compared to the noZP one, coupled with a remarkable decrease of the generated photocurrent.
IPCE measurements at 0 V in LiI 0.1 M show similar trends for the two electrodes, with the ZP one being slightly more efficient (Figure 64). This is in very good agreement with the J-V characteristics data.

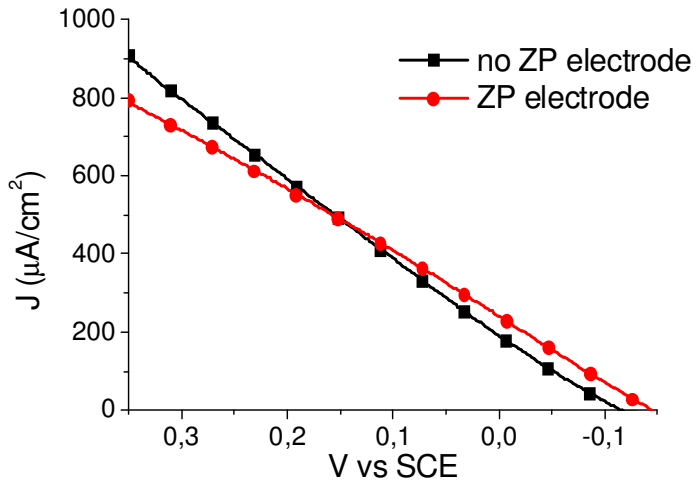

Figure 62: J-V curves for RuP-sensitized ZP and noZP SnO_2 electrodes, collected in 0.1 M LiI in acetonitrile.

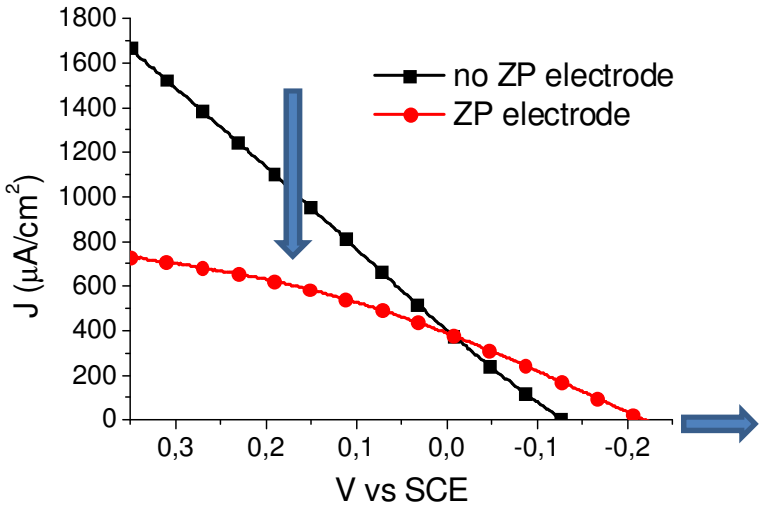

Figure 63:J-V curve for RuP-sensitized ZP and noZP electrodes, aacquired in 0.25 M LiI in acetonitrile.

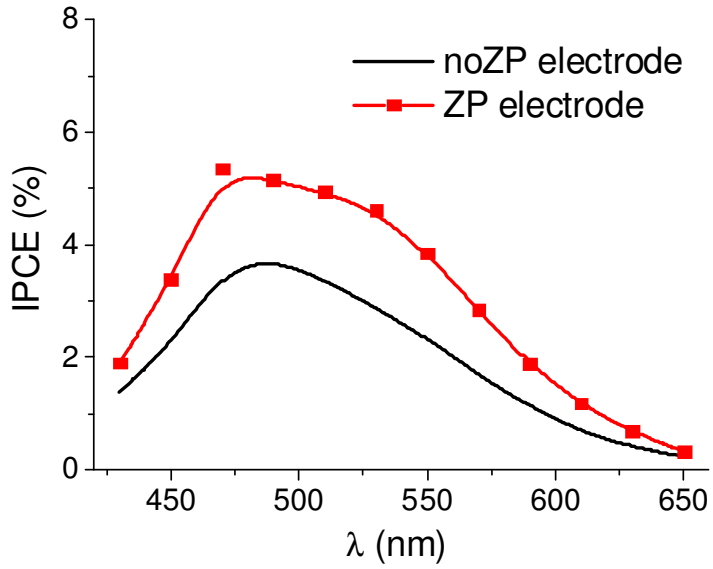

Figure 64: IPCE for RuP-sensitized ZP-SnO_2 electrodes and noZP ones at 0 V

2.2.7. Conclusions

The research work presented in this chapter dealt with investigation of some surface chemistry issues related to the modification *via* molecular anchoring of nanostructured oxide surfaces through the so-called ZP-priming approach. The application of ZP-priming was studied in order to investigate its capability of providing a stable anchoring platform for phosphonate-derivatised photoactive molecules on nanostructured titania surfaces, with perspective application in dye-sensitised electrodes for the development of solar energy conversion devices.

The stepwise priming protocol has been first studied on model flat TiO_2 substrates and then optimised for its application to nanostructured micrometers-thick TiO_2 surfaces. The success of the method in providing an uniform surface functionalisation along the entire oxide layer has been demonstrated by means of ToF-SIMS depth profiling. In particular, through extensive SIMS profiling measurements, the diffusion behaviour upon ZP-priming treatment of Zr(IV) throughout the nanostructured micrometer-thick TiO_2 layer has been studied with respect to different priming experimental conditions. It was possible to understand that a classic diffusion mechanism (diffusion from infinite source) governs the migration of Zr from an aqueous zirconyl chloride solution within the nanostructured layer, and also to identify the best experimental condition for enhancing the diffusion of zirconium until the desired uniform coverage the micrometric TiO_2 layer is reached (i.e. $ZrOCl_2$ in ethanol solution).

The anchoring stability of phosphonate-based photoactive systems on ZP-primed titania surfaces towards thermal stresses in organic solvents and hydrolysis has been studied and compared to the one of the same dye on bare TiO_2. Within the framework of the experimental approaches applied for testing, the anchoring of phosphonate-derivatised molecules on ZP-TiO_2 turns out to be stronger and more stable than the anchoring on bare titania surfaces. Also, the ZP-priming allows to obtain an higher surface density of anchored molecules.

ZP-priming was successfully applied to the assembly of a phosphonic photoactive molecule (dye RuP) on nanostructured titania electrodes. These were studied by means of Time-of-Flight secondary ion mass spectrometry and by UV-Vis spectroscopy, and it was shown that sensitization of ZP-primed nanostructured TiO_2 substrates leads to uniform impregnation of the oxide layer, as along with an higher and more robust dye-loading with respect to bare titania surfaces. Photoelectrochemical measurements on sensitised ZP-titania

demonstrate that the ZP priming has no significant detrimental effect on the electrode performances but, on the contrary, there is evidence of oxide surface passivation that seems to hinder charge recombination, with benefits for the electrode performances.
Finally, the ZP-priming was successfully extended to another nanostructured semiconductor oxide, namely SnO_2. RuP-sensitized ZP-SnO_2 electrodes were prepared and, analogously to ZP-TiO2, higher dye load and the sensitization of the entire nanostructured oxide layer were achieved, as showed by UV-Vis and ToF-SIMS measurements, and the same passivation action coupled with no important detrimental effect on the electrode functionality emerged from the photochemical characterisation.

The increase in molecular binding stability, the non-detrimental effect on the electrical "communication" between molecule and oxide, and the higher molecular loading as a consequences of ZP-priming, allow to propose this priming methodology as a promising solution for the preparation of robust molecular films on oxide surfaces whenever the anchoring stability of the molecules is crucial for their use in real molecular devices (not necessarily in dye-sensitised cells).

2.3. Molecular wires on ZP-primed FTO

In the first chapter, the interest in conductive molecular wires for nanoscale molecular electronics has been discussed. For the fabrication of molecular solid-state circuits and devices it is essential to properly integrate the desired molecules on a convenient conductive or semiconductive substrate. The molecule-surface connection must be strong and stable in time, and it has to guarantee a proper electrical "communication" between the functional system anchored and the surface itself. Therefore, surface modification techniques purposely tailored are necessary in order to achieve this goal.

During this thesis work, the use of ZP-primed oxide surfaces as platform for conductive and photoactive molecular wires growth was investigated. The experimental approach for the assembly of the wires was based on the use of metal ions as "linkers" between the terpyridinic units of a polypyridyl ruthenium compound, namely the Ru(II)-bis[4′,4′′′′-(1,4-phenylene)bis(2,2′:6′,2′′-terpyridine)], henceforth indicated as $RuDT_2$ (Figure 65). This molecule was synthesised by the research group of prof. G. Hanan, of the University of Montreal. The complexation reaction of terpyridine moieties with bivalent metal ions, in particular Fe(II), is fast and easy to carry out in very mild experimental conditions, and leads to very stable compounds with structure $M(tpy)_2$.

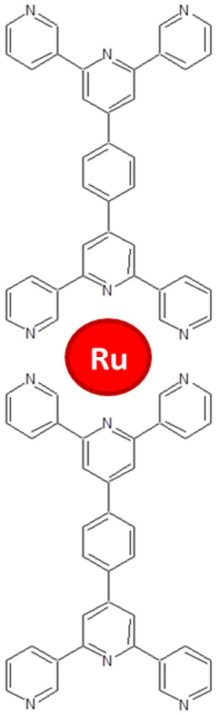

Figure 65: Molecular structure of $RuDT_2$.

The molecule $RuDT_2$ is particularly interesting for perspective application in nanoscale electronics, especially in Photochemical Molecular Devices (PMDs) development. The $Ru(tpy)_2$ core of the molecules is actually a redox photoactive centre, which can undergo reduction-oxidation processes and photoinduced charge separation upon irradiation with visible light. Furthermore, the two free terpyridinic units can be exploited for further metal-coordination reactions, giving the possibility of building more complex aggregates (e.g. molecular wires). Lots of research work has proved that $Ru(tpy)_2$-based complexes can successfully be used as photosensitisers in covalently-linked multicomponent systems.[175]
Polymetallic molecular wires with multiple $M(tpy)_2$ units have already been grown on gold surfaces, with the resulting molecular films showing outstanding electrical properties.[181, 208] However, the possibility of assembling these kind of multi-layered molecular systems onto transparent conductive oxides is still quite unexplored. Just some examples of M-polypyridyl triads [13, 209] and terpyridine-functionalised perylene bisimide metal-complexes on ITO surfaces [195] can be cited. Therefore the work carried out during this thesis can be seen as a contribution to the understanding

and development of the assembly and "functional" behaviour of these systems as well as the possibility of applying them in the technologically-relevant framework of coupling special properties of some functional molecules to the favourable optoelectronic properties of TCOs, for the obtainment of improved solid-state systems exploitable in nanoscale molecular (opto)electronics.

2.3.1. Synthetic approach for the stepwise growth of $RuDT_2$ wires

In order to provide an anchoring site for $RuDT_2$ molecules on FTO surface the latter, after a ZP-priming, has preliminarily been modified with a monolayer of terpyridinic units. The complexation of Fe(II) with a terpyridine group at the surface and one of the two tpy-units of $RuDT_2$ was then carried out to "glue" a layer of $RuDT_2$ onto the oxide surface, by means of a stepwise layer-by-layer approach. This kind of approach allows, in principle, to grow multi-layered architectures directly at the surface via subsequent complexation steps; moreover, it is possible to tailor the growth in terms of number of layers, ligands sequence or chemical nature.

For the tpy-monolayer deposition a synthetic strategy developed by Spampinato et. al was exploited.[103] The experimental approach consists in the anchoring of the ditopic molecule 4-(2,2': 6'-2''-tepryridine-4-yl)benzenephosphonic acid (Figure 66, henceforth PPTP) on ZP-primed oxide surfaces. The PPTP anchoring on ZP-oxide through the phosphonic groups guarantees a stable binding and actually gives a monolayer of free terpyridinic units, the latter being available and for further coordination reaction directly at the surface.

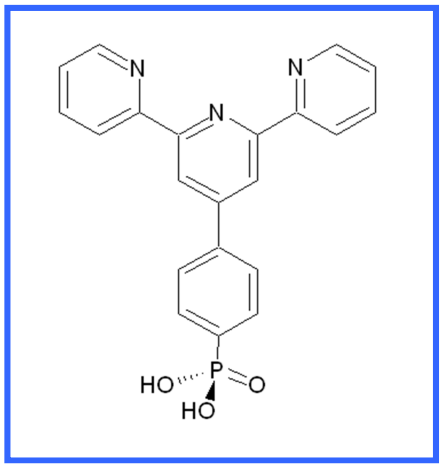

Figure 66: molecular structure of PPTP.

First of all, ZP priming on FTO was carried out, according to the procedure sketched in Figure 67, and already discussed previously in this text (see paragraph 2.2.1). The priming leads to the achievement of a monolayer of zirconium phosphate at the surface, that will able to bind a further phosphate or phosphonate group at the position that, in the scheme of Figure 67, are hold by chlorine.

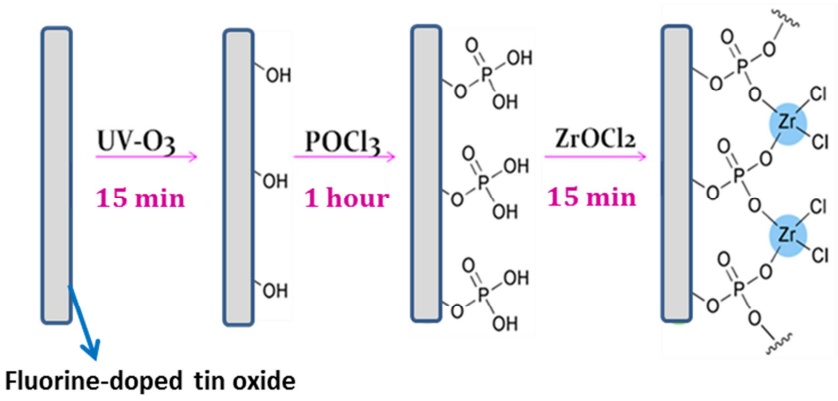

Figure 67: reaction scheme for ZP-priming procedure on FTO surface.

Surface anchoring of PPTP was performed with a protection-deprotection procedure (Figure 68). [103] PPTP was first reacted with a stoichiometric amount of Zn(II) trifluoromethanesulphonate in a DMF-H_2O 1:1 mixture, to

afford a solution of the complex $Zn(PPTP)_2$ (10^{-4} M). ZP-FTO was incubated in this solution for 24 hours, and afterward rinsed with water. The obtained sample was finally dipped in HCl 0.1 M aqueous solution for 15 minutes, in order to dissolve the $Zn(PPTP)_2$ complex and restore the terpyridinic functionality of the molecules anchored at the oxide surface.

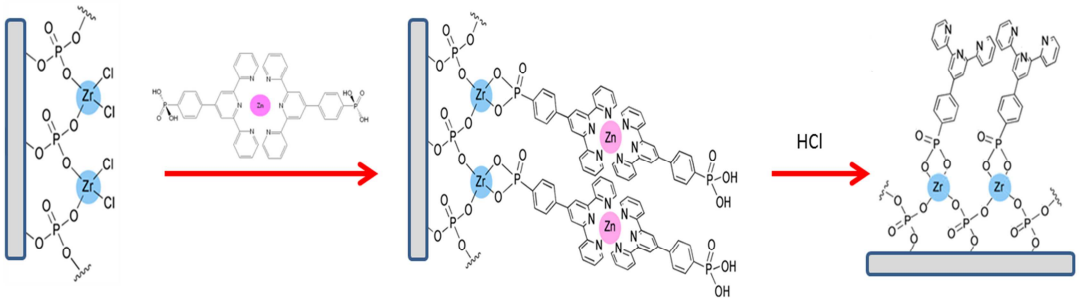

Figure 68: reaction scheme for PPTP anchoring on ZP-FTO *via* protection-deprotection approach.

Once the ZP-FTO surface was functionalised with a monolayer of terpyridinic units, the sample was dipped for 90 seconds in a $FeSO_4 \cdot 7H_2O$ solution (10^{-4} M, H_2O-EtOH 1:1 mixture), then rinsed with water and subsequently immersed for 15 minutes in a 10^{-4} M DMF solution of $RuDT_2$. In this way a complex between Fe(II) at the surface and a terpyridine-unit of $RuDT_2$ would assure the anchoring of the ruthenium complex by means of $Fe(tpy)_2$ complex formation. The last two reaction steps were then repeated iteratively in order to grow the molecular wires of the desired length (Figure 69). It must be pointed out that after each reaction step the samples are carefully rinsed with the appropriate solvents, in order to eliminate residual molecules eventually physisorbed at the surface.

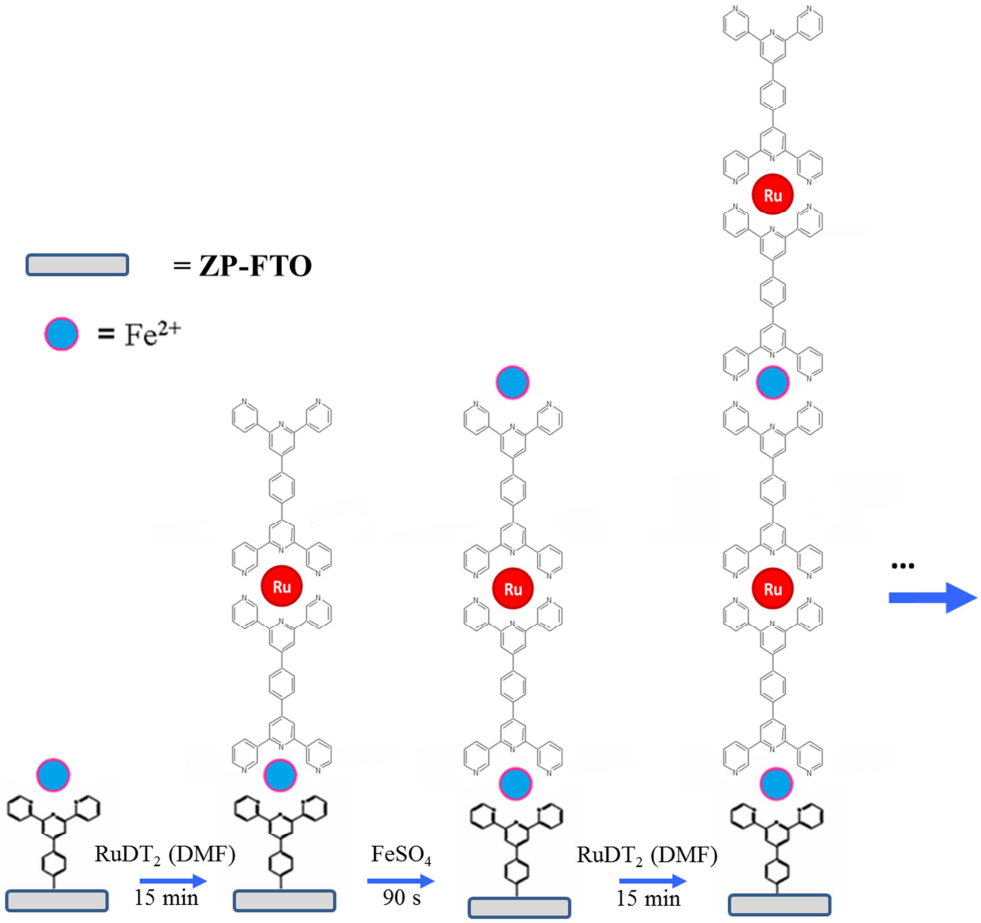

Figure 69: reaction scheme for the stepwise growth of $RuDT_2$ molecular wires.

According to the above described experimental set up, molecular wires of different length were prepared. Given the molecular structure of $RuDT_2$, after each complexation reaction between Fe(II) and $RuDT_2$ a "bilayer" is formed at the surface having Fe-DT-Ru-DT sequence (where DT is 4′,4‴′-(1,4-phenylene)bis(2,2′:6′,2″-terpyridine) unit); this Fe-DT-Ru-DT unit will be indicated, later on, simply as Fe-$RuDT_2$.

Each sample was first studied by means of Time-of-Flight Secondary Ion Mass Spectrometry (ToF-SIMS) and UV-Vis spectroscopy, to gain information about the multi-layered wires composition and growth. Then, preliminary studies on the electrical conduction and charge transport mechanism of these wires were performed by means of EGaIn junction measurements.

2.3.1.1. ToF-SIMS investigation

The formation of the Fe-terpyridine complex and the consequent anchoring of $RuDT_2$ was investigate by ToF-SIMS measurements performed in in static mode, that assures a large amount of molecular information from the uttermost layers of a solid sample.[210] Combined with the extreme sensitivity and high mass resolution, this makes ToF-SIMS a very powerful tool for monitoring of each reaction step of the surface engineering process we are studying.

First of all, ToF-SIMS spectra of the FTO substrate after the ZP-priming were acquired. Two portions of the positive ions mass spectrum are reported for in Figure 70, containing several peaks diagnostic of the ZP-platform, namely Zr^+ (90 uma), ZrO^+ (106 uma), ZrO_2^+ (122 uma), $ZrPO_3^+$ (169 uma), $ZrPO_4H_2^+$ (187 uma) and $ZrPO_5H_2^+$ (203 uma) (for the sake of simplicity, only the mass of the most abundant isotopic combination is indicated). In the mass region interval 80-135 also the characteristic "staircase" isotopic distribution of tin (main isotope $^{120}Sn^+$), coming from FTO substrate, is clearly visible.

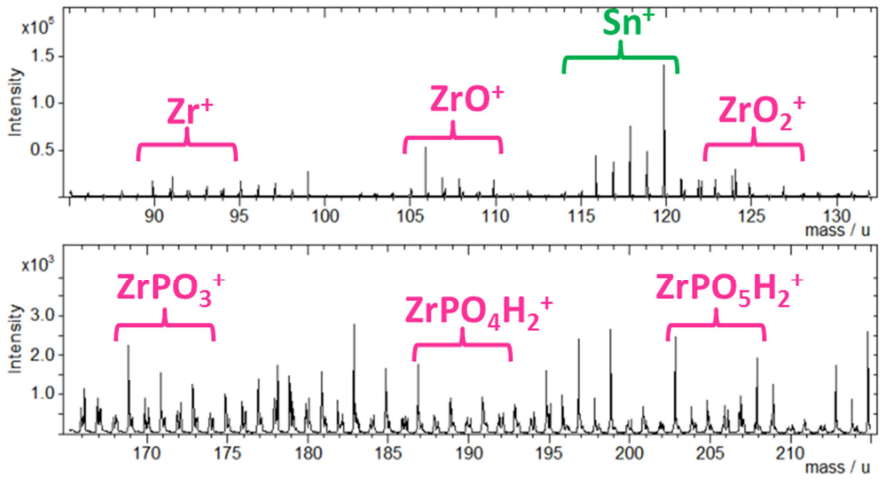

Figure 70: detail of ToF-SIMS positive ions spectrum of ZP-FTO.

The anchoring of the $Zn(PPTP)_2$ onto ZP-FTO, was studied by measuring the ToF-SIMS spectra both before (Figure 71a) and after (Figure 71b) the complex deprotection step. Peak distributions characteristic of PPTP molecule are present in both spectra, namely $C_{21}H_{14}N_3PO_2^+$ (372 uma, PPTP-O quasi-molecular ion) and $C_{21}H_{14}N_3^+$ (308 uma, the PPTP unit missing of the

phosphonic group). In spectrum a) the peak at mass 434 uma corresponds to the fragment $C_{21}H_{14}N_3PO_2Zn^+$, diagnostic of the anchored zinc complex; such fragment, as well as any other zinc-containing fragments, are absent in spectrum b), clearly indicating that the deprotection of the complex and the incorporation of the terpyridinic functionality at the ZP-FTO surface were successful.

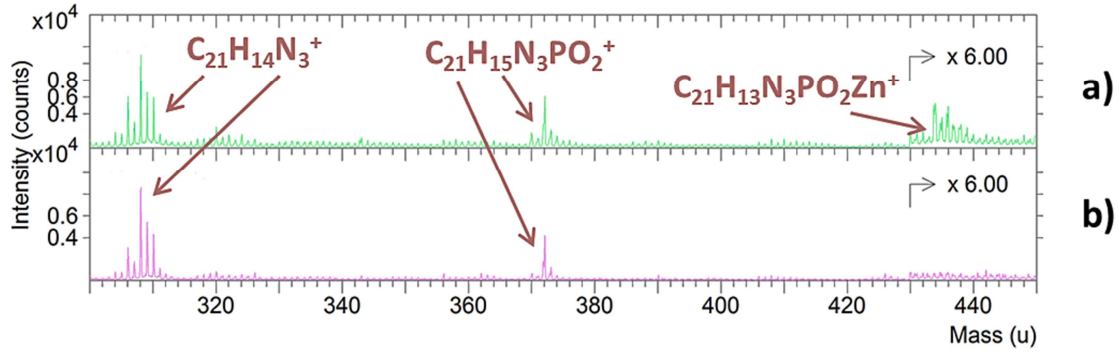

Figure 71: Relevant portion of the positive ions SIMS spectrum of ZP-FTO, a) after the anchoring of $Zn(PPTP)_2$ and b) after the deprotection of the anchored complex.

In Figure 72 two details of the high mass region ToF-SIMS spectrum are shown, for a ZP-FTO sample after the anchoring of PPTP and the stepwise deposition of 5 Fe-$RuDT_2$ units, that are thought to form an assembly of molecular wires.. Here several peak distributions due to large fragments of $RuDT_2$ molecule are present, like $C_{36}H_{24}N_6Ru^+$ (642 uma) and $C_{36}H_{24}N_6RuO^+$ (658 uma). The $RuDT_2$ molecular ion is also present on the spectrum, both as mono-ionised $(C_{36}H_{24}N_6)_2Ru^+$ (m/z 1182) and double-ionised $(C_{36}H_{24}N_6)_2Ru^{++}$ (m/z 591). Another interesting peak is that at m/z 598, pertaining to the fragment $C_{36}H_{25}N_6Fe^+$. The intensity of this peak is evidently quite low with respect to the intensity of the peaks of $RuDT_2$ fragments; this can be explained by making two considerations. First of all, ToF-SIMS provides information about the very upper layer of the surface (sampling depth of the order of nanometre, due to the low mean free path of secondary ions), so the signals relative to Fe-tpy or Fe-DT fragments are "shielded" by the above $RuDT_2$ layer. This signal attenuation argument, of course, holds also for all the other portions of the organic layers progressively closer to the oxide surface. Secondly, the intensity of peaks in ToF-SIMS spectra is not easily quantified, because it is strongly dependent on the fragment ion formation, which in turn is

strongly affected (among others) by the nature of the fragment and by the chemical environment in which it is produced. A reliable method for obtaining quantitative information about the the molecular wires growth is provided, in the case of the systems under investigation, by of UV-Vis spectroscopy, as described in the next paragraph.

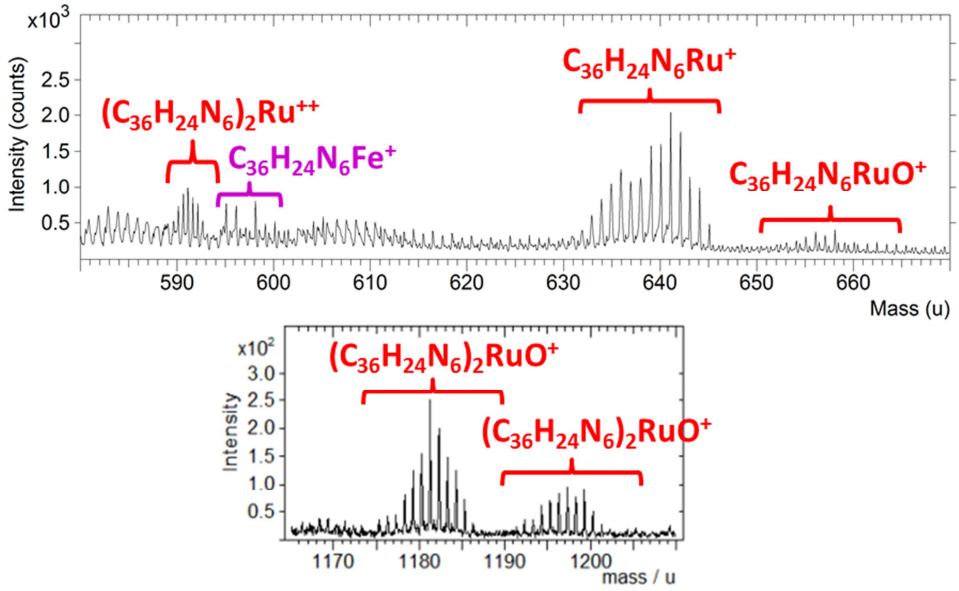

Figure 72: High mass region details of the positive ions spectrum of ZP-FTO functionalised with PPTP and 5 layers of Fe-RuDT$_2$.

2.3.1.2. UV-Vis characterisation

Bis-terpyridinic complexes of Fe(II) and Ru(II) exhibit strong absorption in the visible region of the spectrum, with absorption coefficients of the order of 10^4 M^{-1} cm^{-1};[174, 175] this property allows for a spectroscopic characterisation of Fe(tpy)$_2$- and Ru(tpy)$_2$-based compounds.

In the case of Fe-RuDT$_2$ wires on ZP-FTO-PPTP platform, UV-Vis analysis was used to quantitatively monitor the growth of the wires after each deposition step. A preliminary study of the absorption spectra of the ligands in solution was carried out, namely on RuDT$_2$ solution in DMF (~10^{-4} M) and

$FeDT_2$ solution in $CHCl_3$ (~10^{-4} M, prepared by mixing stoichiometric quantity of $FeSO_4 \cdot 7H_2O$ and 4′,4‴′-(1,4-phenylene)bis(2,2′:6′,2″-terpyridine)). The absorption spectra acquired in the visible region for the two solutions are reported in Figure 73. $RuDT_2$ spectrum shows the absorption band at 490 nm, due to the MLCT transition characteristic of $[Ru\text{-}(tpy)_2]^{2+}$ complex, while that of $FeDT_2$ has the MLCT band at 575 nm.

In Figure 74 the absorption spectra for a sample of ZP-FTO-PPTP are reported, each of them measured after the anchoring of an increasing number of Fe-$RuDT_2$ units.. There is a clear increment of the intensity of the two MLCT bands upon subsequent deposition of Fe-$RuDT_2$ layers, ad this is diagnostic of an increase of number of photoactive $M(tpy)_2$ units at the substrate surface. In addition, the linear correlation between the MLCT bands intensity and the nominal number of layers deposited (Figure 75) indicates that a constant number of $M(tpy)_2$ complexes is formed at each deposition step.

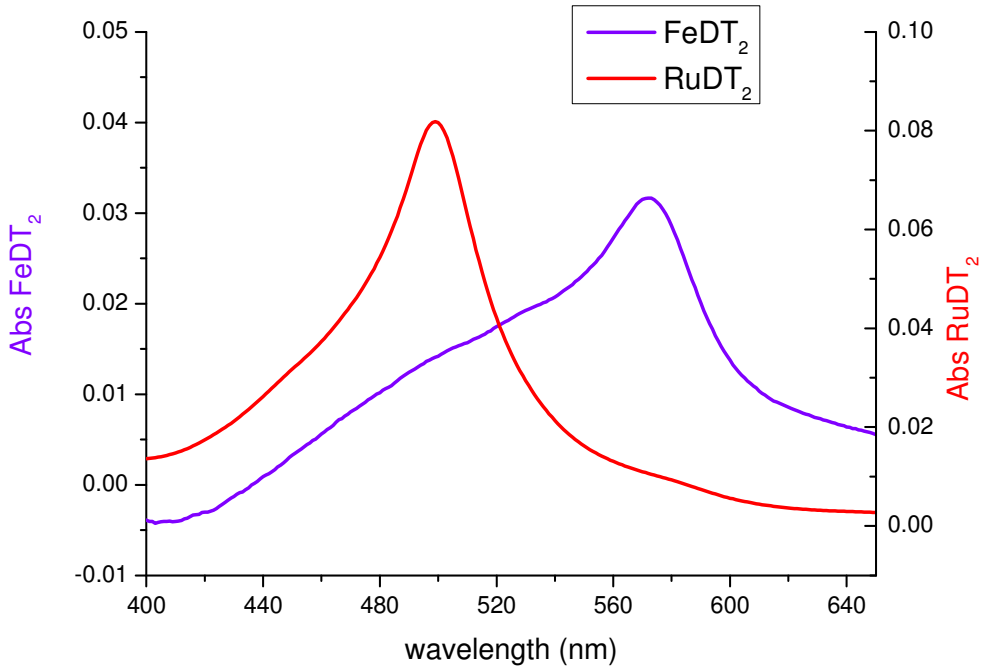

Figure 73: absorption spectra of $RuDT_2$ and $FeDT_2$ solutions (~10^{-4} M).

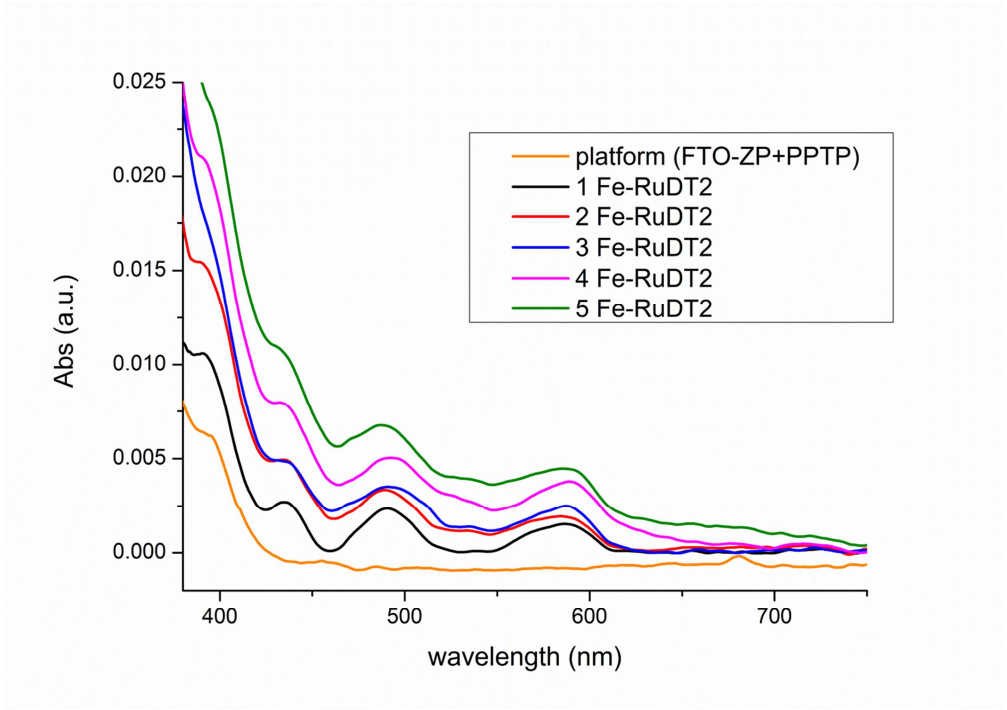

Figure 74: Absorption spectrum for ZP-FTO-PPTP sample acquired at increasing number of Fe-RuDT$_2$ layers.

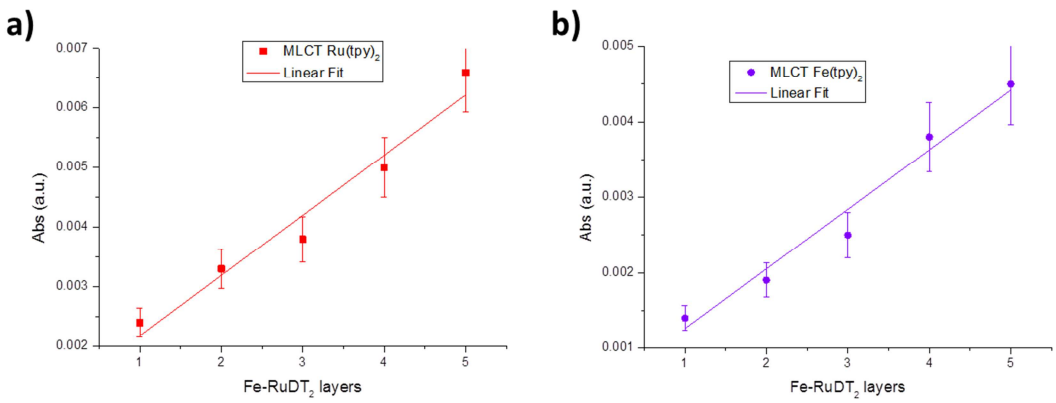

Figure 75: Optical density as a function of the surface number of Fe-RuDT$_2$ layers for a) Ru(tpy)$_2$ MLCT band and b) Fe(tpy)2 MLCT band.

2.3.1.3. EGaIn electrical measurements

In order to gain some insights about the electrical behaviour of Fe-RuDT$_2$ molecular wires, measurements were carried out by using a liquid metal junction made with the eutectic Ga-In alloy (referred as EGaIn). The experimental set-up and a scheme of the EGain-FeRuDT$_2$-FTO junction are sketched in Figure 76. For the acquisition of the J/V characteristics, an EGaIn-drop, suspended from a syringe, was used as top-electrode material and put in contact with the sample by means of a micromanipulator. The contact area between EGaIn and the sample (~0.10 mm^2) was evaluated with a calibrated microscope and it was used to calculate the current density J (A/cm^2) as a function of the applied bias V (V). The voltage was swept between -1 V and 1 V, and 50 I/V traces were collected in different regions of the surface for each sample (see "Material and Methods" for details).

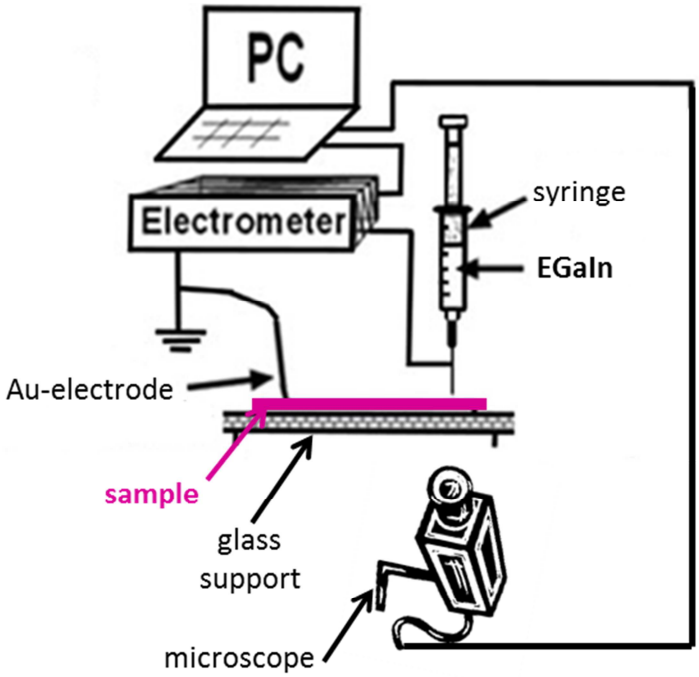

Figure 76: Experimental set-up for EGain junction measurement (adapted from ref. [186]).

The obtained J/V characteristics (averaged over 50 runs) of $FeRuDT_2$ wires are reported in Figure 77. From this plot it is clear that a decrease of the current passing across the organic layer occurs at increasing wire length. These characteristic and the trend of J are very similar to those observed on nFeDT molecular wires on gold, reported by Tuccitto et al., who performed their electrical characterisation by Hg-drop technique.[181]

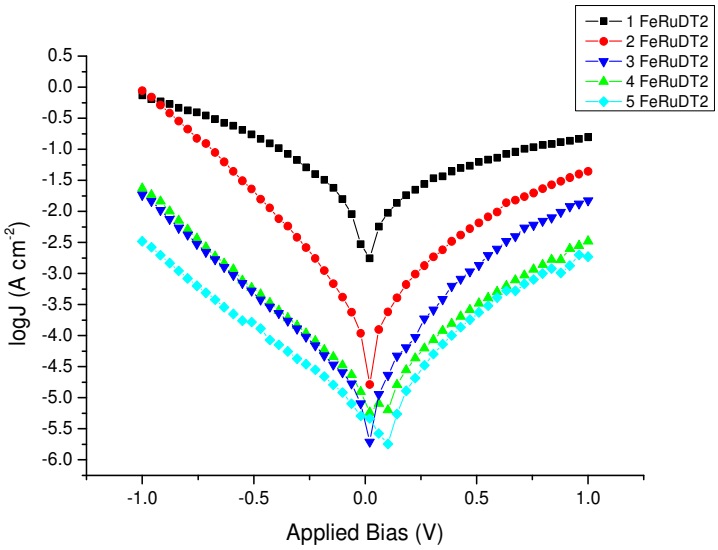

Figure 77: J/V characteristics of nFeRuDT$_2$ systems.

Very useful data can be extracted from the J/V plot about the charge transport mechanism across the wires. In general, in the case of molecular wires, of thin molecular layers junction and of SAM-based junctions, the electrical behaviour is usually described by a simplified form of the Simmons equation[152] for tunnelling across a barrier of arbitrary shape:

$$J = J_0 e^{-\beta d}$$

where J_0 (A/cm^2) is a constant, d (Å) is the width of the tunnelling barrier (corresponding to the thickness of the organic layer) and β (Å^{-1}) is a decay constant, which value depends on the molecular system investigated.

The β parameter is one of the main benchmarks employed for the characterisation of the "good" or "bad" electrical behaviour of a molecular wire, and the smallest the β, the greater the distance that a charge can travel without issues.[182]. This decay factor and the Simmons approximation are by definition valid in the case of exponentially decaying processes (like coherent tunnelling mechanism, the one that usually applies to SAM and molecular wires), but it is actually used for the description of all types of charge transport. From the Simmons equation, lnJ has a linear dependence on the thickness *d* and so from a lnJ/*d* plot one can calculate the β at a chosen voltage, provided that *d* is known. In our case the parameter *d* was estimated to be of ~ 2 nm per Fe-RuDT$_2$ layer, by taking as a reference previous AFM measurement made by Tuccito et al. on Fe-DT molecular wires assembled on gold. The lnJ vs *d* plot for nFe-RuDT$_2$ wires is presented in Figure 78. By fitting the experimental data a β value of 0.071 ± 0.009 Å^{-1} for nFeRuDT$_2$ wires was obtained.

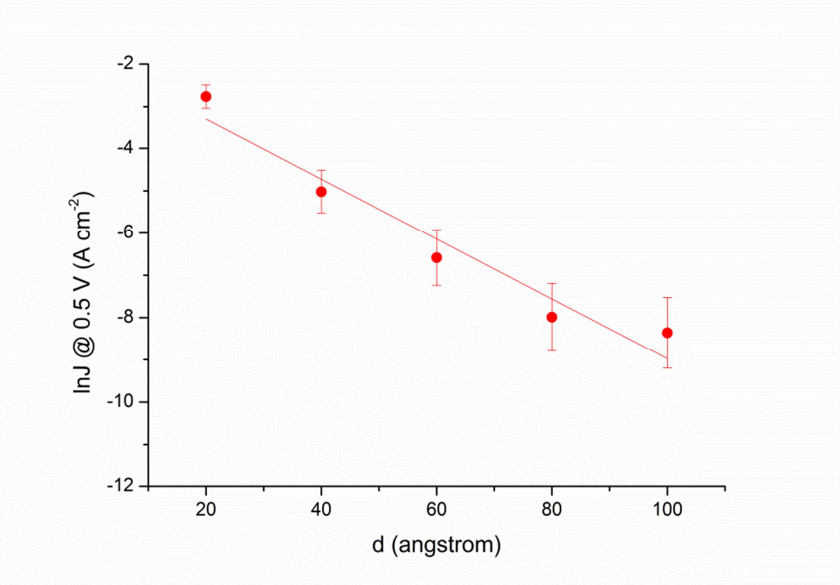

Figure 78: Plot of lnJ as a function of the thickness *d*.

Within the limits of experimental error, this β is two order of magnitude smaller than the value usually obtained for alkanes and one order of magnitude lower than that determined for conjugated wires, like oligophenylenes (see paragraph 1.2.1) but it is in good agreement with the β found on nFeDT systems on gold probed by Hg-drop measurements by Tuccitto et al (0.028 Å^{-1})

and also with β found by Musumeci *et al.* by C-AFM (0.058 ±0.006 $Å^{-1}$) [208] on the same nFeDT systems. Similar decay coefficients were also estimated on analogous bis(terpyridine)-based wires by measuring thermodynamic parameters of electron transfer through electrochemical methods.[211, 212] Such a low value of β and, the other way round, the weak dependences on the wire lengths are typically considered being a signature of a hopping mechanism, i.e. a series of electron transmission events between redox units, even though some cases of long-range tunneling have been reported.[213] As a rule of thumb, coherent tunnelling mechanism appears to be effective for distances smaller than ~25 Å, while for greater distances more complex mechanism are invocated, such as the incoherent diffusive tunnelling or hopping.[149] Given that from tunnelling to hopping the thickness dependence of J changes from, respectively, exponential ($e^{-\beta d}$) to linear (1/d), if there is a transition between different conduction regimes it should be visible as an inflection point on the lnJ vs d plot at some d value.[214] In our case the data fit with a single straight line, which gives a single low attenuation coefficient even at the smallest lengths, and that means that there is apparently no transition. It should be pointed out that the "real" *d* value for $nFeRuDT_2$ wires is not known but only estimated, meaning that the calculated values could suffer from over- or underestimation, that nevertheless is not expected to change the order of magnitude of the decay value.

An indication can be retrieved from the logJ/logV plot (Figure 79) that a transition from a certain transport regime to another is actually likely to exist. A clear inflection point can be noticed at given bias values, for wires containing more than one $Fe\text{-}RuDT_2$ unit; before this transition bias (low bias region) the current density scales linearly with the applied voltage, while after it (high bias) a roughly quadratic dependence is shown. According to literature [215-217] a linear correlation between J and V^2 is usually ascribed to space-charge limited conduction (SCLC).

The same information on the existence of a transition regime for charge transport can be retrieved from the $\ln(J/V^2) - 1/V$ plot for positive bias, called Fowler-Nordheim plot (F-N) (Figure 80). For $1FeRuDT_2$ the current scales logarithmically with 1/V within the whole voltage range explored, according to the Simmons model for tunnelling. On the other hand for longer wires this dependence is valid until a certain applied voltage (low bias), corresponding to an inflection point on the F-N plot; this inflection point likely corresponds to the transition to SCLC regime. On the other hand, a negative slope in the F-N plot in the high bias region would indicate a transition to field emission

(Fowler-Nordheim) transport mechanism;[214, 218, 219] however in the plot of Figure 80 it is not really easy to distinguish if this negative slope is actually present or not.

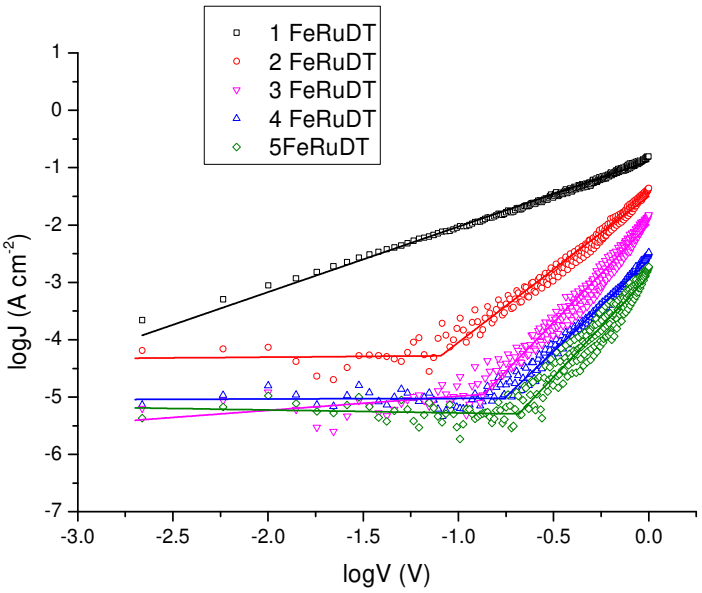

Figure 79: logJ – logV plot for nFeRuDT$_2$ systems (n = 1÷ 5).

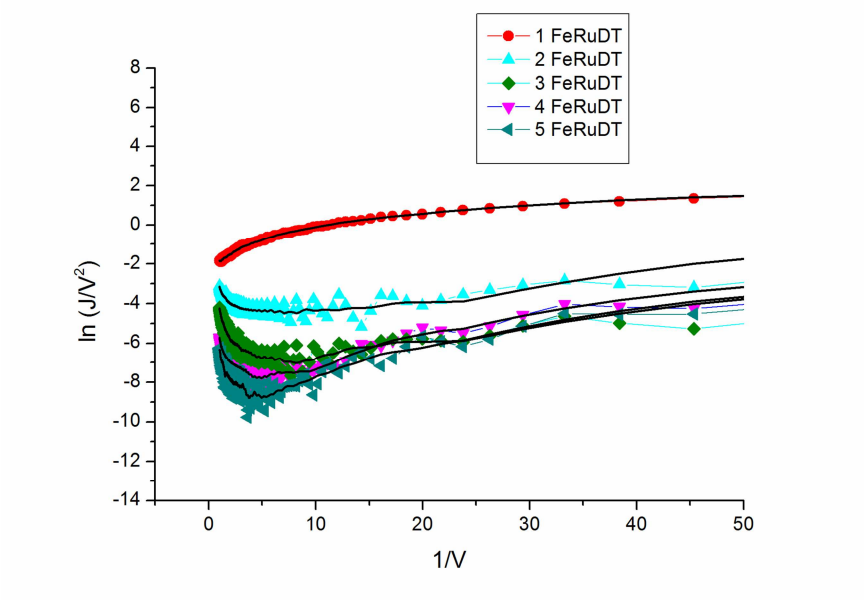

Figure 80: Fowler-Nordheim plot for nFeRuDT$_2$ systems (n = 1÷ 5); the black lines are the results of a smoothing filter, applied to the plots.

In order to discriminate between the different conduction mechanism and try to find the most "suitable" for the description of nFeRuDT$_2$ wires, the dependence of J with varying the wire length can be helpful. In particular, a linear correlation between J and 1/d or $1/d^2$ would be an indication that hopping charge transport mechanism occurs (respectively via intramolecular process or intermolecular diffusion hopping);[133] instead a linear correlation with $1/d^3$ would support a space-charge limited conduction.[217] In Figure 81 the current density is plotted as a function of the inverse distance, as well as inverse quadratic and cubic. A linear variation of J occurs with the inverse of d^3, thus giving further support to the hypothesis that a space-charge limited mechanism occurs.

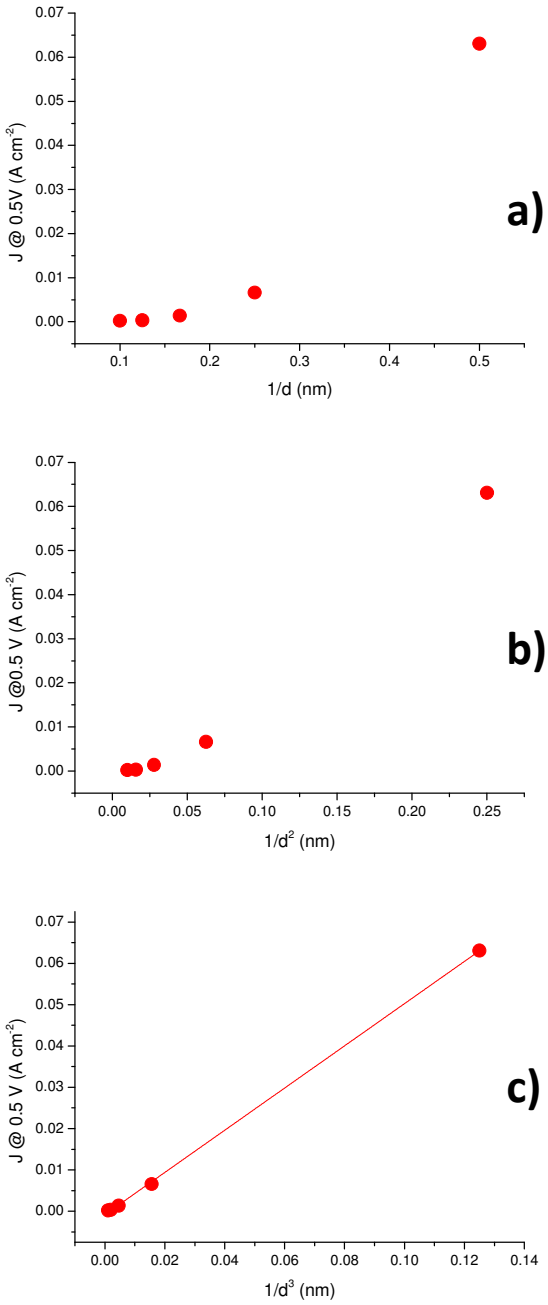

Figure 81: Current density dependence with respect to a) 1/d, b) $1/d^2$, c) $1/d^3$.

The above presented data seem to indicate that for very short wires (1Fe-$RuDT_2$) the conduction mechanism is non-resonant tunnelling (according to Simmons model), whilst for longer wires the available data suggest a space-

charge limited conduction. In order to better clarify the electrical transport along those wires, some work is obviously needed. In particular, temperature-dependent measurements of J/V characteristics would help, considering that some mechanism are indeed temperature dependent (e.g. hopping) and others are not (e.g. tunnelling and field emission).[117] In addition, theoretical simulations of molecular wires electronic structures could be really useful in the interpretation of the charge conduction mechanism and the actual parameters influencing them. Another point that will deserve future investigation is the possible photo-induced activity of the Fe-$RuDT_2$ wires: given that the metal-bisterpyridine units (especially the $Ru(tpy)_2$) are known for their special photophysic and photoelectrochemical properties, the response of the system to light-stimuli and the occurrence of photo-induced phenomena could show interesting outcomes for an application of these conductive wires, amongst other, in the framework of Photochemical Molecular Devices (PMD), light-harvesting and solar energy conversion.

2.3.2. Conclusions

Molecular wires containing multi Fe-$RuDT_2$ units have been grown on ZP-primed FTO surfaces, functionalised with a monolayer of terpyridinic groups by means of a molecular anchoring platform (PPTP film). Molecular wires were grown *via* a self-assembling stepwise method involving direct coordination reactions at the sample surface, in order to study their electrical behaviour for perspective application in molecular photoresponsive electronics. The formation and growth of the molecular films have been assessed by ToF-SIMS and UV-Vis spectroscopy. Electrical measurements carried out by EGaIn junction technique show that the systems investigated in this work display β decay values of the same order of magnitude of the ones measured by means of C-AFM and Hg-drop junctions on nFe-DT wires grown on gold substrates. From the analysis of the J/V characteristics, it seems that for short wires (formed by just 1Fe-$RuDT_2$ unit) a tunnelling mechanism is responsible for charge transport along the wires, whereas for wires containing from 2 to 5 Fe-$RuDT_2$ units a transition to another charge conduction mechanism occurs, likely space-charge limited conduction (SCLC), but further measurement are needed in order to better clarify the actual charge transport mechanism.

The presented data show that these conductive molecular wires can be successfully grown through direct surface reaction onto transparent conductive oxides by means of the ZP-PPTP platform, and moreover, once integrated at the oxide surface they exhibit an interesting electrical behaviour, which could allow perspective applications in nanoscale molecular electronics.

3. Conclusions and perspectives

This thesis work was focused on oxide surfaces modification through functional molecular systems anchoring, for applications in energy and molecular electronics. The main goal was the development of an effective experimental strategy for the robust anchoring of functional molecules onto substrates of technological interest, such as transparent (semi)conducting oxide.
The strategy, exploited for the modification, involved a preliminary stepwise surface priming based on the chemistry of zirconium phosphates/phosphonates (ZP-priming). It was demonstrated that this preliminary surface treatment provides a stable platform for the subsequent anchoring of functional molecules bearing a phosphonic group onto oxides of different chemical nature and morphology. The efficacy of the priming treatment and its effect on the subsequent molecular anchoring were extensively characterised by means of ToF-SIMS technique, UV-Vis spectroscopy and (photo)electric measurements.
The work was focused on the application of this methodology to the integration of functional molecules onto different oxides and with different perspective applications.

First, nanostructured oxides, namely TiO_2 and SnO_2 (micrometres thick layers, deposited onto FTO substrate) were investigated. The ZP-priming methodology was successfully applied to these kind of thick mesoporous substrates: by monitoring each reaction step of the priming by means of SIMS depth profiling, the experimental treatment conditions were optimised for the achievement of a uniform priming of the entire nanostructured layers. ZP-nanostructured TiO_2 and SnO_2 were used as substrate for the preparation of photoactive electrodes with perspective application in dye-sensitised cells for solar energy conversion. It was demonstrated that the preliminary ZP treatment provides a suitable anchoring platform for the sensitisation with RuP photoactive molecular dye (ruthenium terpyridyl-triazin complex containing a phosphonic group). Successful sensitisation of the whole ZP nanostructured layer was demonstrated by ToF-SIMS profiling, and by UV-Vis spectroscopic measurements it was shown that various advantages are brought by the ZP-treatment, such as a more stable binding with respect to untreated substrates (i.e. less desorption of dye molecules from the surface), as well as a higher amount of dye molecules adsorbed at the surface. Moreover, photoelectrochemical measurements (acquisition of JV characteristics upon

irradiation) showed that the presence of the zirconium phosphate layer at the oxide-dye interface has no detrimental effects on the dye-to-oxide charge injection, and, as a consequence, on the functionality of the electrode: the photoelectrochemical properties are maintained and in some cases the electrode performances seem to be even improved from the ZP-treatment.

The second system prepared and characterised during this thesis consists in conductive molecular wires of metal-polypyridinic molecules assembled in a stepwise procedure onto FTO substrates. The preliminar ZP-priming of the oxide followed by the deposition of a thin film of PPTP (4-(2,2': 6'-2''-tepryridine-4-yl)benzenephosphonic acid), resulted in a surface "exposing" a layer of terpyridine functionalities, which were exploited as anchoring sites for the integration of ditopic $RuDT_2$ molecules (Ru(II)-bis[4′,4‴-(1,4-phenylene)bis(2,2′:6′,2″-terpyridine)]) through direct metal-coordination of the terpyridine groups at the surface and one of the two free tepryridine units of $RuDT_2$ by iron(II). The (stepwise) iteration of the coordination reaction led to the growth of molecular wires containing different number of Fe-$RuDT_2$ units, as demonstrated by UV-Vis spectroscopy. The electrical characteristics of the wires were probed by EGaIn liquid metal junction measurements. The electrical behaviour of the nFe-$RuDT_2$ systems, represented by the decay factor β (0.071 ± 0.009 $Å^{-1}$), was found to be very similar to that of analogous wires nFeDT (Fe(II)- [4′,4‴-(1,4-phenylene)bis(2,2′:6′,2″-terpyridine)]) assembled on gold surfaces. From the collected data the actual conduction mechanisms occurring in Fe-$RuDT_2$ wires is still dubious, but clear evidence of a transition from different conduction regimes is given (inflection point in log-log plot of the JV characteristics and Fowler-Nordheim plot). The assembly of these kind of conductive molecular wires directly at the surface of transparent and conductive oxides, and the good current flow taking place when the system is in contact with a second electrode could allow perspective applications within the field of molecular electronic devices, and perhaps also in the framework of devices performing "photoinduced" functions, given the presence of the potentially photoactive $Ru(tpy)_2$ centres.

4. Appendix: Materials and Methods

- **Reagents and solvents**

Zirconyl chloride hydrate ($ZrOCl_2 \cdot xH_2O$, ≥ 99.99% trace metals basis), iron(II) sulfate heptahydrate ($FeSO_4 \cdot 7H_2O$, ≥ 98%), acetonitrile (CH_3CN, anhydrous, 99.8%), chloroform ($CHCl_3$, anhydrous, ≥99%, ethanol-stabilised), dimethylformamide (DMF, $HCON(CH_3)_2$, anhydrous, 99.8%), ethanol (EtOH, CH_3CH_2OH, puriss. p.a., ACS reagent, absolute alcohol ≥99.8%), phosphorous (V) oxychloride ($POCl_3$, Reagent Plus, 99%), titanium(IV) chloride ($TiCl_4$ puriss. ≥99%) and zinc(II) trifluoromethanesulphonate ($((CF_3SO_3)_2Zn$, 98%) were purchased by Sigma-Aldrich. Ti-Nanoxide T/SP serigraphic TiO_2 paste (anatase titania nanoparticle paste, average NPs size: 20 nm, Solaronix SA), and cis-diisothiocyanato-bis(2,2'-bipyridyl-4,4'-dicarboxylato) ruthenium(II) bis(tetrabutylammonium) (N719 dye) and Surlyn foils (25 μm thickness) were purchased from Solaronix SA. All reagents (unless otherwise indicated) were used as-supplied.

[Ru^{II}(4'-(tolyl)-2,2':6',2"-terpyridine)(dihydroxy-4-(4,6-di(pyridine-2-yl)-1,3,5-triazin-2-yl) phenylphosphonate)]$(PF_6)_2$ (RuP) and 4-(2,2': 6'-2''-tepryridine-4-yl)benzenphosphonic acid (PPTP) were synthesised as reported in the literature respectively by Ronconi[206] and Spampinato[103].
Ru^{II}-bis[4′,4‴′-(1,4-phenylene)bis(2,2′:6′,2″-terpyridine)] ($RuDT_2$) was synthesised in collaboration with the University of Montreal (Canada), from the research group of prof. G. Hanan. Rhodamine-B phosphonic derivative (RhB-P) was synthesised in collaboration with prof. M.E. Amato (University of Catania).

Water used for solution preparation was ultrapure MilliQ® water with resistivity of 18 MΩ·cm (Merck Millipore purification system).

- **Substrates and samples preparation**

Prior to any utilisation, FTO-covered glass slides were always cleaned by generous rinsing with, subsequently, warm chloroform, ethanol and water.
Flat TiO_2 substrates were prepared onto FTO. TiO_2 (anatase phase) flat film was deposited on substrates by hydrolysis at 70°C of a 0.4M $TiCl_4$ aqueous

solution, prepared according to literature procedure.[220] FTO was dipped overnight in the titanium tetrachloride solution, and afterwards washed with water and annealed at 450 °C for 30 minutes.
Unless differently stated, TiO_2 nanostructured substrates were prepared by "doctor blade" technique, depositing a layer (4÷10 μm thick) of TiO_2 paste onto FTO substrates (previously cleaned by washing with, subsequently, hot chloroform and ethanol). After titania layer deposition, the substrates were sintered at 450°C for 30 minutes.
Nanostructured SnO_2 substrates were prepared by spin-coating (600 rpm for 6s, plus 20s high speed spinning at 2000 rmp) of a tin dioxide colloidal paste (1 μm thick layer, average NPs size: 20 nm), prepared according to literature procedures.[221] Similarly to titania substrates, after the SnO_2 paste deposition the substrate was sintered for 30 minutes at 450°C.
For the stability tests, monolayers of RhB-P and RuP on flat TiO_2 and ZP-TiO_2 were prepared by immersing the substrates in a 10-4 M solution in, respectively, ethanol and acetonitrile, for 24 hours. Then samples were washed with the respective solvents, in order to remove eventually physisorbed molecules, and dried in a stream of nitrogen.
For the preparation of Fe-$RuDT_2$ molecular wires on ZP-FTO, first of all the surface anchoring of PPTP was performed, following with a protection-deprotection procedure.[103] PPTP was first reacted with a stoichiometric amount of Zn(II) trifluoromethanesulphonate in a DMF-H_2O 1:1 mixture, to afford a solution of the complex $Zn(PPTP)_2$ (10^{-4} M). ZP-FTO was incubated in this solution for 24 hours, and afterward rinsed with water. The obtained sample was finally dipped in HCl 0.1 M aqueous solution for 15 minutes, in order to dissolve the $Zn(PPTP)_2$ complex and restore the terpyridinic functionality of the molecules anchored at the oxide surface.
Once the ZP-FTO surface was functionalised with a monolayer of terpyridinic units, the sample was dipped for 90 seconds in a $FeSO_4 \cdot 7H_2O$ solution (10^{-4} M, H_2O-EtOH 1:1 mixture), then rinsed with water and subsequently immersed for 15 minutes in a 10^{-4} M DMF solution of $RuDT_2$. In this way a complex between Fe(II) at the surface and a terpy-unit of $RuDT_2$ would assure the anchoring of the ruthenium complex by means of $Fe(tpy)_2$ complex formation. The last two reaction steps were then repeated iteratively in order to grow the molecular wires of the desired length.

- **Measurement conditions, instrumental parameters**

SIMS depth profiles and surface spectra were acquired using a TOFSIMS IV (ION-TOF GmbH, Münster, Germany). The instrument is equipped with a liquid metal ion source with Bi emitter for analysis and a Cs ion source for sputtering. This technique provides elemental as well as molecular information on the composition of solid surfaces with great sensitivity. With the appropriate experimental conditions, it is also possible the depth profiling of a sample.
Surface spectra were acquired using 25 keV Bi^+ primary ions gun (~ 0.5 pA), rastered over 150 μm x 150 μm. Static conditions were used (Bi^+ primary ion fluence< 10^{12} ions·cm^{-2}) in order to preserve the molecular information from the surface. Mass calibration of ToF spectra was obtained by using eight known peaks in the mass range 1-350 u. Typical mass accuracy was of the order of 20 ppm.
Negative ions profiles of nanostructured TiO_2 were obtained in dual beam mode (in "non-interlaced" mode): sputtering cycles (9.996 s) with 10 keV Cs^+ ion beam (60 nA) rastered over 80 μm x 80 μm area, alternated with analysis cycles with a low current 25 keV Bi^+ ion beam (0.4 pA) rastered over 30 μm x 30 μm area concentric to the sputter crater. For nanostructured SnO_2 samples Cs+ sputter gun was rastered over an area of 150 μm x 150 μm, and Bi+ primary ions beam was rastered concentrically over 50 μm x 50 μm area. In some experiments, SIMS depth profiles were obtained in a Cameca IMS-4f instrument by using a 14.5 keV Cs^+ beam (150 nA) rastered over 125 μm x 125 μm area while collecting negative secondary ions from a central area of the crater. In these measurements, the instrument was operated at low resolution ($M/\Delta M \approx 300$) and the absence of mass interferences at the chosen masses was assessed from the high resolution ToF-SIMS spectra. In all profiling measurements electron flooding was used for charge compensation. Where reported on profiles graph, depth scale calibration was done by measuring the crater depth with a profilometer (P7 KLA Tencor) and assuming a constant sputtering rate.
Being SIMS technique able to discriminate between different elemental isotopes, for convenience the mass and m/z values reported in the text for each peak are referred to the most abundant isotope; otherwise the specific isotope is clearly indicated.

For the acquisition of the J/V characteristics by EGaIn liquid metal junction, a single drop of liquid gallium-indium eutectic (≥99.99 %, trace metal basis, Sigma-Aldrich) was suspended from a syringe, and was used as top-electrode material and put in contact with the sample by means of a micromanipulator. The contact area between EGain and the sample (~0.10 mm^2) was evaluated with a calibrated microscope put behind the transparent substrate and used to calculate the current density J (A/cm^2) as a function of the applied bias V (V). The voltage was swept between -1 V and 1 V, and 50 I/V traces were collected in different regions of the surface for each sample, by means of a Keithley 2611B multimeter.

Photoelectrochemical experiments on dye-sensitised nanostructured samples were performed with a PGSTAT 30 workstation in a three electrode configuration (SCE as reference electrode and Pt-counterelectrode). The samples were exposed to a solar sunlight simulator (LOT-Oriell LS0100-1000), generating AM 1.5 G illumination. A 420 nm cutoff filter was placed in front of the measurement cell to eliminate the contribution due to light absorption from the oxide (either TiO_2 or SnO_2). The experiments were carried out at a scan rate of 20 $mV \cdot s^{-1}$, in aqueous $NaClO_4$ 0.1 M at pH 3 or LiI (different concentrations) in acetonitrile.

The electrical characteristics of N719 –sensitised nanostructured TiO_2 and ZP-TiO_2 were measured by inserting the photoanodes in a "real" standard Grätzel cell, by following a literature procedure. [222]. The photoanodes the Pt counter-electrode were assembled into a sandwich type cell, which was sealed using a thermopress with a hot melt gasket made of Surlyn. The electrolyte solution (LiI 0.8M, I2 0.05M) was introduced into the cell by putting a drop on a hole previously drilled on the Pt-electrode and then by vacuum backfilling. For measuring the functional parameters of dye-sensitized solar cells, devices were exposed to a solar sunlight simulator (LOT-Oriell LS0100-1000) and the I-V curves registered with a digital Keithley 236 multimeter.

UV-Vis spectra were collected with a Jasco V650 instrument, within the range 200-800 nm, at 200 nm/min scanspeed (1 nm data pitch).

References

[1] P. M. Martin, "Front Matter," in *Introduction to Surface Engineering and Functionally Engineered Materials*: John Wiley & Sons, Inc., 2011, pp. i-xv.

[2] A. V. Kiselev, "Non-specific and specific interactions of molecules of different electronic structures with solid surfaces," *Discussions of the Faraday Society,* 10.1039/DF9654000205 vol. 40, no. 0, pp. 205-218, 1965.

[3] S. F. Bent, "Chapter 5 - Semiconductor Surface Chemistry A2 - Nilsson, Anders," in *Chemical Bonding at Surfaces and Interfaces*, L. G. M. Pettersson and J. K. Nørskov, Eds. Amsterdam: Elsevier, 2008, pp. 323-395.

[4] R. F. Pease and S. Y. Chou, "Lithography and other patterning techniques for future electronics," (in English), *Proceedings of the Ieee,* Article vol. 96, no. 2, pp. 248-270, Feb 2008.

[5] U. Diebold, S. C. Li, and M. Schmid, "Oxide Surface Science," in *Annual Review of Physical Chemistry, Vol 61*, vol. 61, S. R. Leone, P. S. Cremer, J. T. Groves, M. A. Johnson, and G. Richmond, Eds. (Annual Review of Physical Chemistry, Palo Alto: Annual Reviews, 2010, pp. 129-148.

[6] A. Stadler, "Transparent Conducting Oxides-An Up-To-Date Overview," (in English), *Materials,* Article vol. 5, no. 4, pp. 661-683, Apr 2012.

[7] J. Wu and R. L. McCreery, "Solid-State Electrochemistry in Molecule/TiO2 Molecular Heterojunctions as the Basis of the TiO2 "Memristor"," (in English), *Journal of the Electrochemical Society,* Article vol. 156, no. 1, pp. P29-P37, 2009.

[8] Z. R. Wang *et al.*, "Role of redox centre in charge transport investigated by novel self-assembled conjugated polymer molecular junctions," (in English), *Nature Communications,* Article vol. 6, p. 10, Jun 2015, Art. no. 7478.

[9] P. Tarakeshwar *et al.*, "SERS as a Probe of Charge-Transfer Pathways in Hybrid Dye/Molecule-Metal Oxide Complexes," (in English), *Journal of Physical Chemistry C,* Article vol. 118, no. 7, pp. 3774-3782, Feb 2014.

[10] D. K. Aswal, S. Lenfant, D. Guerin, J. V. Yakhmi, and D. Vuillaume, "Self assembled monolayers on silicon for molecular electronics," (in English), *Analytica Chimica Acta,* Review vol. 568, no. 1-2, pp. 84-108, May 2006.

[11] J. Wu and R. L. McCreery, "Solid-State Electrochemistry in Molecule/TiO2 Molecular Heterojunctions as the Basis of the TiO2 "Memristor"," (in English), *Journal of the Electrochemical Society,* Article vol. 156, no. 1, pp. P29-P37, 2009.

[12] H. J. Bolink *et al.*, "Molecular Ionic Junction for Enhanced Electronic Charge Transfer," (in English), *Langmuir,* Article vol. 25, no. 1, pp. 79-83, Jan 2009.

[13] R. Farran, D. Jouvenot, F. Loiseau, J. Chauvin, and A. Deronzier, "Photoelectric conversion at a Ru(bpy)(3) (2+)-based metallic triad anchored on ITO surface," (in English), *Dalton Transactions,* Article vol. 43, no. 32, pp. 12156-12159, Aug 2014.

[14] M. B. Gawande, R. K. Pandey, and R. V. Jayaram, "Role of mixed metal oxides in catalysis science-versatile applications in organic synthesis," (in English), *Catalysis Science & Technology,* Review vol. 2, no. 6, pp. 1113-1125, 2012.

[15] J. Monot *et al.*, "Towards zirconium phosphonate-based microarrays for probing DNA-protein interactions: Critical influence of the location of the probe anchoring groups," (in English), *Journal of the American Chemical Society,* Article vol. 130, no. 19, pp. 6243-6251, May 2008.

[16] E. Topoglidis, B. M. Discher, C. C. Moser, P. L. Dutton, and J. R. Durrant, "Functionalizing nanocrystalline metal oxide electrodes with robust synthetic redox proteins," (in English), *Chembiochem,* Article vol. 4, no. 12, pp. 1332-1339, Dec 2003.

[17] V. Balzani, L. Moggi, and F. Scandola, "Towards a Supramolecular Photochemistry: Assembly of Molecular Components to Obtain Photochemical Molecular Devices," in *Supramolecular Photochemistry*, V. Balzani, Ed. Dordrecht: Springer Netherlands, 1987, pp. 1-28.

[18] L. Caranzi *et al.*, "Photoactive Molecular Junctions Based on Self-Assembled Monolayers of Indoline Dyes," (in English), *Acs Applied Materials & Interfaces,* Article vol. 6, no. 22, pp. 19774-19782, Nov 2014.

[19] A. Ulman, *An Introduction to ultrathin organic films : from Langmuir-Blodgett to self-assembly*. Boston, Mass.: Academic Press Inc, 1991.

[20] M. A. Hasan and K. Sumathy, "Photovoltaic thermal module concepts and their performance analysis: A review," (in English), *Renewable & Sustainable Energy Reviews,* Review vol. 14, no. 7, pp. 1845-1859, Sep 2010.

[21] J. R. Durrant, "Molecular approaches to solar energy conversion: the energetic cost of charge separation from molecular-excited states," (in English), *Philosophical Transactions of the Royal Society a-Mathematical Physical and Engineering Sciences,* Review vol. 371, no. 1996, p. 10, Aug 2013, Art. no. 20120195.

[22] S. Caramori *et al.*, "Solar Energy Conversion in Photoelectrochemical Systems," in *Applied Photochemistry: When Light Meets Molecules*, G. Bergamini and S. Silvi, Eds. Cham: Springer International Publishing, 2016, pp. 67-143.

[23] B. Oregan and M. Gratzel, "A LOW-COST, HIGH-EFFICIENCY SOLAR-CELL BASED ON DYE-SENSITIZED COLLOIDAL TIO2 FILMS," (in English), *Nature,* Article vol. 353, no. 6346, pp. 737-740, Oct 1991.

[24] Y. Bai, I. Mora-Sero, F. De Angelis, J. Bisquert, and P. Wang, "Titanium Dioxide Nanomaterials for Photovoltaic Applications," (in English), *Chemical Reviews,* Review vol. 114, no. 19, pp. 10095-10130, Oct 2014.

[25] J. W. Gong, J. Liang, and K. Sumathy, "Review on dye-sensitized solar cells (DSSCs): Fundamental concepts and novel materials," (in English), *Renewable & Sustainable Energy Reviews,* Review vol. 16, no. 8, pp. 5848-5860, Oct 2012.

[26] K. Keis, J. Lindgren, S. E. Lindquist, and A. Hagfeldt, "Studies of the adsorption process of Ru complexes in nanoporous ZnO electrodes," (in English), *Langmuir,* Article vol. 16, no. 10, pp. 4688-4694, May 2000.

[27] K. Keis *et al.*, "Nanostructured ZnO electrodes for dye-sensitized solar cell applications," (in English), *Journal of Photochemistry and Photobiology a-Chemistry,* Article; Proceedings Paper vol. 148, no. 1-3, pp. 57-64, May 2002, Art. no. Pii s1010-6030(02)00039-4.

[28] Q. F. Zhang, C. S. Dandeneau, X. Y. Zhou, and G. Z. Cao, "ZnO Nanostructures for Dye-Sensitized Solar Cells," (in English), *Advanced Materials,* Review vol. 21, no. 41, pp. 4087-4108, Nov 2009.

[29] S. Ferrere, A. Zaban, and B. A. Gregg, "Dye sensitization of nanocrystalline tin oxide by perylene derivatives," (in English), *Journal of Physical Chemistry B,* Letter vol. 101, no. 23, pp. 4490-4493, Jun 1997.

[30] I. Bedja, S. Hotchandani, and P. V. Kamat, "PREPARATION AND PHOTOELECTROCHEMICAL CHARACTERIZATION OF THIN SNO(2) NANOCRYSTALLINE SEMICONDUCTOR-FILMS AND THEIR SENSITIZATION WITH BIS(2,2'-BIPYRIDINE)(2,2'-BIPYRIDINE-4,4'-DICARBOXYLIC ACID)RUTHENIUM(II) COMPLEX," (in English), *Journal of Physical Chemistry,* Article vol. 98, no. 15, pp. 4133-4140, Apr 1994.

[31] K. Sayama, H. Sugihara, and H. Arakawa, "Photoelectrochemical properties of a porous Nb2O5 electrode sensitized by a ruthenium dye," (in English), *Chemistry of Materials,* Article vol. 10, no. 12, pp. 3825-3832, Dec 1998.

[32] A. Le Viet, R. Jose, M. V. Reddy, B. V. R. Chowdari, and S. Ramakrishna, "Nb2O5 Photoelectrodes for Dye-Sensitized Solar Cells: Choice of the Polymorph," (in English), *Journal of Physical Chemistry C,* Article vol. 114, no. 49, pp. 21795-21800, Dec 2010.

[33] H. Y. Zhang, W. G. Wang, H. Liu, R. Wang, Y. M. Chen, and Z. W. Wang, "Effects of TiO2 film thickness on photovoltaic properties of dye-sensitized solar cell and its enhanced performance by graphene combination," (in English), *Materials Research Bulletin,* Article vol. 49, pp. 126-131, Jan 2014.

[34] K. H. Park, T. Y. Kim, J. H. Kim, H. J. Kim, C. K. Hong, and J. W. Lee, "Adsorption and electrochemical properties of photoelectrodes depending on TiO2 film thickness for dye-sensitized solar cells," (in English), *Journal of Electroanalytical Chemistry,* Article vol. 708, pp. 39-45, Nov 2013.

[35] R. Escalante *et al.*, "Influence of TiO2 Film Thickness on the Performance of Dye-Sensitized Solar Cells: Relation Between Optimum Film Thickness and Electron Diffusion Length," *Energy and Environment Focus,* vol. 2, no. 4, pp. 280-286, // 2013.

[36] D. P. Macwan, P. N. Dave, and S. Chaturvedi, "A review on nano-TiO2 sol-gel type syntheses and its applications," (in English), *Journal of Materials Science,* Review vol. 46, no. 11, pp. 3669-3686, Jun 2011.

[37] Q. F. Zhang and G. Z. Cao, "Nanostructured photoelectrodes for dye-sensitized solar cells," (in English), *Nano Today,* Review vol. 6, no. 1, pp. 91-109, 2011.

[38] L. L. Deng, C. X. Zhao, Y. Q. Ma, S. S. Chen, and G. Xu, "Low cost acetone sensors with selectivity over water vapor based on screen printed TiO2 nanoparticles," (in English), *Analytical Methods,* Article vol. 5, no. 15, pp. 3709-3713, 2013.

[39] M. Gratzel, "Dye-sensitized solar cells," (in English), *Journal of Photochemistry and Photobiology C-Photochemistry Reviews,* Review vol. 4, no. 2, pp. 145-153, Oct 2003.

[40] A. Devos, "THERMODYNAMICS OF PHOTOCHEMICAL SOLAR-ENERGY CONVERSION," (in English), *Solar Energy Materials and Solar Cells,* Article; Proceedings Paper vol. 38, no. 1-4, pp. 11-22, Aug 1995.

[41] A. Luque and G. L. Araújo, "Physical limitations to photovoltaic energy conversion," Bristol; Philadelphia; New York: A. Hilger.

[42] A. Hagfeldt, G. Boschloo, L. C. Sun, L. Kloo, and H. Pettersson, "Dye-Sensitized Solar Cells," (in English), *Chemical Reviews,* Review vol. 110, no. 11, pp. 6595-6663, Nov 2010.

[43] S. Campagna, F. Puntoriero, F. Nastasi, G. Bergamini, and V. Balzani, "Photochemistry and photophysics of coordination compounds: Ruthenium," in *Photochemistry and Photophysics of Coordination Compounds I*, vol. 280, V. Balzani and S. Campagna, Eds. (Topics in Current Chemistry, Berlin: Springer-Verlag Berlin, 2007, pp. 117-214.

[44] M. I. J. Polson *et al.*, "Ruthenium complexes of easily accessible tridentate ligands based on the 2-aryl-4,6-bis(2-pyridyl)-s-triazine motif: Absorption spectra, luminescence properties, and redox behavior," (in English), *Chemistry-a European Journal,* Article vol. 10, no. 15, pp. 3640-3648, Aug 2004.

[45] M. K. Nazeeruddin *et al.*, "CONVERSION OF LIGHT TO ELECTRICITY BY CIS-X2BIS(2,2'-BIPYRIDYL-4,4'-DICARBOXYLATE)RUTHENIUM(II) CHARGE-TRANSFER SENSITIZERS (X = CL-, BR-, I-, CN-, AND SCN-) ON NANOCRYSTALLINE TIO2 ELECTRODES," (in English), *Journal of the American Chemical Society,* Article vol. 115, no. 14, pp. 6382-6390, Jul 1993.

[46] M. K. Nazeeruddin *et al.*, "Acid-base equilibria of (2,2 '-bipyridyl-4,4 '-dicarboxylic acid)ruthenium(II) complexes and the effect of protonation on charge-transfer sensitization of nanocrystalline titania," (in English), *Inorganic Chemistry,* Article vol. 38, no. 26, pp. 6298-6305, Dec 1999.

[47] M. K. Nazeeruddin *et al.*, "Engineering of efficient panchromatic sensitizers for nanocrystalline TiO2-based solar cells," (in English), *Journal of the American Chemical Society,* Article vol. 123, no. 8, pp. 1613-1624, Feb 2001.

[48] H. Park, E. Bae, J. J. Lee, J. Park, and W. Choi, "Effect of the anchoring group in Ru-bipyridyl sensitizers on the photoelectrochemical behavior of dye-sensitized TiO2 electrodes: Carboxylate versus phosphonate linkages," (in English), *Journal of Physical Chemistry B,* Article vol. 110, no. 17, pp. 8740-8749, May 2006.

[49] C. E. Taylor and D. K. Schwartz, "Octadecanoic acid self-assembled monolayer growth at sapphire surfaces," (in English), *Langmuir,* Article vol. 19, no. 7, pp. 2665-2672, Apr 2003.

[50] P. Pechy *et al.*, "PREPARATION OF PHOSPHONATED POLYPYRIDYL LIGANDS TO ANCHOR TRANSITION-METAL COMPLEXES ON OXIDE SURFACES - APPLICATION FOR THE CONVERSION OF LIGHT TO ELECTRICITY WITH

NANOCRYSTALLINE TIO2 FILMS," (in English), *Journal of the Chemical Society-Chemical Communications,* Article no. 1, pp. 65-66, Jan 1995.

[51] I. Gillaizeau-Gauthier *et al.*, "Phosphonate-based bipyridine dyes for stable photovoltaic devices," (in English), *Inorganic Chemistry,* Article vol. 40, no. 23, pp. 6073-6079, Nov 2001.

[52] K. Hanson *et al.*, "Photostability of Phosphonate-Derivatized, Ru-II Polypyridyl Complexes on Metal Oxide Surfaces," (in English), *Acs Applied Materials & Interfaces,* Article vol. 4, no. 3, pp. 1462-1469, Mar 2012.

[53] B. J. Brennan, M. J. L. Portoles, P. A. Liddell, T. A. Moore, A. L. Moore, and D. Gust, "Comparison of silatrane, phosphonic acid, and carboxylic acid functional groups for attachment of porphyrin sensitizers to TiO2 in photoelectrochemical cells," (in English), *Physical Chemistry Chemical Physics,* Article vol. 15, no. 39, pp. 16605-16614, 2013.

[54] S. A. Trammell *et al.*, "Sensitization of TiO2 by phosphonate-derivatized proline assemblies," (in English), *Inorganic Chemistry,* Article vol. 38, no. 16, pp. 3665-3669, Aug 1999.

[55] L. Alibabaei, H. L. Luo, R. L. House, P. G. Hoertz, R. Lopez, and T. J. Meyer, "Applications of metal oxide materials in dye sensitized photoelectrosynthesis cells for making solar fuels: let the molecules do the work," (in English), *Journal of Materials Chemistry A,* Article vol. 1, no. 13, pp. 4133-4145, 2013.

[56] X. Luo, J. H. Wang, M. Dooner, and J. Clarke, "Overview of current development in electrical energy storage technologies and the application potential in power system operation," (in English), *Applied Energy,* Article vol. 137, pp. 511-536, Jan 2015.

[57] J. R. Bolton, "Solar fuels," (in English), *Science (New York, N.Y.),* vol. 202, no. 4369, pp. 705-11, 1978 Nov 1978.

[58] A. Bard and L. Faulkner, *Electrochemical Methods: Fundamentals and Applications*. John Wiley & Sons, Inc, 2001.

[59] W. Song *et al.*, "Interfacial Dynamics and Solar Fuel Formation in Dye-Sensitized Photoelectrosynthesis Cells," *ChemPhysChem,* vol. 13, no. 12, pp. 2882-2890, 2012.

[60] J. A. Treadway, J. A. Moss, and T. J. Meyer, "Visible region photooxidation on TiO2 with a chromophore-catalyst molecular assembly," (in English), *Inorganic Chemistry,* Article vol. 38, no. 20, pp. 4386-+, Oct 1999.

[61] K. J. Takeuchi, M. S. Thompson, D. W. Pipes, and T. J. Meyer, "Redox and spectral properties of monooxo polypyridyl complexes of ruthenium and osmium in aqueous media," *Inorganic Chemistry,* vol. 23, no. 13, pp. 1845-1851, 1984/06/01 1984.

[62] S. Hackwood, L. M. Schiavone, W. C. Dautremont-Smith, and G. Beni, "Anodic Evolution of Oxygen on Sputtered Iridium Oxide Films," *Journal of The Electrochemical Society,* vol. 128, no. 12, pp. 2569-2573, December 1, 1981 1981.

[63] M. Yagi, E. Tomita, and T. Kuwabara, "Remarkably high activity of electrodeposited IrO2 film for electrocatalytic water oxidation," (in English),

Journal of Electroanalytical Chemistry, Article vol. 579, no. 1, pp. 83-88, May 2005.

[64] A. Harriman, J. M. Thomas, and G. R. Millward, "CATALYTIC AND STRUCTURAL-PROPERTIES OF IRIDIUM-IRIDIUM DIOXIDE COLLOIDS," (in English), *New Journal of Chemistry,* Article vol. 11, no. 11-12, pp. 757-762, Nov-Dec 1987.

[65] A. Harriman, I. J. Pickering, J. M. Thomas, and P. A. Christensen, "METAL-OXIDES AS HETEROGENEOUS CATALYSTS FOR OXYGEN EVOLUTION UNDER PHOTOCHEMICAL CONDITIONS," (in English), *Journal of the Chemical Society-Faraday Transactions I,* Article vol. 84, pp. 2795-2806, 1988.

[66] N. D. Morris, M. Suzuki, and T. E. Mallouk, "Kinetics of electron transfer and oxygen evolution in the reaction of Ru(bpy)(3) (3+) with colloidal iridium oxide," (in English), *Journal of Physical Chemistry A,* Article vol. 108, no. 42, pp. 9115-9119, Oct 2004.

[67] W. J. Youngblood *et al.*, "Photoassisted Overall Water Splitting in a Visible Light-Absorbing Dye-Sensitized Photoelectrochemical Cell," (in English), *Journal of the American Chemical Society,* Article vol. 131, no. 3, pp. 926-+, Jan 2009.

[68] W. J. Youngblood, S. H. A. Lee, K. Maeda, and T. E. Mallouk, "Visible Light Water Splitting Using Dye-Sensitized Oxide Semiconductors," (in English), *Accounts of Chemical Research,* Review vol. 42, no. 12, pp. 1966-1973, Dec 2009.

[69] G. M. Cheniae and I. F. Martin, "Sites of function of manganese within photosystem II. Roles in O2 evolution and system II," (in English), *Biochimica et biophysica acta,* vol. 197, no. 2, pp. 219-39, 1970 Mar 1970.

[70] K. Sauer, "A role for manganese in oxygen evolution in photosynthesis," *Accounts of Chemical Research,* vol. 13, no. 8, pp. 249-256, 1980/08/01 1980.

[71] C. F. Yocum, C. T. Yerkes, R. E. Blankenship, R. R. Sharp, and G. T. Babcock, "Stoichiometry, inhibitor sensitivity, and organization of manganese associated with photosynthetic oxygen evolution," *Proceedings of the National Academy of Sciences,* vol. 78, no. 12, pp. 7507-7511, December 1, 1981 1981.

[72] C. W. Cady, R. H. Crabtree, and G. W. Brudvig, "Functional models for the oxygen-evolving complex of photosystem II," (in English), *Coordination Chemistry Reviews,* Review vol. 252, no. 3-4, pp. 444-455, Feb 2008.

[73] H. Y. Chen *et al.*, "New linear high-valent tetranuclear manganese-oxo cluster relevant to the oxygen-evolving complex of photosystem II with oxo, hydroxo, and aqua coordinated to a single Mn(IV)," (in English), *Inorganic Chemistry,* Article vol. 44, no. 25, pp. 9567-9573, Dec 2005.

[74] C. S. Mullins and V. L. Pecoraro, "Reflections on small molecule manganese models that seek to mimic photosynthetic water oxidation chemistry," (in English), *Coordination Chemistry Reviews,* Review vol. 252, no. 3-4, pp. 416-443, Feb 2008.

[75] M. W. Kanan and D. G. Nocera, "In situ formation of an oxygen-evolving catalyst in neutral water containing phosphate and Co2+," (in English), *Science,* Article vol. 321, no. 5892, pp. 1072-1075, Aug 2008.

[76] M. W. Kanan, J. Yano, Y. Surendranath, M. Dinca, V. K. Yachandra, and D. G. Nocera, "Structure and Valency of a Cobalt-Phosphate Water Oxidation Catalyst Determined by in Situ X-ray Spectroscopy," (in English), *Journal of the American Chemical Society,* Article vol. 132, no. 39, pp. 13692-13701, Oct 2010.

[77] R. Chakrabarty, S. J. Bora, and B. K. Das, "Synthesis, structure, spectral and electrochemical properties, and catalytic use of cobalt(III)-Oxo cubane clusters," (in English), *Inorganic Chemistry,* Article vol. 46, no. 22, pp. 9450-9462, Oct 2007.

[78] G. La Ganga *et al.*, "Light-driven water oxidation with a molecular tetra-cobalt(III) cubane cluster," (in English), *Faraday Discussions,* Article vol. 155, pp. 177-190, 2012.

[79] N. S. McCool, D. M. Robinson, J. E. Sheats, and G. C. Dismukes, "A Co4O4 "Cubane" Water Oxidation Catalyst Inspired by Photosynthesis," (in English), *Journal of the American Chemical Society,* Article vol. 133, no. 30, pp. 11446-11449, Aug 2011.

[80] A. Sartorel, M. Bonchio, S. Campagna, and F. Scandola, "Tetrametallic molecular catalysts for photochemical water oxidation," (in English), *Chemical Society Reviews,* Review vol. 42, no. 6, pp. 2262-2280, 2013.

[81] Y. Umena, K. Kawakami, J. R. Shen, and N. Kamiya, "Crystal structure of oxygen-evolving photosystem II at a resolution of 1.9 angstrom," (in English), *Nature,* Article vol. 473, no. 7345, pp. 55-U65, May 2011.

[82] M. Vazylyev, D. Sloboda-Rozner, A. Haimov, G. Maayan, and R. Neumann, "Strategies for oxidation catalyzed by polyoxometalates at the interface of homogeneous and heterogeneous catalysis," (in English), *Topics in Catalysis,* Article; Proceedings Paper vol. 34, no. 1-4, pp. 93-99, May 2005.

[83] A. Sartorel *et al.*, "Water Oxidation at a Tetraruthenate Core Stabilized by Polyoxometalate Ligands: Experimental and Computational Evidence To Trace the Competent Intermediates," (in English), *Journal of the American Chemical Society,* Article vol. 131, no. 44, pp. 16051-+, Nov 2009.

[84] Y. V. Geletii *et al.*, "Structural, Physicochemical, and Reactivity Properties of an All-inorganic, Highly Active Tetraruthenium Homogeneous Catalyst for Water Oxidation," (in English), *Journal of the American Chemical Society,* Article vol. 131, no. 47, pp. 17360-17370, Dec 2009.

[85] Y. V. Geletii, Z. Q. Huang, Y. Hou, D. G. Musaev, T. Q. Lian, and C. L. Hill, "Homogeneous Light-Driven Water Oxidation Catalyzed by a Tetraruthenium Complex with All Inorganic Ligands," (in English), *Journal of the American Chemical Society,* Article vol. 131, no. 22, pp. 7522-+, Jun 2009.

[86] F. M. Toma *et al.*, "Efficient water oxidation at carbon nanotube-polyoxometalate electrocatalytic interfaces," (in English), *Nature Chemistry,* Article vol. 2, no. 10, pp. 826-831, Oct 2010.

[87] M. Orlandi *et al.*, "Ruthenium polyoxometalate water splitting catalyst: very fast hole scavenging from photogenerated oxidants," (in English), *Chemical Communications,* Article vol. 46, no. 18, pp. 3152-3154, 2010.

[88] X. H. Lu, S. L. Xie, H. Yang, Y. X. Tong, and H. B. Ji, "Photoelectrochemical hydrogen production from biomass derivatives and water," (in English), *Chemical Society Reviews,* Review vol. 43, no. 22, pp. 7581-7593, Nov 2014.

[89] Y. Fukai, Y. Kondo, S. Mori, and E. Suzuki, "Highly efficient dye-sensitized SnO2 solar cells having sufficient electron diffusion length," (in English), *Electrochemistry Communications,* Article vol. 9, no. 7, pp. 1439-1443, Jul 2007.

[90] J. Bandara and K. Tennakone, "Interparticle charge transfer in dye-sensitized films composed of two kinds of semiconductor crystallites," (in English), *Journal of Colloid and Interface Science,* Article vol. 236, no. 2, pp. 375-378, Apr 2001.

[91] A. N. M. Green, E. Palomares, S. A. Haque, J. M. Kroon, and J. R. Durrant, "Charge transport versus recombination in dye-sensitized solar cells employing nanocrystalline TiO2 and SnO2 films," (in English), *Journal of Physical Chemistry B,* Article vol. 109, no. 25, pp. 12525-12533, Jun 2005.

[92] P. Tiwana, P. Docampo, M. B. Johnston, H. J. Snaith, and L. M. Herz, "Electron Mobility and Injection Dynamics in Mesoporous ZnO, SnO2, and TiO2 Films Used in Dye-Sensitized Solar Cells," (in English), *Acs Nano,* Article vol. 5, no. 6, pp. 5158-5166, Jun 2011.

[93] C. Prasittichai and J. T. Hupp, "Surface Modification of SnO2 Photoelectrodes in Dye-Sensitized Solar Cells: Significant Improvements in Photovoltage via Al2O3 Atomic Layer Deposition," (in English), *Journal of Physical Chemistry Letters,* Article vol. 1, no. 10, pp. 1611-1615, May 2010.

[94] H. J. Snaith and C. Ducati, "SnO2-Based Dye-Sensitized Hybrid Solar Cells Exhibiting Near Unity Absorbed Photon-to-Electron Conversion Efficiency," (in English), *Nano Letters,* Article vol. 10, no. 4, pp. 1259-1265, Apr 2010.

[95] L. Alibabaei, B. D. Sherman, M. R. Norris, M. K. Brennaman, and T. J. Meyer, "Visible photoelectrochemical water splitting into H-2 and O-2 in a dye-sensitized photoelectrosynthesis cell," (in English), *Proceedings of the National Academy of Sciences of the United States of America,* Article vol. 112, no. 19, pp. 5899-5902, May 2015.

[96] T. W. Hamann, R. A. Jensen, A. B. F. Martinson, H. Van Ryswyk, and J. T. Hupp, "Advancing beyond current generation dye-sensitized solar cells," (in English), *Energy & Environmental Science,* Review vol. 1, no. 1, pp. 66-78, 2008.

[97] E. Palomares, J. N. Clifford, S. A. Haque, T. Lutz, and J. R. Durrant, "Control of charge recombination dynamics in dye sensitized solar cells by the use of conformally deposited metal oxide blocking layers," (in English), *Journal of the American Chemical Society,* Article vol. 125, no. 2, pp. 475-482, Jan 2003.

[98] A. Kay and M. Gratzel, "Dye-sensitized core-shell nanocrystals: Improved efficiency of mesoporous tin oxide electrodes coated with a thin layer of an

insulating oxide," (in English), *Chemistry of Materials,* Article vol. 14, no. 7, pp. 2930-2935, Jul 2002.

[99] J. Brillet *et al.*, "Highly efficient water splitting by a dual-absorber tandem cell," (in English), *Nature Photonics,* Article vol. 6, no. 12, pp. 823-827, Dec 2012.

[100] P. Wang, S. M. Zakeeruddin, R. Humphry-Baker, J. E. Moser, and M. Gratzel, "Molecular-scale interface engineering of TiO2 nanocrystals: Improving the efficiency and stability of dye-sensitized solar cells," (in English), *Advanced Materials,* Article vol. 15, no. 24, pp. 2101-+, Dec 2003.

[101] H. J. Son *et al.*, "Dye Stabilization and Enhanced Photoelectrode Wettability in Water-Based Dye-Sensitized Solar Cells through Post-assembly Atomic Layer Deposition of TiO2," (in English), *Journal of the American Chemical Society,* Article vol. 135, no. 31, pp. 11529-11532, Aug 2013.

[102] D. H. Kim *et al.*, "Stabilizing chromophore binding on TiO2 for long-term stability of dye-sensitized solar cells using multicomponent atomic layer deposition," (in English), *Physical Chemistry Chemical Physics,* Article vol. 16, no. 18, pp. 8615-8622, 2014.

[103] V. Spampinato *et al.*, "Functionalization of Oxide Surfaces by Terpyridine Phosphonate Ligands: Surface Reactions and Anchoring Geometry," (in English), *Langmuir,* Article vol. 26, no. 11, pp. 8400-8406, Jun 2010.

[104] S. Vitale, G. Zappala, N. Tuccitto, A. Torrisi, E. Napolitani, and A. Licciardello, "SIMS characterization of surface-modified nanostructured titania electrodes for solar energy conversion devices," (in English), *Journal of Vacuum Science & Technology B,* Article vol. 34, no. 3, p. 5, May-Jun 2016, Art. no. 03h110.

[105] G. E. Moore, "Cramming more components onto integrated circuits (Reprinted from Electronics, pg 114-117, April 19, 1965)," (in English), *Proceedings of the Ieee,* Reprint vol. 86, no. 1, pp. 82-85, Jan 1998.

[106] R. P. Feynman, "There's Plenty of Room at the Bottom," ed, 1959.

[107] B. Mann and H. Kuhn, "Tunneling through Fatty Acid Salt Monolayers," *Journal of Applied Physics,* vol. 42, no. 11, pp. 4398-4405, 1971.

[108] E. E. Polymeropoulos and J. Sagiv, "Electrical conduction through adsorbed monolayers," *The Journal of Chemical Physics,* vol. 69, no. 5, pp. 1836-1847, 1978.

[109] G. Binnig, H. Rohrer, C. Gerber, and E. Weibel, "Surface Studies by Scanning Tunneling Microscopy," *Physical Review Letters,* vol. 49, no. 1, pp. 57-61, 07/05/ 1982.

[110] M. A. Reed, C. Zhou, C. J. Muller, T. P. Burgin, and J. M. Tour, "Conductance of a molecular junction," (in English), *Science,* Article vol. 278, no. 5336, pp. 252-254, Oct 1997.

[111] D. Xiang, H. Jeong, T. Lee, and D. Mayer, "Mechanically Controllable Break Junctions for Molecular Electronics," (in English), *Advanced Materials,* Review vol. 25, no. 35, pp. 4845-4867, Sep 2013.

[112] C. Zhou, M. R. Deshpande, M. A. Reed, L. Jones, and J. M. Tour, "Nanoscale metal self-assembled monolayer metal heterostructures," (in English), *Applied Physics Letters,* Article vol. 71, no. 5, pp. 611-613, Aug 1997.

[113] H. Song, Y. Kim, Y. H. Jang, H. Jeong, M. A. Reed, and T. Lee, "Observation of molecular orbital gating," (in English), *Nature,* Article vol. 462, no. 7276, pp. 1039-1043, Dec 2009.

[114] H. S. J. Van der Zant, E. A. Osorio, M. Poot, and K. O'Neill, "Electromigrated molecular junctions," (in English), *Physica Status Solidi B-Basic Solid State Physics,* Article; Proceedings Paper vol. 243, no. 13, pp. 3408-3412, Nov 2006.

[115] C. Z. Li, H. X. He, and N. J. Tao, "Quantized tunneling current in the metallic nanogaps formed by electrodeposition and etching," (in English), *Applied Physics Letters,* Article vol. 77, no. 24, pp. 3995-3997, Dec 2000, Art. no. Pii [s0003-6951(00)00651-3].

[116] X. L. Li *et al.*, "Measurement of electron transport properties of molecular junctions fabricated by electrochemical and mechanical methods," (in English), *Surface Science,* Article; Proceedings Paper vol. 573, no. 1, pp. 1-10, Dec 2004.

[117] D. Xiang, X. L. Wang, C. C. Jia, T. Lee, and X. F. Guo, "Molecular-Scale Electronics: From Concept to Function," (in English), *Chemical Reviews,* Review vol. 116, no. 7, pp. 4318-4440, Apr 2016.

[118] A. Ulman, "Formation and structure of self-assembled monolayers," (in English), *Chemical Reviews,* Review vol. 96, no. 4, pp. 1533-1554, Jun 1996.

[119] K. Slowinski, R. V. Chamberlain, C. J. Miller, and M. Majda, "Through-bond and chain-to-chain coupling. Two pathways in electron tunneling through liquid alkanethiol monolayers on mercury electrodes," (in English), *Journal of the American Chemical Society,* Article vol. 119, no. 49, pp. 11910-11919, Dec 1997.

[120] G. Wang, Y. Kim, M. Choe, T. W. Kim, and T. Lee, "A New Approach for Molecular Electronic Junctions with a Multilayer Graphene Electrode," (in English), *Advanced Materials,* Article vol. 23, no. 6, pp. 755-+, Feb 2011.

[121] J. Chen, M. A. Reed, A. M. Rawlett, and J. M. Tour, "Large on-off ratios and negative differential resistance in a molecular electronic device," (in English), *Science,* Article vol. 286, no. 5444, pp. 1550-1552, Nov 1999.

[122] G. Wang, T. W. Kim, Y. H. Jang, and T. Lee, "Effects of metal-molecule contact and molecular structure on molecular electronic conduction in nonresonant tunneling regime: Alkyl versus conjugated molecules," (in English), *Journal of Physical Chemistry C,* Article vol. 112, no. 33, pp. 13010-13016, Aug 2008.

[123] A. Nitzan and M. A. Ratner, "Electron transport in molecular wire junctions," (in English), *Science,* Review vol. 300, no. 5624, pp. 1384-1389, May 2003.

[124] J. C. Ellenbogen and J. C. Love, "Architectures for molecular electronic computers: 1. Logic structures and an adder designed from molecular electronic diodes," (in English), *Proceedings of the Ieee,* Review vol. 88, no. 3, pp. 386-426, Mar 2000.

[125] C. Zhou, "Atomic and molecular wires," Yale University, 1999.

[126] M. A. Ratner, B. Davis, M. Kemp, V. Mujica, A. Roitberg, and S. Yaliraki, "Molecular wires: Charge transport, mechanisms, and control," (in English), *Molecular Electronics: Science and Technology,* Article; Proceedings Paper vol. 852, pp. 22-37, 1998.

[127] S. Datta, *Electronic Transport in Mesoscopic Systems*. Cambridge: Cambridge University Press, 1995.
[128] P. G. Collins, A. Zettl, H. Bando, A. Thess, and R. E. Smalley, "Nanotube nanodevice," (in English), *Science,* Article vol. 278, no. 5335, pp. 100-103, Oct 1997.
[129] S. J. Tans *et al.*, "Individual single-wall carbon nanotubes as quantum wires," (in English), *Nature,* Article vol. 386, no. 6624, pp. 474-477, Apr 1997.
[130] J. W. G. Wildoer, L. C. Venema, A. G. Rinzler, R. E. Smalley, and C. Dekker, "Electronic structure of atomically resolved carbon nanotubes," (in English), *Nature,* Article vol. 391, no. 6662, pp. 59-62, Jan 1998.
[131] F. R. F. Fan, Y. X. Yao, L. T. Cai, L. Cheng, J. M. Tour, and A. J. Bard, "Structure-dependent charge transport and storage in self-assembled monolayers of compounds of interest in molecular electronics: Effects of tip material, headgroup, and surface concentration," (in English), *Journal of the American Chemical Society,* Article vol. 126, no. 12, pp. 4035-4042, Mar 2004.
[132] R. W. Murray, "Polymer Modification of Electrodes," *Annual Review of Materials Science,* vol. 14, no. 1, pp. 145-169, 1984.
[133] N. A. Surridge *et al.*, "ELECTRON SELF-EXCHANGE DYNAMICS BETWEEN REDOX SITES IN POLYMERS," (in English), *Faraday Discussions,* Editorial Material vol. 88, pp. 1-+, 1989.
[134] N. J. Tao, "Probing potential-tuned resonant tunneling through redox molecules with scanning tunneling microscopy," (in English), *Physical Review Letters,* Article vol. 76, no. 21, pp. 4066-4069, May 1996.
[135] E. Tran, M. A. Rampi, and G. M. Whitesides, "Electron transfer in a Hg-SAM//SAM-Hg junction mediated by redox centers," (in English), *Angewandte Chemie-International Edition,* Article vol. 43, no. 29, pp. 3835-3839, 2004.
[136] Y. Nishimori, K. Kanaizuka, M. Murata, and H. Nishihara, "Synthesis of molecular wires of linear and branched bis(terpyridine)-complex oligomers and electrochemical observation of through-bond redox conduction," (in English), *Chemistry-an Asian Journal,* Article vol. 2, no. 3, pp. 367-376, 2007.
[137] C. Silva *et al.*, "Exciton and polaron dynamics in a step-ladder polymeric semiconductor: the influence of interchain order," (in English), *Journal of Physics-Condensed Matter,* Article vol. 14, no. 42, pp. 9803-9824, Oct 2002, Art. no. Pii s0953-8984(02)53317-8.
[138] N. Fukuda, M. Mitsuishi, A. Aoki, and T. Miyashita, "Photocurrent enhancement for polymer Langmuir-Blodgett monolayers containing ruthenium complex by surface plasmon resonance," (in English), *Journal of Physical Chemistry B,* Article vol. 106, no. 28, pp. 7048-7052, Jul 2002.
[139] A. A. Bakulin, D. Martyanov, D. Y. Paraschuk, P. H. M. van Loosdrecht, and M. S. Pshenichnikov, "Charge-transfer complexes of conjugated polymers as intermediates in charge photogeneration for organic photovoltaics," (in English), *Chemical Physics Letters,* Article vol. 482, no. 1-3, pp. 99-104, Nov 2009.

[140] P. Heremans, D. Cheyns, and B. P. Rand, "Strategies for Increasing the Efficiency of Heterojunction Organic Solar Cells: Material Selection and Device Architecture," (in English), *Accounts of Chemical Research,* Review vol. 42, no. 11, pp. 1740-1747, Nov 2009.

[141] A. P. Kulkarni, K. M. Noone, K. Munechika, S. R. Guyer, and D. S. Ginger, "Plasmon-Enhanced Charge Carrier Generation in Organic Photovoltaic Films Using Silver Nanoprisms," (in English), *Nano Letters,* Article vol. 10, no. 4, pp. 1501-1505, Apr 2010.

[142] Y. D. Huan *et al.*, "A New Type of Charge-Transfer Salts Based on Tetrathiafulvalene-Tetracarboxylate Coordination Polymers and Methyl Viologen," (in English), *Inorganic Chemistry,* Article vol. 53, no. 7, pp. 3480-3487, Apr 2014.

[143] Y. Kobori and T. Miura, "Overcoming Coulombic Traps: Geometry and Electronic Characterizations of Light-Induced Separated Spins at the Bulk Heterojunction Interface," (in English), *Journal of Physical Chemistry Letters,* Article vol. 6, no. 1, pp. 113-123, Jan 2015.

[144] G. A. Shagisultanova, I. A. Orlova, and A. N. Borisov, "Synthesis and properties of photoactive and electroactive polymers based on transition metal complexes," (in English), *Journal of Photochemistry and Photobiology a-Chemistry,* Article vol. 103, no. 3, pp. 249-255, Mar 1997.

[145] H. Hamidi *et al.*, "Photocurrent Generation from Thylakoid Membranes on Osmium-Redox-Polymer-Modified Electrodes," (in English), *Chemsuschem,* Article vol. 8, no. 6, pp. 990-993, Mar 2015.

[146] B. Y. Ren, D. L. Zhao, S. S. Liu, X. X. Liu, and Z. Tong, "Synthesis and characterization of poly(ferrocenylsilanes) with coumarin side groups and their photochemical reactivity and electrochemical behavior," (in English), *Macromolecules,* Article vol. 40, no. 13, pp. 4501-4508, Jun 2007.

[147] J.-P. Launay and C. Coudret, "Wires Based on Metal Complexes," in *Electron Transfer in Chemistry*: Wiley-VCH Verlag GmbH, 2008, pp. 2-47.

[148] A. Vlček, "Electron-Transfer Processes in Mononuclear Polypyridine Metal Complexes," in *Electron Transfer in Chemistry*: Wiley-VCH Verlag GmbH, 2008, pp. 804-877.

[149] R. L. McCreery, "Molecular electronic junctions," (in English), *Chemistry of Materials,* Review vol. 16, no. 23, pp. 4477-4496, Nov 2004.

[150] B. Q. Xu and N. J. J. Tao, "Measurement of single-molecule resistance by repeated formation of molecular junctions," (in English), *Science,* Article vol. 301, no. 5637, pp. 1221-1223, Aug 2003.

[151] L. D. A. Siebbeles and F. C. Grozema, *Charge and exciton transport through molecular wires*. Weinheim: Wiley-VCH, 2011.

[152] J. G. Simmons, "Generalized Formula for the Electric Tunnel Effect between Similar Electrodes Separated by a Thin Insulating Film," *Journal of Applied Physics,* vol. 34, no. 6, pp. 1793-1803, 1963.

[153] F. Barigelletti *et al.*, "RIGID ROD-LIKE DINUCLEAR RU(II) OS(II) TERPYRIDINE-TYPE COMPLEXES - ELECTROCHEMICAL-BEHAVIOR, ABSORPTION-SPECTRA, LUMINESCENCE PROPERTIES, AND ELECTRONIC-ENERGY TRANSFER

THROUGH PHENYLENE BRIDGES," (in English), *Journal of the American Chemical Society,* Article vol. 116, no. 17, pp. 7692-7699, Aug 1994.

[154] E. A. Weiss, M. J. Ahrens, L. E. Sinks, A. V. Gusev, M. A. Ratner, and M. R. Wasielewski, "Making a molecular wire: Charge and spin transport through para-phenylene oligomers," (in English), *Journal of the American Chemical Society,* Article vol. 126, no. 17, pp. 5577-5584, May 2004.

[155] Y. Selzer, A. Salomon, and D. Cahen, "Effect of molecule-metal electronic coupling on through-bond hole tunneling across metal-organic monolayer-semiconductor junctions," (in English), *Journal of the American Chemical Society,* Article vol. 124, no. 12, pp. 2886-2887, Mar 2002.

[156] P. S. Weiss, L. A. Bumm, T. D. Dunbar, T. P. Burgin, J. M. Tour, and D. L. Allara, "Probing electronic properties of conjugated and saturated molecules in self-assembled monolayers," (in English), *Molecular Electronics: Science and Technology,* Article; Proceedings Paper vol. 852, pp. 145-168, 1998.

[157] E. C. Constable, C. E. Housecroft, M. Neuburger, S. Schaffner, and E. J. Shardlow, "Formation of a 2+2 -heterotetranuclear macrocycle from reaction of a platina-homoditopic ligand with iron(II)," (in English), *Dalton Transactions,* Article no. 2, pp. 234-235, 2005.

[158] F. Wurthner, C. C. You, and C. R. Saha-Moller, "Metallosupramolecular squares: from structure to function," (in English), *Chemical Society Reviews,* Review vol. 33, no. 3, pp. 133-146, Mar 2004.

[159] L. J. Chen *et al.*, "Smart Stimuli-Responsive Spherical Nanostructures Constructed from Supramolecular Metallodendrimers via Hierarchical Self-Assembly," (in English), *Journal of the American Chemical Society,* Article vol. 136, no. 16, pp. 5993-6001, Apr 2014.

[160] S. Bodige *et al.*, "First-generation chiral metallodendrimers: Stereoselective synthesis of rigid D-3-symmetric tetranuclear ruthenium complexes," (in English), *Journal of the American Chemical Society,* Article vol. 119, no. 43, pp. 10364-10369, Oct 1997.

[161] O. Mamula and A. von Zelewsky, "Supramolecular coordination compounds with chiral pyridine and polypyridine ligands derived from terpenes," (in English), *Coordination Chemistry Reviews,* Review vol. 242, no. 1-2, pp. 87-95, Jul 2003.

[162] S. Schmatloch, A. M. J. van den Berg, A. S. Alexeev, H. Hofmeier, and U. S. Schubert, "Soluble high-molecular-mass poly(ethylene oxide)s via self-organization," (in English), *Macromolecules,* Article vol. 36, no. 26, pp. 9943-9949, Dec 2003.

[163] E. C. Constable, A. Thompson, P. Harveson, L. Macko, and M. Zehnder, "METAL-MEDIATED SYNTHESIS OF MULTIDOMAIN LIGANDS - A NEW STRATEGY FOR METALLOSUPRAMOLECULAR CHEMISTRY," (in English), *Chemistry-a European Journal,* Article vol. 1, no. 6, pp. 360-367, Sep 1995.

[164] G. T. Morgan and F. H. Burstall, "3. Dehydrogenation of pyridine by anhydrous ferric chloride," *Journal of the Chemical Society (Resumed),* 10.1039/JR9320000020 no. 0, pp. 20-30, 1932.

[165] G. Morgan and F. H. Burstall, "347. Researches on residual affinity and co-ordination. Part XXXVII. Complex metallic salts containing 2 : 6-di-2[prime or minute]-pyridylpyridine (2 : 2[prime or minute] : 2[double prime]-tripyridyl)," *Journal of the Chemical Society (Resumed),* 10.1039/JR9370001649 no. 0, pp. 1649-1655, 1937.

[166] G. T. Morgan and F. H. Burstall, "323. Researches on residual affinity and co-ordination. Part XXXV. 2 : 2[prime or minute] : 2[double prime]-Tripyridylplatinum salts," *Journal of the Chemical Society (Resumed),* 10.1039/JR9340001498 no. 0, pp. 1498-1500, 1934.

[167] V. Duprez, M. Biancardo, H. Spanggaard, and F. C. Krebs, "Synthesis of conjugated polymers containing terpyridine-ruthenium complexes: Photovoltaic applications," (in English), *Macromolecules,* Article vol. 38, no. 25, pp. 10436-10448, Dec 2005.

[168] F. C. Krebs and M. Biancardo, "Dye sensitized photovoltaic cells: Attaching conjugated polymers to zwitterionic ruthenium dyes," (in English), *Solar Energy Materials and Solar Cells,* Article vol. 90, no. 2, pp. 142-165, Jan 2006.

[169] C. W. Hu, T. Sato, J. Zhang, S. Moriyama, and M. Higuchi, "Multi-colour electrochromic properties of Fe/Ru-based bimetallo-supramolecular polymers," (in English), *Journal of Materials Chemistry C,* Article vol. 1, no. 21, pp. 3408-3413, 2013.

[170] N. Tuccitto *et al.*, "Controlled Density Patterning of Tolylterpyridine-Tagged Oligonucleotides," (in English), *Langmuir,* Article vol. 27, no. 14, pp. 8595-8599, Jul 2011.

[171] N. Tuccitto, N. Giamblanco, A. Licciardello, and G. Marletta, "Patterning of lactoferrin using functional SAMs of iron complexes," (in English), *Chemical Communications,* Article no. 25, pp. 2621-2623, 2007.

[172] A. Auditore *et al.*, "Organized assemblies of thiol-terpyridine and thiophenol on gold surfaces: preferential composition of mixed species evidence," (in English), *Chemical Communications,* Article no. 19, pp. 2494-2495, Oct 2003.

[173] A. Auditore *et al.*, "ToF-SIMS investigation of functional mixed aromatic thiol monolayers on gold," (in English), *Applied Surface Science,* Article; Proceedings Paper vol. 231, pp. 314-317, Jun 2004.

[174] U. S. Schubert, A. Winter, and G. R. Newkome, "Chemistry and Properties of Terpyridine Transition Metal Ion Complexes," in *Terpyridine-Based Materials*: Wiley-VCH Verlag GmbH & Co. KGaA, 2011, pp. 65-127.

[175] J. P. Sauvage *et al.*, "RUTHENIUM(II) AND OSMIUM(II) BIS(TERPYRIDINE) COMPLEXES IN COVALENTLY-LINKED MULTICOMPONENT SYSTEMS - SYNTHESIS, ELECTROCHEMICAL-BEHAVIOR, ABSORPTION-SPECTRA, AND PHOTOCHEMICAL AND PHOTOPHYSICAL PROPERTIES," (in English), *Chemical Reviews,* Review vol. 94, no. 4, pp. 993-1019, Jun 1994.

[176] H. H. Race and S. I. Reynolds, "Electrical Properties of Multimolecular Films," *Journal of the American Chemical Society,* vol. 61, no. 6, pp. 1425-1432, 1939/06/01 1939.

[177] M. L. Chabinyc *et al.*, "Molecular rectification in a metal-insulator-metal junction based on self-assembled monolayers," (in English), *Journal of the*

American Chemical Society, Article vol. 124, no. 39, pp. 11730-11736, Oct 2002.

[178] M. A. Rampi and G. M. Whitesides, "A versatile experimental approach for understanding electron transport through organic materials," (in English), *Chemical Physics,* Review vol. 281, no. 2-3, pp. 373-391, Aug 2002, Art. no. Pii s0301-0104(02)00445-7.

[179] R. E. Holmlin *et al.*, "Electron transport through thin organic films in metal-insulator-metal junctions based on self-assembled monolayers," (in English), *Journal of the American Chemical Society,* Review vol. 123, no. 21, pp. 5075-5085, May 2001.

[180] K. Slowinski, H. K. Y. Fong, and M. Majda, "Mercury-mercury tunneling junctions. 1. Electron tunneling across symmetric and asymmetric alkanethiolate bilayers," (in English), *Journal of the American Chemical Society,* Article vol. 121, no. 31, pp. 7257-7261, Aug 1999.

[181] N. Tuccitto *et al.*, "Highly conductive similar to 40-nm-long molecular wires assembled by stepwise incorporation of metal centres (vol 8, pg 41, 2009)," (in English), *Nature Materials,* Correction vol. 8, no. 4, pp. 359-359, Apr 2009.

[182] E. A. Weiss, J. K. Kriebel, M. A. Rampi, and G. M. Whitesides, "The study of charge transport through organic thin films: mechanism, tools and applications," (in English), *Philosophical Transactions of the Royal Society a-Mathematical Physical and Engineering Sciences,* Article vol. 365, no. 1855, pp. 1509-1537, Jun 2007.

[183] R. C. Chiechi, E. A. Weiss, M. D. Dickey, and G. M. Whitesides, "Eutectic gallium-indium (EGaIn): A moldable liquid metal for electrical characterization of self-assembled monolayers," (in English), *Angewandte Chemie-International Edition,* Article vol. 47, no. 1, pp. 142-144, 2008.

[184] C. A. Nijhuis, W. F. Reus, and G. M. Whitesides, "Molecular Rectification in Metal-SAM-Metal Oxide-Metal Junctions," (in English), *Journal of the American Chemical Society,* Article vol. 131, no. 49, pp. 17814-17827, Dec 2009.

[185] W. F. Reus, M. M. Thuo, N. D. Shapiro, C. A. Nijhuis, and G. M. Whitesides, "The SAM, Not the Electrodes, Dominates Charge Transport in Metal-Monolayer//Ga2O3/Gallium-Indium Eutectic Junctions," (in English), *Acs Nano,* Article vol. 6, no. 6, pp. 4806-4822, Jun 2012.

[186] M. M. Thuo *et al.*, "Odd-Even Effects in Charge Transport across Self-Assembled Monolayers," (in English), *Journal of the American Chemical Society,* Article vol. 133, no. 9, pp. 2962-2975, Mar 2011.

[187] A. Clearfield and G. David Smith, "The Crystallography and Structure of α-Zirconium Bis(monohydrogen orthophosphate) Monohydrate " vol. 8, ed. Inorganic Chemistry, 1969, pp. 431 - 436.

[188] A. Clearfield and K. Demadis, *Metal Phosphonate Chemistry: From Synthesis to Applications*. Royal Society of Chemistry, 2012.

[189] H. Lee, L. J. Kepley, H. G. Hong, and T. E. Mallouk, "INORGANIC ANALOGS OF LANGMUIR-BLODGETT FILMS - ADSORPTION OF ORDERED ZIRCONIUM 1,10-DECANEBISPHOSPHONATE MULTILAYERS ON SILICON SURFACES," (in

English), *Journal of the American Chemical Society,* Note vol. 110, no. 2, pp. 618-620, Jan 1988.
[190] H. Lee, L. J. Kepley, H. G. Hong, S. Akhter, and T. E. Mallouk, "ADSORPTION OF ORDERED ZIRCONIUM PHOSPHONATE MULTILAYER FILMS ON SILICON AND GOLD SURFACES," (in English), *Journal of Physical Chemistry,* Article vol. 92, no. 9, pp. 2597-2601, May 1988.
[191] S. B. Bakiamoh and G. J. Blanchard, "Demonstration of oriented multilayers through asymmetric metal coordination chemistry," (in English), *Langmuir,* Article vol. 15, no. 19, pp. 6379-6385, Sep 1999.
[192] P. Kohli and G. J. Blanchard, "Design and growth of robust layered polymer assemblies with molecular thickness control," (in English), *Langmuir,* Article vol. 15, no. 4, pp. 1418-1422, Feb 1999.
[193] P. Kohli and G. J. Blanchard, "Probing interfaces and surface reactions of zirconium phosphate/phosphonate multilayers using P-31 NMR spectrometry," (in English), *Langmuir,* Article vol. 16, no. 2, pp. 695-701, Jan 2000.
[194] T. Morotti *et al.*, "Zirconium phosphate phosphonate multilayered films based on push-pull stilbazolium salt: synthesis, characterization and second harmonic generation," (in English), *Dalton Transactions,* Article no. 22, pp. 2974-2982, 2008.
[195] V. Spampinato *et al.*, "ToF-SIMS of metal-complex-based supramolecular architectures on oxide surfaces," (in English), *Surface and Interface Analysis,* Article vol. 45, no. 1, pp. 206-210, Jan 2013.
[196] A. Clearfield and K. Demadis, *Metal phosphonate chemistry : from synthesis to applications*. Cambridge: Royal Society of Chemistry, 2012.
[197] J. Crank, *The mathematics of diffusion*, 2nd ed. ed. Oxford: Clarendon Press, 1975.
[198] R. G. Wilson, F. A. Stevie, and C. W. Magee, *Secondary ion mass spectrometry : a practical handbook for depth profiling and bulk impurity analysis*. New York: Wiley, 1989.
[199] J. C. Vickerman and D. Briggs, *ToF-SIMS : surface analysis by mass spectrometry*. Chichester: IM, 2001.
[200] K. Hanson *et al.*, "Self-Assembled Bilayer Films of Ruthenium(II)/Polypyridyl Complexes through Layer-by-Layer Deposition on Nanostructured Metal Oxides," (in English), *Angewandte Chemie-International Edition,* Article vol. 51, no. 51, pp. 12782-12785, 2012.
[201] T. Fujii, A. Ishii, and M. Anpo, "ABSORPTION AND FLUORESCENCE-SPECTRA OF RHODAMINE-B MOLECULES ENCAPSULATED IN SILICA-GEL NETWORKS AND THEIR THERMAL-STABILITY," (in English), *Journal of Photochemistry and Photobiology a-Chemistry,* Article vol. 54, no. 2, pp. 231-237, Nov 1990.
[202] T. J. Meyer, "PHOTOCHEMISTRY OF METAL COORDINATION-COMPLEXES - METAL TO LIGAND CHARGE-TRANSFER EXCITED-STATES," (in English), *Pure and Applied Chemistry,* Article vol. 58, no. 9, pp. 1193-1206, Sep 1986.
[203] H. Seo, M. K. Son, S. Park, H. J. Kim, and M. Shiratani, "The blocking effect of charge recombination by sputtered and acid-treated ZnO thin film in dye-

sensitized solar cells," (in English), *Journal of Photochemistry and Photobiology a-Chemistry,* Article vol. 248, pp. 50-54, Nov 2012.

[204] M. P. Santoni *et al.*, "Dinuclear Ru(II) complexes of bis-(dipyrid-2 '-yl)triazine (bis-dpt) ligands as efficient electron reservoirs," (in English), *Chemical Communications,* Article vol. 47, no. 12, pp. 3586-3588, 2011.

[205] F. Puntoriero *et al.*, "Photoinduced water oxidation using dendrimeric Ru(II) complexes as photosensitizers," (in English), *Coordination Chemistry Reviews,* Review vol. 255, no. 21-22, pp. 2594-2601, Nov 2011.

[206] F. Ronconi *et al.*, "Charge injection into nanostructured TiO2 electrodes from the photogenerated reduced form of a new Ru(ii) polypyridine compound: the "anti-biomimetic" mechanism at work," *Dalton Transactions,* 10.1039/C6DT01970F vol. 45, no. 36, pp. 14109-14123, 2016.

[207] V. Johansson, L. Ellis-Gibbings, T. Clarke, M. Gorlov, G. G. Andersson, and L. Kloo, "On the correlation between dye coverage and photoelectrochemical performance in dye-sensitized solar cells," (in English), *Physical Chemistry Chemical Physics,* Article vol. 16, no. 2, pp. 711-718, 2014.

[208] C. Musumeci *et al.*, "Nanoscale Electrical Investigation of Layer-by-Layer Grown Molecular Wires," (in English), *Advanced Materials,* Article vol. 26, no. 11, pp. 1688-1693, Mar 2014.

[209] R. Farran, D. Jouvenot, B. Gennaro, F. Loiseau, J. Chauvin, and A. Deronzier, "Photoinduced Charge Separation within Metallo-supramolecular Wires Built around a Ru(bpy)(3) (2+)-Bisterpyridine Linear Entity," (in English), *Acs Applied Materials & Interfaces,* Article vol. 8, no. 25, pp. 16136-16146, Jun 2016.

[210] A. Benninghoven, "CHEMICAL-ANALYSIS OF INORGANIC AND ORGANIC-SURFACES AND THIN-FILMS BY STATIC TIME-OF-FLIGHT SECONDARY-ION MASS-SPECTROMETRY (TOF-SIMS)," (in English), *Angewandte Chemie-International Edition in English,* Review vol. 33, no. 10, pp. 1023-1043, Jun 1994.

[211] Y. Nishimori *et al.*, "Superior Electron-Transport Ability of pi-Conjugated Redox Molecular Wires Prepared by the Stepwise Coordination Method on a Surface," (in English), *Chemistry-an Asian Journal,* Article vol. 4, no. 8, pp. 1361-1367, 2009.

[212] R. Sakamoto, S. Katagiri, H. Maeda, and H. Nishihara, "Bis(terpyridine) metal complex wires: Excellent long-range electron transfer ability and controllable intrawire redox conduction on silicon electrode," (in English), *Coordination Chemistry Reviews,* Review vol. 257, no. 9-10, pp. 1493-1506, May 2013.

[213] G. Sedghi *et al.*, "Comparison of the Conductance of Three Types of Porphyrin-Based Molecular Wires: beta,meso,beta-Fused Tapes, meso-Butadiyne-Linked and Twisted meso-meso Linked Oligomers," (in English), *Advanced Materials,* Article vol. 24, no. 5, pp. 653-+, Feb 2012.

[214] S. H. Choi, B. Kim, and C. D. Frisbie, "Electrical resistance of long conjugated molecular wires," (in English), *Science,* Article vol. 320, no. 5882, pp. 1482-1486, Jun 2008.

[215] S. M. Sze and K. K. Ng, "Physics and Properties of Semiconductors—A Review," in *Physics of Semiconductor Devices*: John Wiley & Sons, Inc., 2006, pp. 5-75.
[216] M. A. Lampert, "Simplified Theory of Space-Charge-Limited Currents in an Insulator with Traps," *Physical Review,* vol. 103, no. 6, pp. 1648-1656, 09/15/ 1956.
[217] M. A. Lampert and P. Mark, *Current injection in solids*. New York ; London: Academic Press, 1970.
[218] J. M. Beebe, B. Kim, J. W. Gadzuk, C. D. Frisbie, and J. G. Kushmerick, "Transition from direct tunneling to field emission in metal-molecule-metal junctions," (in English), *Physical Review Letters,* Article vol. 97, no. 2, p. 4, Jul 2006, Art. no. 026801.
[219] R. H. Fowler and L. Nordheim, "Electron Emission in Intense Electric Fields," *Proceedings of the Royal Society of London. Series A,* vol. 119, no. 781, pp. 173-181, 1928.
[220] S.-J. Kim, S.-D. Park, Y. H. Jeong, and S. Park, "Homogeneous Precipitation of TiO2 Ultrafine Powders from Aqueous TiOCl2 Solution," *Journal of the American Ceramic Society,* vol. 82, no. 4, pp. 927-932, 1999.
[221] F. Ronconi *et al.*, "Modification of Nanocrystalline WO3 with a Dicationic Perylene Bisimide: Applications to Molecular Level Solar Water Splitting," (in English), *Journal of the American Chemical Society,* Article vol. 137, no. 14, pp. 4630-4633, Apr 2015.
[222] G. Calogero, I. Citro, G. Di Marco, S. Armeli Minicante, M. Morabito, and G. Genovese, "Brown seaweed pigment as a dye source for photoelectrochemical solar cells," *Spectrochimica Acta Part A: Molecular and Biomolecular Spectroscopy,* vol. 117, pp. 702-706, 1/3/ 2014.